The Hong Kong Polytechnic University

Department of Electronic and Information Engineering

A Pseudo Two-Dimensional Two-Phase Proton Exchange Membrane Fuel Cell Model and its Applications for Water Management Study

Ka Hung Wong

A thesis submitted in partial fulfillment of the requirements

for the degree of Master of Philosophy

July 2011

CERTIFICATE OF ORIGINALITY:

I hereby declare that this thesis is my own work and that, to the best of my knowledge and belief, it reproduces no material previously published or written, nor material that has been accepted for the award of any other degree or diploma, except where due acknowledgement has been made in the text.

_____(Signed)

Ka Hung Wong (Name of student)

Abstract

Numerical studies of the water transport in proton exchange membrane (PEM) fuel cell are presented in this thesis in order to develop an effective active water management scheme for achieving an adequate water distribution in PEM fuel cell. A computational efficient two-phase gas channel model is derived in order to correlate the liquid water flooding in gas channel to the inlet operating conditions. The proposed model is then coupled to the membrane electrolyte assembly (MEA) model to develop a steady-state pseudo two-dimensional two-phase PEM fuel cell model as a framework for analyzing the role of inlet operating conditions. It is found that inlet operating conditions can have significant influences on the performance of PEM fuel cell and can act as effective control parameters for optimizing its performance. In particular, since the performance of PEM fuel cell is highly sensitive to the water distribution within the MEA and water flooding can have detrimental effects on both the performance and the lifetime of PEM fuel cell. The influences of the inlet relative humidity at anode and cathode are systematically investigated by the developed numerical model. A general trend is observed that the influences of the inlet relative humidity at anode and cathode are highly

asymmetrical, so a fully humidified anode and dry cathode are generally preferred for maximizing the output power density of PEM fuel cell by means of achieving a good protonic conduction and an unimpeded diffusion of reactant gases. The usefulness of inlet relative humidity control as a simple and effective method for optimizing PEM fuel cell's performance are demonstrated theoretically by using two examples, in which the use of inlet relative humidity control for maximizing the power density (in static condition) and extending the operating range of PEM fuel cell (in moving-static condition) are presented. In order to realize the proposed inlet relative humidity control, a fast two-phase dynamic PEM fuel cell model is further developed. A short computational time can be achieved by assuming that the concentrations of reactant gases are in steady state, while the dynamic responses of the water content in membrane and the liquid water saturation in gas diffusion layer, which have significantly larger characteristic time constants, are considered. The asymmetrical influences of inlet relative humidity at anode and cathode and the dynamic responses of PEM fuel cell under step changes of current density are realistically captured by the model.

Publications

Journal Papers

[1] K.H. Wong, K.H. Loo, Y.M. Lai, S.C. Tan, and C.K. Tse, A theoretical study of inlet relative humidity control in PEM fuel cell, *International Journal of Hydrogen Energy*, 36(18):11871-11885, 2011.

[2] K.H. Wong, K.H. Loo, Y.M. Lai, S.C. Tan, and C.K. Tse, Treatment of two-phase flow in cathode gas channel for an improved one-dimensional PEM fuel cell model, *International Journal of Hydrogen Energy*, 36(6):3941-3955, 2011.

[3] K.H. Loo, K.H. Wong, Y.M. Lai, S.C. Tan, C.K. Tse, Characterization of the dynamic response of proton exchange membrane fuel cells - a numerical study, *International Journal of Hydrogen Energy*, 35(21): 11861-11877, 2010.

Conference Papers

[1] K.H. Wong, K.H. Loo, Y.M. Lai, and C.K. Tse, Derivation of a computationally efficient two-phase dynamic PEM fuel cell model for control system simulation,

11th International Conference on Clean Energy (ICCE-2011), November 2-5, 2011, Taichung, Taiwan.

[2] K.H. Wong, K.H. Loo, Y.M. Lai, S.C. Tan, and C.K. Tse, Treatment of two-phase flow in gas channel for an improved one-dimensional PEM fuel cell model, *ASME 2010 8th International Fuel Cell Science, Engineering and Technology Conference*, June 14-16, 2010, New York, USA.

Acknowledgements

I would like to thank Dr. Ka Hong Loo, Dr. Siew Chong Tan, Dr. Yuk Ming Lai and Prof. Chi Kong Tse, who have been great teachers throughout my graduate studies. I am truly indebted and thankful for their inspiration and encouragement for getting me interested in the development of PEM fuel cell and guiding me in all aspects of my research.

I have been fortunate to be with Applied Nonlinear Circuits and Systems Research Group. It is a great time to having engaging discussions about research and life with the group members.

I would also like to acknowledge support from the University Grants Committee of the Hong Kong Special Administrative Region.

Last but not least, I want to give my sincerest thanks to my family for their love and support. Without them, I could not focus on my study and accomplish this thesis.

Contents

List of Figures

List of Tables

Chapter 1

Introduction

1.1 Background

Fuel cell is an energy conversion device that converts the energy stored in chemical fuel directly into electric energy. This one-step energy conversion is an advantage of fuel cell, which has initiated the development of fuel cell as a power source since the first fuel cell invented by William Grove in 1839. During the process of its development, various types of fuel cells have been demonstrated including alkaline fuel cell (AFC), phosphoric acid fuel cell (PAFC), solid oxide fuel cell (SOFC) and proton exchange membrane (PEM) fuel cell, but it was PEM fuel cell that demonstrates a great potential in various applications, especially in transportation application. Moreover, with the latest developments of PEM fuel cell, it becomes one of the most promising device that harvests hydrogen power and achieves an environmentally friendly and sustainable

energy generation [1–4].

Hydrogen and oxygen are used as the fuel and oxidant, respectively, in the operation of PEM fuel cell, and consequently water and heat are the only by-products produced at the end of the electrochemical reaction that occurs in PEM fuel cell. The reaction rate is enhanced by the catalyst such that the operating temperature is relatively low ($< 100\,^{\circ}\mathrm{C}$) compared to other high-temperature fuel cells and internal combustion engines, and the warm-up time is typically short. A rapid start-up is thus possible that makes PEM fuel cell suitable for portable and automotive applications. Some demonstrations on these aspects [5–14] have been presented recently. PEM fuel cell is a scalable power source since its core components are thin enough to have a compact design that offers the ability of scaling of the output power up to megawatt capacity. The scalability of output power allows PEM fuel cell to meet the need of a stationary power generation, and some PEM-fuel-cell-based stationary power generations have been demonstrated [15–20].

PEM fuel cell has a compact structure as shown in Fig. 1.1. This structure is designed to effectively distribute reactants within the fuel cell for energy conversion. When PEM fuel cell is operated, the reactants, in general, hydrogen (or hydrogen-rich gases) and oxygen (or compressed air), are fed into the anode and cathode inlets respectively. First, these gaseous reactants reach the gas channel (GC) located between the bipolar plates and the gas diffusion layer (GDL). Then, the gaseous reactants diffuse through the GDL and finally reach the catalyst layer (CL) where electrochemical

reaction occurs. At anode, hydrogen is oxidized to produce protons and electrons. On one hand, electrons flow through the carbon fibers in GDL and CL, to the bipolar plates, and then to the cathode via the external circuit. On the other hand, the protons migrate through the membrane to the cathode. At cathode, oxygen reacts with protons and electrons and form water that is subsequently removed from the fuel cell. The conditions under which these transport phenomena take place significantly affect the energy conversion efficiency of PEM fuel cell. An effective fuel cell operation relies on the realization of an effective transportation of all the reactants and reaction by-products in the fuel cell.

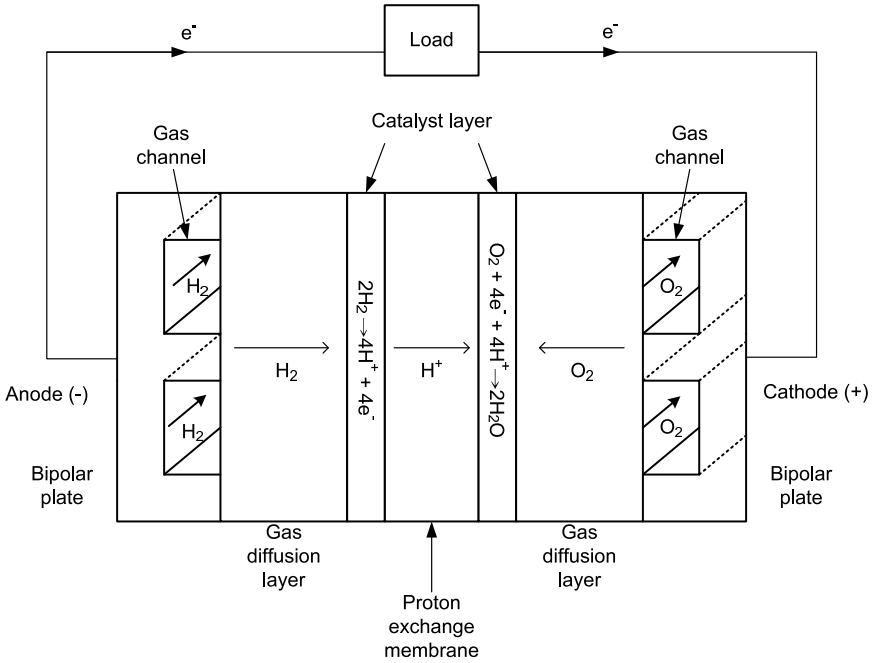

Figure 1.1: A schematic diagram of the structure of a PEM fuel cell.

Poor proton conduction and reliability of the electrolyte had been the great barri-

ers in the last few decades of the development of PEM fuel cell, and these problems were alleviated by the use of perfuorosulfonic acid (PFSA) membranes, for instance Nafion, as an electrolyte due to its electrical, structural and chemical properties it possesses [21,22]. In particular, since PFSA membrane conducts protons (hence it is known as the proton exchange membrane) and is impermeable to gases, it becomes a critical component in PEM fuel cell for carrying protons between anode and cathode and to minimize the cross-over of reactant gases. Although the use of this membrane is considered to be one of the most important milestones in the development of PEM fuel cell [21], hydration of the membrane is required to maintain a high protonic conductivity.

Water concentration that is measured in the terms of water content critically affects the conductivity of membrane. Generally, a higher water content gives rise to a better protonic conductivity. A lack of water supply to fuel cell dehydrates membrane and reduces the mobility of protons in membrane, which increases the ohmic overpotential in the fuel cell. In addition to a degraded performance, dehydration of membrane and the membrane phase in CL can potentially cause irreversible physical degradation to the fuel cell. Significant reactant gases crossover that causes PEM fuel cell's failure is observed when PEM fuel cell is operated under low or unsaturated humidification [23–26]. It is believed that the significant crossover of hydrogen and oxygen is related to membrane degradation accompanied by the formation of cracks or pinholes under these unfavorable operating conditions [23,25,26], even though the exact mechanism that initiates the

membrane degradation in operating PEM fuel cell remains under investigation [24, 27]. Therefore, in order to maintain a membrane in a well-hydrated and healthy state, an adequate humidification is required by feeding humidified reactant gases to the fuel cell.

An adequate amount of water should be maintained in a fuel cell; however, the presence of excessive amount of water has many undesirable effects. Water flooding might happen if excess water accumulates in the fuel cell. Flooding in CL and GDL directly reduces the performance of PEM fuel cell since it hinders the transportation of reactant gases and reduces the surface area of the electrochemically reactive sites, which results in an increased concentration overpotential. The excess water can also lead to flooding in GC, resulting in channel clogging and non-uniform gaseous distribution [28, 29], hence more power must be consumed by compressor for inlet gas feeding. Furthermore, water flooding can accelerate the physical and chemical degradations and shorten the life-time of PEM fuel cell. Non-uniform distribution of gases triggers reactant gas starvation [30], causing cell reversal that accelerates the corrosion (of the carbon fibers) of CL and GDL [30, 31]. Ice-forming at CL under freezing temperature results in the delamination of CL from membrane and GDL, which significantly lowers the physical and electrical contact between these layers [32]. All these damages are irreversible, therefore water flooding should be prevented to enhance the durability and performance of PEM fuel cell.

1.2 Motivation

Water transport significantly affects the proton and reactant gases transport and is a determining factor to the energy conversion efficiency of PEM fuel cell. Dehydration leads to a poor proton transport, and flooding leads to a poor reactant gases transport, both of which result in a low energy conversion efficiency. Moreover, dehydration and flooding lead to irreversible damages to PEM fuel cell and shortens its life-time. These improper water distribution should be avoided by applying a suitable control over the water transport in PEM fuel cell. This gives rise to the requirement of water management for optimizing the performance of PEM fuel cell. The work reported in this thesis is motivated by this important objective that aims to develop a water management scheme to improve the energy conversion efficiency and extend the operating range of PEM fuel cell.

External humidification has been used to enable a flexible water management for PEM fuel cell by directly controlling the relative humidity of inlet reactant gases. In more advanced systems, a feedback control should be implemented and the relative humidity of inlet reactant gases are adjusted dynamically according to real-time operating conditions for constantly achieving a balanced water distribution in a fuel cell. However, in early systems, where the objective of water management has been simply reduced to the essential idea of improving the protonic conductivity of the membrane [33], fully

humidified reactant gases are normally fed to PEM fuel cell indiscriminately. Although a constant and high external humidification increases the possibility of water flooding in PEM fuel cell, especially when PEM fuel cell is operated at high current density, it remains as one standard water management scheme for PEM fuel cell because it can efficiently hydrate the membrane and is simple to implement.

In order to overcome the flooding issue caused by external humidification, some researchers had worked on developing water management schemes that reduce the level of water flooding. In general, these water management schemes are designed to prevent water flooding in cathode and minimize the concentration overpotential. The schemes adopted for this purpose include the design of bilayer diffusion media [34–40] and interdigitated flow field [41–45].

Although external humidification is easy to implement, humidifier is an indispensable component for humidifying the reactant gases but it has the main drawback of occupation of system volume and auxiliary energy consumption [1]. Some researchers suggested that humidifiers should be removed from fuel cell systems for a simplified structure and reduced volume and control complexity through dry-gas operation [46–50]. However, feeding dry reactant gases leads a sub-optimum performance in a conventional PEM fuel cell because it is detrimental to the conductivity of membrane. In view of the poor conductivity, some researchers had proposed some advanced PEM fuel cell's designs with enhanced water-retaining ability for maintaining the fuel cell performance

without external humidification. These designs include self-humidified membrane and anode CL [51–57], innovative gas delivery subsystems [58, 59] and the integration of wicking components [60–62]. These designs have strengthened the feasibility of dry-gas operation, but they also involve more advanced designs and increase the complexity of a fuel cell system.

The main drawback associated with these water management schemes discussed is that only a passive control of water distribution is possible since the amount of by-product water available is restricted by the fuel cell's operating conditions. Therefore, there is no guarantee that the water distribution is optimized under all operating conditions. On the contrary, external humidification is more flexible and provides an active control over water distribution by directly monitoring and adjusting the relative humidity of inlet reactant gases. As discussed above, full humidification and dry-gas operation represent two extreme operating conditions, and both give rise to sub-optimum PEM fuel cell's performance. In view of these drawbacks, an intermediate relative humidity control is required to match the relative humidity of inlet reactant gases to the specific fuel cell's operating conditions such that an optimized water distribution within the fuel cell is constantly achieved over a wide range of operating conditions. Although humidifiers are required for inlet relative humidity control, the recently developed membrane humidifier that employs proton exchange membrane as the water exchange material [63, 64] has enabled a low-cost implementation of external humidification with a

greatly reduced space and power consumption. Moreover, several studies [63–68] that focus on the design and modeling of membrane humidifier were conducted with the aim of developing a more compact membrane humidifier so that inlet relative humidity control can be more conveniently applied to PEM fuel cell.

A comprehensive study of the influences of external humidification on water distribution is vitally important to identify the pathway for achieving an optimized water distribution in PEM fuel cell. Recently, several studies have provided valuable information on the understanding of the effects and applications of external humidification on PEM fuel cell [33, 69–76], and they provided great insights to the work presented in this thesis.

In this thesis, the role of external humidification is considered and the feasibility of applying active control on the inlet relative humidity for optimizing fuel cell's performance is discussed. In order to discuss the role of external humidification, a detailed two-phase PEM fuel cell model is necessary. It is our objective to develop a detailed two-phase PEM fuel cell that aims to provide a more realistic capture of the influences of inlet operating conditions on the liquid water transport within PEM fuel cell. Specifically, liquid water transport in GC is included since its influence on the water distribution inside MEA is vitally important and is closely associated with inlet operating conditions.

The proposed model enables a systemical analysis on the individual roles of inlet

anode and cathode humidification, and their influences on PEM fuel cell's electrical performance. It follows that the maximum power density point of a PEM fuel cell is strongly dependent on the combination of the inlet anode and cathode humidification conditions. Their influences, however, are predicted to be highly asymmetrical. The physical explanation to this asymmetry is given in this thesis. Finally, the developed understanding of their influences are employed to formulate two examples on the use of inlet relative humidity control as a simple and effective method for maximizing the volumetric power density and adjusting the operating range of PEM fuel cell, respectively.

The optimization of PEM fuel cell through external humidification requires a two-phase dynamic PEM fuel cell model since the dynamic response of PEM fuel cell is a determining factor that affects the design of its feedback control system. In this respect, some fast dynamic models have been developed and presented in the literature [77, 78]. These models are based on simplified PEM fuel cell models that do not include all the important water transport phenomena in PEM fuel cell. For instance, two-phase water transport in cathode is often neglected. The complexities of the models are reduced, and thus the physical quantities can be solved in real-time simulation that is essential to developing a feedback control system. However, the simplification would raise concerns about the accuracy of the feedback control system derived using a highly simplified fuel cell model, and, more importantly, these models cannot capture the influences of inlet relative humidity on the water transport in PEM fuel cell. Moreover, it was reported

that the transient response of PEM fuel cell is strongly related to the two-phase water transport [79–83] because the response time of two-phase water transport is much longer than that of other transport phenomena such as gas transport [84, 85]. Therefore, two-phase water transport should be considered in a fast dynamic model.

Most of the two-phase dynamic PEM fuel cell models developed in the literature provide a sophisticated treatment of water transport phenomena that a long computational time is required [79–83]. The sophisticated treatment provides great insights to the understanding of PEM fuel cell and their preferred designs, but it is difficult to apply sophisticated models for control-type simulation studies. The complexities of two-phase water transport in PEM fuel cell has been the main obstacle in the derivation of computationally efficient PEM fuel cell models, and thus it is important to balance the level of sophistication and the required computational time.

So far there are several published works aimed to develop computational efficient two-phase dynamic PEM fuel cell by means of reducing the complexities of existing detailed two-phase dynamic models [86–88]. The liquid water transport in PEM fuel cell is considered, but a static membrane distribution is assumed in these models, which related to initial undershoot of fuel cell's voltage when the current density undergoes a step-wise increase. This motivates the development of a fast two-phase dynamic model following the same idea but with the inclusion of two-phase water transport in GDL and membrane treated with fast computation technique, as is presented in this thesis.

1.3 Organization

This thesis is organized into seven chapters. The first chapter is an introduction of the thesis. Background, motivation and the organization of the thesis are given. In Chapter 2, a detailed literature review is given. Prior research works by others on two-phase PEM fuel cell modeling are discussed and summarized. Moreover, an overview of the main ideas of water management strategies presented in the literature is given.

The next four chapters are the main body of the thesis. In Chapter 3, the mathematical models that describe the transport phenomena in MEA are developed. In Chapter 4, derivation of a two-phase GC submodel is presented, and an improved one-dimensional steady-state two-phase PEM fuel cell model incorporating this submodel is presented. The main objective is to discuss the effects of inlet operating conditions on GC flooding and its effects on the fuel cell's performance. In Chapter 5, the feasibility of inlet relative humidity control for achieving an optimum fuel cell's output power density and a maximum operating range of PEM fuel cell is studied. In Chapter 6, the development of a computationally efficient two-phase dynamic PEM fuel cell model is presented.

Finally, conclusions are given in Chapter 7, along with the proposed future works of research.

Chapter 2

Literature Review

2.1 Water Management Studies

Water management is a critical aspect of PEM fuel cell's operation for preventing the improper water distribution in PEM fuel cell, and many water management schemes have been proposed in literature. They are mainly divided in two categories: 1) Prevention of water flooding; 2) Improvement of dry-gas operation or development of self-humidified fuel cell. The first category aims to prevent water flooding in PEM fuel cell and improve the fuel cell power output capability by reducing as much as possible the concentration overpotential. The second category aims to fully utilize the water generated or to generate extra water from electrochemical reaction in PEM fuel cell for hydrating the membrane and reduce the ohmic overpotential. In this section, an overview of these two water management approaches is given.

2.1.1 Prevention of Water Flooding

The use of bilayer diffusion medium has been suggested for reducing the level of water flooding in PEM fuel cell and has been discussed widely in literature [34–40, 89]. The first detailed numerical analysis on the concept of bilayer diffusion medium was provided by Nam *et al.* [34]. In this article, the discontinuity of liquid water saturation across the boundary formed by a fine and coarse layer due to continuous capillary pressure at this boundary was studied, and it was shown that by inserting a fine layer (compared to GDL) between CL and GDL, the liquid water saturation at the interface of the fine layer and GDL can be reduced, thus possibly improving the fuel cell's performance.

The fine diffusion layer consists of micro-pores and thus it is also called a microporous layer (MPL). Its structure has a significant effect on the liquid water transport in fuel cells, which was numerically studied by Pasaogullari *et al.* [35] and Zhan *et al.* [38, 39]. Pasaogullari *et al.* [35] showed that the liquid water saturation at the CL-MPL boundary can be reduced by using a very thin and high hydrophobic MPL adjacent to CL (compared to the case of single-layer GDL). Zhan *et al.* [38, 39] showed that a thinner MPL gives a lower liquid water saturation st the CL-MPL boundary. Although the lower liquid water saturation at CL-MPL boundary by inserting a MPL was observed, the influences of MPL on the overall liquid water saturation in CL cannot be drawn since CL was not included in those numerical studies.

Pasaogullari *et al.* [36] and Weber *et al.* [37] showed that a higher liquid water pressure is observed by inserting a MPL due to its low permeability. Moreover, it was reported that the water flux toward the anode is increased due to higher liquid water pressure, and hence demonstrating the advantages of MPL in the prevention of water flooding in PEM fuel cells. However, the higher liquid water pressure can also act as a barrier for the liquid water transport at cathode and a high liquid water saturation is thus generated at CL that was reported by Meng's numerical study [89]. Recently, in a short communication by Shi *et al.* [40], the effects of bilayer diffusion media on two-phase water transport were studied under various operating temperatures, and it was reported that water flooding can become worse in MPL and GDL under a higher operating temperature. Moreover, the liquid water saturation in cathode with bi-layer GDL increases with the current density as observed in the numerical results in Pasaogullari *et al.* [36] and Weber *et al.* [37]. Those results suggested that inserting MPL in GDL cannot totally eliminate the water flooding in PEM fuel cell according to real-time operating conditions.

The use of interdigitated flow field for enhancing liquid water removal in GDL and CL was first introduced in [41, 42]. Later, He *et al.* [43], Wang *et al.* [44] and Le *et al.* [45] developed a two-phase model to capture the effects of interdigitated flow field on liquid water removal at GDL. They showed that the liquid water transport is enhanced by the shear force of reactant gas flow due to the use of interdigitated gas

distributor. However, it was mentioned that the high water removal rate can reduce the ionic conductivity of PEM fuel cell, and hence more power loss in the form of ohmic overpotential [45]. Moreover, the convection creates a high pressure drop along the GC, and hence more power needs to be consumed for generating a high gas pressure at the inlet [90].

2.1.2 Dry-gas Operation and Self-Humidified Fuel Cell

Dry-gas operation, *i.e.*, operating PEM fuel cell without external humidification, was proposed in order to eliminate the space and energy consumed by the operation of external humidifiers. Some prior works were done by Buchi *et al.* [46] who conducted modeling studies and experiments to validate the feasibility of dry-gas operation. Some recent experiments reported in [47, 48] explored the influences of operating conditions, such as cell temperature, anode and cathode stoichiometries, on the performance of PEM fuel cell under dry-gas operation, and demonstrated that dry-gas operation is practical under certain well-controlled operating conditions. Furthermore, there are experimental works that examined the reactant species and current distributions [49], and the transient behavior [50] of PEM fuel cell under dry-gas operation. The idea of dry-gas operation is inherently attractive as there is no external humidification subsystem, but the previously reported experimental works [46–48] indicate that the performance of PEM fuel cell under dry-gas operation is low compared to the conventionally operated fuel cell with external humidification, since in the former case the required water for

hydrating membrane originates solely from the by-product water generated within the fuel cell, which is incapable of fulfilling the required level of humidification [47, 48].

Since a sub-optimum performance is resulted under dry-gas operation of an ordinary PEM fuel cell, several approaches that employ the principle of internal humidification were introduced in the literature. These approaches aim to utilize the by-product water more efficiently for an improved fuel cell's performance without external humidification. In this respect, modified PEMs with enhanced water-retaining ability have received a significant research interest. Watanabe *et al.* [51, 52] is one of the pioneers who developed and proposed the use of the self-humidified membrane. This kind of membrane is modified from the conventional membrane by inserting nano-crystallites of platinum (Pt) and hygroscopic oxide that are highly dispersed in the membrane. The Pt particles embedded in the membrane catalyzes the reaction between permeated hydrogen and oxygen forming water that is absorbed by the oxide in nanocrystallites form acting as water storage. The self-humidified membrane utilizes permeated hydrogen and oxygen for generating water for self-humidification. However, the water generation rate is limited by the slow cross-over rate of hydrogen and oxygen as discussed in [53]. Generally, a satisfactory performance is achieved under dry-gas operation solely for low to medium output current density. The relatively small limiting current density can be extended by slight external humidification [52–54]. Despite numerous efforts have been made to improve self-humidified membrane, including optimization of its fabrica-

tion [53, 54] and Pt loading [55], it still requires a more complex membrane preparation and high consumption of Pt.

Several authors [56,57] extended the concept of self-humidified membrane by introducing a self-humidified anode with high water-retaining ability. In this self-humidified anode, hygroscopic oxide is highly dispersed for absorbing the water and enhancing its water content. It was shown that, similar to self-humidified membrane, the modified anode shows a satisfactory performance under dry-gas operation for low to medium output current density, but gives rise to a poorer performance at concentration overpotential dominated region.

There are several studies on the design of innovative gas delivery subsystems [58,59] or the integration of wicking components [60–62] to recirculate the by-product water for humidifying membrane without external humidification. For the development of gas delivery subsystems, Qi *et al*. [58] and Hogarth *et al*. [59] developed a double-path-type flow field design and a channel-less, self-draining PEM fuel cell, respectively, and the effectiveness of these designs were demonstrated. Ge *et al.* [60, 61] mounted an absorbent wicking material to the flow field for absorbing the water produced by fuel cell. Similarly, Litster *et al.* [62] developed a porous plate where the liquid water produced is wicked to this plate, and the stored water can be used for humidification of the membrane. These designs have strengthened the feasibility and aided the practical implementation of dry-gas operation, but they involve more advanced designs and in-

crease the complexity of the fuel cell system. The system's durability with these added complexities should become a design issue when adopting this operation approach.

2.2 Numerical Studies on Two-Phase Water Transport

In the last decade, two-phase PEM fuel cell model has been used to provide fundamental understandings on liquid water transport phenomenon. The understanding provides insights to enhance the design of PEM fuel cell and to develop effective water management schemes, which shorten the development time of PEM fuel cell products. These advantages have motivated researchers to improve the accuracy and details of two-phase PEM fuel cell model. Although PEM fuel cell has a relatively simple and compact structure, two-phase water transport is a complicated phenomenon to model because a variety of complex mass-transport phenomena have to be considered. The complexity is mainly due to the highly specialized components used in PEM fuel cell, which have stimulated research interests toward the understanding of different cell materials and structures and their influences on mass transport. Various sophisticated models have been developed for describing the properties of these specialized components; these complex models are often developed for some given objective of study.

Some early two-phase PEM fuel cell models were developed and introduced by several researchers [34, 91, 92]. Although the modeling formulation were different in these models, Darcy's law that is the fundamental mechanism for liquid water transport in

porous electrode, GDL or CL, was adopted. By including two-phase water transport, some general features of liquid water transport were discussed in these work. Wang *et al*. [91] reported that liquid water transport is likely to occur under high current density due to the high water generation at the cathode CL, and the liquid water is subsequently driven away from GDL toward GC resulting by capillary action. The capillary action is significantly affected by the capillary pressure in GDL, which was systematically studied by Nam *et al*. [34]. The authors studied not only the effects of various gradients of capillary pressure but also the effects of various fiber diameters and porosities of GDL on the level of liquid water saturation since the magnitude of capillary pressure strongly depends on fiber diameter and porosity. According to their results, the authors suggested that the level of liquid water saturation in GDL should decrease with increasing fiber diameter or porosity. Pasaogullari *et al*. [92] derived an analytical solution of the governing equation that describes capillary action, *i.e.*, Darcy's law. The solution showed that the level of liquid water saturation in GDL significantly affects oxygen transport in cathode, hence the performance of fuel cell. From these studies, it is found that capillary action is vital in modeling two-phase water transport. Thus, inclusion of capillary action has become a standard ingredient in describing two-phase water transport in PEM fuel cell.

The development of multi-dimensional model is one possibility for achieving a higher accuracy or improve the predicting capability of two-phase PEM fuel cell in

relation to the influences of cell geometry/material including GC, bipolar plate's shoulder, in-plane-directional mass transport, anisotropic properties of GDL, *etc*. The understanding of these properties is significantly important in the design of passive water management through optimizing the material and structure of PEM fuel cell's stack. This objective has motivated researchers to develop various multi-dimensional models [43, 69, 70, 93, 94]. The two-dimensional models developed by He *et al*. and Natarajan *et al*. [43, 69] consider the same geometrical dimensions, including the through-plane direction and the cross-channel direction, but different flow field designs were employed. He *et al*. [43] focused on interdigitated gas distributor and discussed its influences on liquid water transport when cathode GDL is stacked with the interdigitated gas distributor. The authors reported that the shear force in the cross-channel direction facilitates the removal of liquid water in GDL and showed that the thickness of electrode and the geometry of GC/bipolar plate's shoulders can be designed to optimize the liquid water removal. On the other hand, Natarajan *et al*. [69] focused on conventional gas distributor. Their results suggested that the geometry of GC and bipolar plate are important considerations when fabricating PEM fuel cell for improving its performance. Later, Natarajan *et al*. extended their previous model [69] to include the along-channel direction, forming a three-dimensional model [70]. It was shown that the water flooding in cathode has a more significant drawback on oxygen transport in the context of a three-dimensional model compared with the results obtained with a two-dimensional

one described in their previous work [69]. These studies emphasized on the structure of gas distributors, while other researchers focused on other aspects such as liquid water distribution. For example, Berning *et al*. [93] used a three-dimensional model to discuss the effects of cell geometry on the transport mechanisms of various physical parameters such as reactant concentration, temperature, pressure, and water level. Pasaogullari *et al*. [94] focused on the operating conditions and reported that inlet reactant gases stoichiometry and humidification can have important influences on the two-phase water transport characteristics.

Although these models are multi-dimensional and include GC in the models, the researchers focused on the water flooding phenomena in GDL or CL rather than GC. For instance, He *et al*. [43] focused on the effects of convection force on the liquid water transport in GDL due to the use of interdigitated flow field but did not discuss the effects of the GC conditions on the liquid water transport in GDL. This has motivated some researchers to study the liquid water transport in GC [95–99], where gas and liquid water interact and two-phase flow is modeled using volume-of-fluid (VOF) approach. Quan *et al*. [95] and Jiao *et al*. [96] described the liquid water distribution in a GC with serpentine flow field. Jiao *et al*. [97] further studied the effects of straight GC on liquid water transport. In general, it was shown that reactant gases are un-evenly distributed in GDL/GC when liquid water is found in GC. The mechanism of water droplets emerging from GDL to GC was investigated using the multi-dimensional models developed

by Zhu *et al*. [98, 99], and they showed that the emergence of water droplet involves a cyclical formation process, including growth, deformation, detachment, and finally removal of water droplet.

However, in these studies, electrochemical reactions were not included, and the effects of GC flooding on cell voltage were not discussed. This motivated Le *at al.* [100, 101] to develop a full two-phase fuel cell model that included the electrochemical submodel. They reported that GC flooding creates a barrier for oxygen transport, and a reduced current density is observed at CL when liquid water accumulates in GC and causes a lower oxygen concentration.

In PEM fuel cell's fabrication, the resulting CL would have a variety of morphological and wetting properties. However, in general, CL consists of a structure with numerous agglomerates, which is covered by a thin layer of membrane phase or liquid water, forming a network structure for multi-mass transport. The influences of these structure were described by detailed CL models developed by several authors [72,80,81,102,103]. Siegel *et al*. [102] developed a detailed CL model with the assumption that the agglomerate is spherical without liquid water layer formed on the surface of agglomerates. Lin *et al*. used a thin-film-agglomerate approach to model the morphological properties of CL by describing the agglomerate using cylindrical geometry. Unlike Siegel's model [102], the agglomerate was assumed to be covered by a thin layer of liquid water in the model of Lin *et al*.. The results showed that severe water flooding can occur in CL,

which will significantly affect oxygen transport. The authors suggested that the details of CL should be included to enhance the accuracy of two-phase PEM fuel cell model. Others models developed by Shah *et al*. [72, 80] and Gerteisen *et al*. [81] assumed a spherical agglomerate covered with a thin layer of liquid water, whose thickness is dependent on the level of liquid water saturation in CL.

Some researchers enhanced the accuracy of two-phase PEM fuel cell by studying the effect of capillary action on liquid water transport. The simplest approach adopts the approximation of capillary pressure by a constant known as the capillary diffusion coefficient, which was adopted by He *et al*. [43]. Other detailed approaches employing capillary pressure function fitted from experimental polarization curve [69, 70] or the Leverett function derived from sand physics [34, 91, 92, 94]. These approaches were not fully accurate when it comes to modeling the morphological and wetting properties of GDL and CL. This has motivated Ye *et al*. [104] to develop a more sophisticated model that describes the capillary action in GDL and CL by using experimental capillary function. The work of Ye *et al*. [104] provided an understanding of the effects of the properties of GDL and CL on capillary pressure. Since capillary pressure varies with different materials and structures of GDL and CL, this work also provided insights on the design of GDL/CL providing effective liquid water removal and simulated the work of Wang *et al.* [105]. Wang *et al*. [105] conducted a systematic numerical study on the effects of capillary pressure on the level of liquid water saturation and the performance

of PEM fuel cell. They simulated the polarization curves of PEM fuel cell with various functional forms of capillary pressure. According to their numerical results, it is feasible to increase the limiting current density with a suitable design of GDL/CL that gives rise to the desired capillary properties, and hence a reduction in the level of liquid water flooding.

Several aspects of the developments of two-phase modeling of PEM fuel cell have been discussed, but most of them have focused on passive water management, for instance, the development of gas distributors, design of the cathode CL, design of GDL and MPL, *etc*. In contrast, there were few studies that discussed the issue of active water management, especially the role of inlet relative humidity on the water transport in PEM fuel cell.

Natarajan *et al*. developed two [69] and three-dimensional [70] two-phase PEM fuel cell models and used these models to study the effects of inlet humidification on the performance of PEM fuel cell. The authors showed that the cathode overpotential increases with increasing inlet cathode humidification. It is interesting to point out that both two and three-dimensional models are capable of predicting the same trend. However, protonic transport was not included in these models, and the effect of ohmic overpotential due to dehydration was neglected. Later, Lee *et al*. [71] and Min *et al*. [76] developed more detailed two-phase PEM fuel cell models, from their simulation results, the concentration overpotential is significantly affected by the inlet cathode relative humidity.

When the cathode humidification increases, the concentration overpotential increases, thus leading to a lower limiting current density. In [71], Lee *et al*. also discussed the effect of inlet relative humidity on the liquid water distribution along GC. The author reported that the level of liquid water flooding in cathode decreases with decreasing inlet cathode relative humidity. So far, according to these studies, it is found that the inlet relative humidity significantly affects the liquid water saturation and thus the concentration overpotential in PEM fuel cell. On the other hand, the effect of inlet relative humidity on ohmic overpotential was not emphasized. Shah *et al*. [72] studied the liquid water distribution in the through-plane direction in MEA. Although only two cases of humidification were studied, they showed that the membrane becomes drier at lower humidification, which causes a higher ohmic overpotential at intermediate current density region. However, the study conducted by Shah *et al*. [72] did not provide a systematic and comprehensive analysis on the role of inlet relative humidity on PEM fuel cell's performance. Those studies have provided great insights about the role of inlet relative humidity on the water transport in PEM fuel cell; however, a comprehensive analysis on inlet relative humidity has not been conducted. This motivates the research work in this thesis on the development of a pseudo two-dimensional two-phase model to conduct a detailed analysis on the role of inlet relative humidity.

Chapter 3

Two-Phase MEA Model

Membrane electrolyte assembly (MEA) is the central part of PEM fuel cell stack consisting of GDL, CL and PEM, in which electrochemical reactions and mass transports occur. In the operation of PEM fuel cell, electrons are produced during the electrochemical reactions and are driven by an electric potential difference across the anode and cathode known as the cell voltage. A higher cell voltage, *i.e.*, a lower overall overpotential, relies on an effective mass transport in MEA since most of the overpotentials are a consequence of poor mass transport in MEA. Concentration overpotential is a result of poor mass transport of reactants that leads a deficit of reactant concentration for electrochemical reactions at the CL. Ohmic overpotential is mainly contributed by the poor proton transport across the membrane in MEA. Therefore, the development of materials for and structure of MEA aims to facilitate the mass transport and to enhance the efficiency of electrochemical reactions.

The structure of MEA is compact and simple, but the mass transport phenomena are in fact complicated. In order to have a good description on PEM fuel cell's operation, various mass transport phenomena and electrochemical reactions should be studied. In this chapter, the roles of different components in MEA on mass transport and electrochemical reactions are discussed, and mathematical descriptions of these mass transport and electrochemical reactions are presented.

3.1 MEA Components

During PEM fuel cell's fabrication, anode, cathode and PEM are compressed mechanically together to form a compact, multi-layer structure, including GDLs, CLs and PEM. The schematic of this structure is shown in Fig. 3.1. Each layer is intended to play different roles and has multiple functions in the operation of PEM fuel cell. Therefore, each layer has their own structure and material that are different from each other. Although the structural and material designs provide other functions such as mechanical support and thermal conduction, in this section, only the electrochemical reactions and mass transport occurring in each layer that have significant effects on the performance of PEM fuel cell are discussed.

3.1.1 GDL

GDL is the outermost layer of MEA and is embedded between CL and GC (and bipolar plate). It plays the role in providing passage for mass transport including reactant gases,

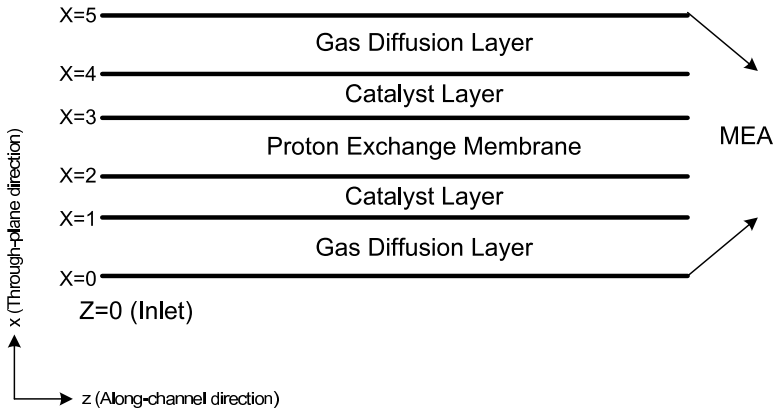

Figure 3.1: The schematic of the multi-layer structure of MEA. A typical MEA includes GDLs, CLs and PEM that are compressed mechanically into a single multi-layer structure.

liquid water and electrons. The requirement for multi-species transport in GDL restricts the available of choices of materials for using as GDL. The suitable materials should have high gas permeability and diffusivity, electron conductivity and should be effective in aiding the removal of liquid water. Currently, carbon-fiber (woven) papers or (unwoven) cloths are the most promising candidates because they satisfy these requirements. In general, carbon papers or cloths have void space for reactant gases transport from GC to the reactive sites in CL. The void space also provide the path for removing of liquid water. However, the volume of void space is limited, therefore when excessive amount of water is transported from CL to GC, liquid water may condense in the void space and occupy part of the space and greatly reduces the rate of reactant gas transport. This is usually referred to as the GDL water flooding phenomenon. The solid matrix of carbon paper or cloth consists of carbon fiber that conduct electrons from anode to cathode for delivering electric power to the external circuit.

Concentration overpotential due to the restriction of reactant gas transport in GDL can be reduced by improving the porosity of GDL. However, GDL with a higher porosity gives rise a larger ohmic overpotential due to poor electron conduction via the remaining carbon fibers. In view of this, the ratio between void space and solid matrix significantly affects the overall performance of GDL and must be optimized.

3.1.2 CL

Low-temperature PEM fuel cell can start up instantly. However, the rates of hydrogen oxidation and oxygen reduction are very low at low-temperature operating condition ($< 100\ ^{\circ}\mathrm{C}$). Therefore, catalyst is used to speed up these electrochemical reactions in order to deliver a reasonable output power density. An expensive metal, platinum, is currently used as the catalyst. Platinum particles are supported by carbon particles forming a porous solid matrix in CL, and membrane phase, *i.e.*, Nafion, penetrates the void space of CL and cover the solid matrix. This gives rise to the basic structure of CL, which is called agglomerate structure.

In similarity to GDL, multi-species mass transport occurs in CL. The solid matrix provides the path for electron transport, the membrane phase provides the path for proton transport, and the void space provides the path for reactant gases transport. All these species finally reach the reactive sites for electrochemical reactions.

3.1.3 Electrolyte

Electrolyte is located at the center of MEA that is embedded between anode and cathode CLs. Its basic function is to interconnect the CLs and transport the protons produced at the anode CL to the cathode CL for completing the electrochemical reactions. Currently, Nafion is used as an electrolyte due to its high protonic conductivity (when it is hydrated). Although Nafion allows proton transport, it is an electron insulator that forbids electron transport. The electron produced in the anode CL is driven to the cathode CL via the external circuit by the potential difference between the anode and cathode. Moreover, Nafion has a very low gas permeability, and it effectively separates the hydrogen in anode and oxygen in cathode, and prevent them from reacting directly. The cross-over of reactant gases is thus prevented and the utilization of the reactants is enhanced. In addition to proton conduction, Nafion also provides the path for water transport in PEM fuel cell.

3.2 Model Assumptions and Descriptions

In this thesis, transport phenomena of six species that determines most of the important transport phenomena and contributes most of the overptentials in PEM fuel cell are described. These transport phenomena of interest include the liquid water transport in cathode, hydrogen transport in anode, oxygen transport in cathode, water vapor transport in both anode and cathode, dissolved water and proton transport in membrane. In

particular, in this chapter, these transport phenomena in MEA including an anode, a cathode and a PEM are discussed, and mathematical model describing these transport phenomena are also presented.

The continuum modeling approach is a traditionally used to describe fluid phenomena within the MEA of PEM fuel cell, which is formulated based upon a macroscopic description thus the knowledge of the constitutive relations are required. Despite there is a huge collection of literature on the continuum modeling of PEM fuel cell [34, 36, 38–40, 72, 79–81, 92, 103, 105–110] , it must be admitted that there is a general lack of realistic constitutive relations that accurately describe the properties of MEA, especially GDL and CL. The macroscopic two-phase flow that is widely adopted for modeling GDL and CL has its origin in the formulation of two-phase flow in porous media that is widely adopted in various engineering applications such as oil recovery, soil and rock mechanics, and chemical reactors. The constitutive relations such as the dependencies of capillary pressure and relative permeability on water saturation are usually taken from empirical relations derived from experiments in these engineering fields, but they are not specific enough to describe the two-phase phenomena in the GDL and CL. As a result, the predicted results obtained from the two-phase flow are not always reliable.

An alternative approach to modeling the two-phase flow in GDL, which has received attention recently, is called the pore network modeling [34, 111–118]. This approach is

a microscopic modeling technique with which the micro-structure of GDL is captured by means of reconstructing the geometry and topology of GDL such that the pore-level physics can be taken into account. This advantage leads to pore network modeling providing a more realistic treatment of the two-phase transport in GDL, which is useful to provide details, such as the capillary pressure of GDL and CL, for constructing realistic continuum two-phase modeling.

An advantage of the continuum modeling is that it is easy to adopt the constitute relations obtained from the microscopic modeling like pore-network modeling in the model to give a more reliable predicted results. Therefore, the continuum modeling approach is adopted in this thesis to earn this flexility in enhancing the accuracy of the model in the future.

Since continuum modeling is adopted, the governing equation for MEA can be rewritten in the conservation form $\nabla \cdot \mathbf{J}_i = S_i$, where $\mathbf{J}_i$ and S_i are respectively the flux and source terms for species i. The expressions of flux and source terms depend on the region of PEM fuel cell.

The physical parameters that are related to electrochemical reactions and mass transport and some constitutive relation of transport properties are listed in Table 3.1.

Table 3.1: Physical Parameters and Constitutive Relations of Mass Transport Properties in MEA.

Parameter/Transport property	Value/Expression
Faraday constant, $F\ (\mathrm{C\ mol^{-1}})$	96487
Gas constant, $R\ (\mathrm{J\ mol\ K^{-1}})$	8.314
Water viscosity, $\mu_\mathrm{l}\ (\mathrm{Pa\ s^{-1}})$ [119]	$2.73 \times 10^{-3} - 6.69 \times 10^{-6} T$
Air viscosity, $\mu_\mathrm{g}\ (\mathrm{Pa\ s^{-1}})$ [120]	2.04×10^{-5}
Water surface tension, $\tau\ (\mathrm{N\ m^{-1}})$ [119]	$0.12398 - 0.00017393T$
Water concentration, $c_\mathrm{l}\ (\mathrm{mol\ m^{-3}})$ [119]	$64500 - 29.84T$
Water molecular mass, $M_\mathrm{v}\ (\mathrm{kg\ mol^{-1}})$	1.8×10^{-2}
Oxygen molecular mass, $M_{\mathrm{O_2}}\ (\mathrm{kg\ mol^{-1}})$	3.2×10^{-2}
Mole fraction of nitrogen of air, $\chi_{\mathrm{N_2,air}}$	0.8
Mole fraction of oxygen of air, $\chi_{\mathrm{O_2,air}}$	0.2
Condensation rate, $k_\mathrm{cond}\ (\mathrm{s^{-1}})$ [121]	1
Evaporation rate, $k_\mathrm{evap}\ (\mathrm{Pa^{-1}\ s^{-1}})$ [121]	5×10^{-5}
Water transfer coefficient of the membrane, $k_\mathrm{d}\ (\mathrm{Pa^{-1}\ s^{-1}})$Modified from [104]	1.5
Binary diffusion coefficient	
Oxygen and nitrogen, $D_{\mathrm{O_2,N_2}}\ (\mathrm{m^2\ s^{-1}})$ [122]	$6.488 \times 10^{-5} T^{1.823} p^{-1}$
Water vapor and nitrogen, $D_{\mathrm{v,N_2}}\ (\mathrm{m^2\ s^{-1}})$ [122]	$4.452 \times 10^{-6} T^{2.334} p^{-1}$
Hydrogen and water vapor, $D_{\mathrm{H_2,v}}\ (\mathrm{m^2\ s^{-1}})$ [122]	$2.2 \times 10^{-5} T^{2.334} p^{-1}$
Oxygen and water vapor, $D_{\mathrm{O_2,v}}\ (\mathrm{m^2\ s^{-1}})$ [122]	$4.257 \times 10^{-6} T^{1.823} p^{-1}$
Oxygen diffusion coefficient	
In electrolyte, $D_{\mathrm{m,O_2}}\ (\mathrm{m^2\ s^{-1}})$ [123]	$3.1 \times 10^{-7} \exp\left(-2768/T\right)$
In water, $D_{\mathrm{l,O_2}}\ (\mathrm{m^2\ s^{-1}})$ [104]	$1.98 \times 10^{-9} \left(\mu_{293\mathrm{K}}/\mu_\mathrm{T}\right) \left(T/293\right)$
Henry's constant of oxygen	
At electrolyte,$H_{\mathrm{m,O_2}}$ [123]	$1.348 \times 10^{5} \exp\left(-666/T\right)$
At water,$H_{\mathrm{l,O_2}}$ [124]	$5.147 \times 10^{5} \exp\left(-498/T\right)$

3.3 Transport of Gas Species

3.3.1 Flux Term

For the PEM fuel cell with parallel or serpentine flow field distributor, diffusion is the primary transport mechanism for gas species at the porous electrodes including GDL and CL. In general, the flux term of gas species i, represented by the symbol $\mathbf{J}_i$, is expressed by the following equation:

$$\mathbf{J}_i = -D_i^{\text{eff}} \nabla c_i, \tag{3.1}$$

where D_i^{eff} is the effective diffusion coefficient of gas species i. This coefficient depends on the morphological structure and wetting properties of the medium and the level of liquid water saturation in the medium. In particular, it can be expressed as follows in GDL [34]:

$$D_i^{\text{eff}} = f(\varepsilon) g(s) D_i. \tag{3.2}$$

Here D_i is the diffusion coefficient of species i in the open space. In an operating PEM fuel cell, the diffusion coefficient of the species i equals or approximates to the binary diffusion coefficient $D_{i,j}$ of species i and its corresponding species j [125].

In anode GDL, humidified hydrogen contains water vapor and hydrogen, hence we

have:

$$D_{\mathrm{v}} = D_{\mathrm{H_2}} = D_{\mathrm{v,H_2}}. \tag{3.3}$$

If humidified oxygen is fed into the cathode of PEM fuel cell, the diffusion coefficient of oxygen and vapor are calculated from binary diffusion coefficient as follows, in which the calculation is similar to anode, *i.e.*,

$$D_{\mathrm{O_2}} = D_{\mathrm{v}} = D_{\mathrm{O_2,v}}. \tag{3.4}$$

On the other hand, if humidified air is used instead to supply the oxidant, the diffusion coefficient of oxygen and water vapor can also be described by binary diffusion coefficient without significant loss of generality because nitrogen constitutes a great proportion of air. In this case, the diffusion coefficient of oxygen and vapor are calculated by the binary diffusion coefficient as expressed in the following equation.

$$\begin{aligned} D_{\mathrm{O_2}} &\approx D_{\mathrm{O_2,N_2}}, \\ D_{\mathrm{v}} &\approx D_{\mathrm{v,N_2}}. \end{aligned} \tag{3.5}$$

Binary diffusion coefficient is a function of temperature and pressure, and their expressions can be estimated based on the kinetic theory of gases. Expressions for some

useful gases that used in this thesis are listed in Table 3.1 for reference.

The first correction factor $f(\varepsilon)$ in Eq. (3.2) accounts for the combined effect of the permeability and tortuosity for a porous medium, and the magnitude of $f(\varepsilon)$ depends on the intrinsic porosity of the medium, ε, and decreases with decreasing intrinsic porosity due to the lesser void space for diffusion. The presence of liquid water decreases the porosity and increases the tortuosity when the medium is flooded and part of the void space is occupied by liquid water. Therefore, the second correction term, $g(s)$ in Eq. (3.2) [34, 126] is introduced to describe the impeding effect of liquid water on the transport of gas species.

Several expressions have been suggested for the correction factor $f(\varepsilon)$ in GDL. In [34], the expression was predicted by percolation theory (pore-network model) and is expressed as follows:

$$f(\varepsilon) = \varepsilon \left(\frac{\varepsilon - 0.11}{1 - 0.11} \right)^{0.785} . \tag{3.6}$$

In [127], the expression was calculated and is expressed as follows:

$$f(\varepsilon) = 1.01 \left(\varepsilon - 0.24 \right)^{1.83} . \tag{3.7}$$

The correction term $g(s)$ was suggested to be $(1 - s)^2$ in the GDL [34].

In CL, the effective diffusion coefficient is suggested as the follows [126]:

$$D_i^{\text{eff}} = \left[(1-s)\,\varepsilon\right]^{1.5} \left(\frac{1}{D_i} + \frac{1}{D_i^{\text{knu}}}\right)^{-1}. \tag{3.8}$$

In this expressions, D_i^{knu} represent Knudsen diffusion coefficient for gas species i. This coefficient describes the transport phenomenon of gas molecules due to the molecule-wall collisions that plays an important role in CL since the pore size of CL is comparable to the mean free path of the gas molecules [128]. The value of Kundsen diffusion coefficient can be calculated by Eq. (3.9).

$$D_i^{\text{knu}} = \frac{2r_{\text{crit}}}{3\sqrt{8RT/\pi M_i}}, \tag{3.9}$$

where r_{crit} is the critical pore radius.

3.3.2 Reaction Kinetics

In cathode CL, oxygen reduction reaction has a slow kinetic that oxygen is not likely to be reacted completely at the reactive sites located at the surface of agglomerate. The remaining oxygen continuously diffuses towards the center of agglomerate and is continuously reacted to give water by the reactive sites located at the center of agglomerate. Diffusion of oxygen in agglomerate gives rise an additional mass-transport resistance that further lower the concentration of oxygen at the reactive sites in agglomerate.

Therefore, a thin film-agglomerate approach is adopted to describe the simultaneous actions of the diffusion of oxygen and the electrochemical reactions [103, 105].

The consumption rate of oxygen is the product of dissolved oxygen concentration and electrochemical reaction rate:

$$S_{\mathrm{O_2}} = c_{\mathrm{O_2}}^{\mathrm{Pt}} k_{\mathrm{r}}. \tag{3.10}$$

The electrochemical reaction rate k_{r} is described by the Butler-Volmer equation, in which the cathode overpotential η_{c} is the driving force for the oxygen reduction reaction, *i.e.*,

$$k_{\mathrm{r}} = \frac{a^{\mathrm{eff,Pt}} i_{\mathrm{ref}}}{4F c_{\mathrm{O_2,ref}}} \exp\left(-\frac{F\eta_{\mathrm{c}}}{RT}\right) \text{ where } \eta_{\mathrm{c}} = V_{\mathrm{cell}} - \phi_{\mathrm{p}} - V_{\mathrm{oc}}. \tag{3.11}$$

In these equations, the effective specific area of the Pt catalyst $a^{\mathrm{eff,Pt}}$, is the product of the specific area of the Pt catalyst a^{Pt}, catalyst loading m^{Pt}, and the inverse of CL thickness l^{CL}. Moreover, V_{cell} is a output voltage of the fuel cell and V_{oc} is the open-circuit voltage of the fuel cell, which can be calculated from Eq. (3.12).

$$V_{\mathrm{oc}} = 1.229 - \frac{\Delta s}{2F}(T - T_{\mathrm{ref}}) + \frac{RT}{2F} \ln\left[\frac{p_{\mathrm{H_2}}^{\mathrm{ACL}}}{p_{\mathrm{H_2,ref}}} + \left(\frac{p_{\mathrm{O_2}}^{\mathrm{CCL}}}{p_{\mathrm{O_2,ref}}}\right)^{0.5}\right], \tag{3.12}$$

where $-\Delta s/2F$ equals 8.46×10^{-4} when the reference temperature, T_{ref}, is 298.15 K.

Oxygen initially dissolves in the electrolyte and water film located at the surface of agglomerates, and then diffuses to the active reaction sites inside the agglomerates. The dissolved oxygen concentration $c_{\mathrm{O_2}}^{\mathrm{Pt}}$ at the active reaction sites is lower than the bulk oxygen concentration in the gas phase of void space external to the agglomerates. To model this concentration drop, $c_{\mathrm{O_2}}^{\mathrm{Pt}}$ is described by:

$$c_{\mathrm{O_2}}^{\mathrm{Pt}} = \frac{c_{\mathrm{O_2}}}{(\Xi_{\mathrm{film}} + \Xi_{\mathrm{agg}})}. \tag{3.13}$$

The first dimensionless constant Ξ_{film} describes the diffusive resistance to oxygen transport due to the presence of water film and electrolyte, and the expression is suggested by Lin *et al.* and Wang *et al.* [103, 105] as:

$$\Xi_{\mathrm{film}} = \frac{k_{\mathrm{r}}}{a^{\mathrm{agg}} RT} \left(\frac{d_{\mathrm{l}} H_{\mathrm{l,O_2}}}{D_{\mathrm{l,O_2}}} + \frac{d_{\mathrm{m}} H_{\mathrm{m,O_2}}}{D_{\mathrm{m,O_2}}} \right). \tag{3.14}$$

The subscripts l and m denotes the liquid and membrane phase, respectively. The parameters a^{agg} and $D_{\alpha,\mathrm{O_2}}$, which are defined as the outer surface area of agglomerates per unit volume of the CL and the diffusivity of oxygen in liquid water or electrolyte, respectively, both tend to reduce the overall diffusive resistance. On the other hand, increases in the electrochemical reaction rate k_{r}, thickness of the film d_α, and the Henry constant $H_{\alpha,\mathrm{O_2}}$, have the opposite effects. The thickness of membrane film is a constant, while the thickness of water film is assumed to have a linear dependence on the liquid

water saturation [103, 105]:

$$d_{\mathrm{l}} = \frac{\varepsilon^{\mathrm{CL}} s}{a^{\mathrm{agg}}}. \tag{3.15}$$

The parameter Ξ_{agg} described the diffusive resistance to oxygen transport due to the structure of the agglomerates is expressed below:

$$\Xi_{\mathrm{agg}} = \frac{H_{\mathrm{m,O_2}}}{\xi RT}. \tag{3.16}$$

Here ξ is the effectiveness factor for the cathode CL agglomerate, defined as a function of the Thiele modulus Φ, which correlates the oxygen reduction reaction to the diffusion process. Their expressions are given by the following expressions:

$$\begin{aligned} \xi &= \frac{3\Phi \coth 3\Phi - 1}{3\Phi^2}, \text{ where} \\ \Phi &= \frac{r^{\mathrm{agg}}}{3}\sqrt{\frac{k_{\mathrm{r}}}{D_{\mathrm{m,O_2}}(\varepsilon_{\mathrm{m}}^{\mathrm{agg}})^{1.5}\left(1-\varepsilon^{\mathrm{CL}}\right)^{1.5}}}. \end{aligned} \tag{3.17}$$

Hydrogen is oxidized at anode CL, and protons are produced. Since the oxidization of hydrogen has a fast kinetic, the Butler-Volmer equation is used to compute the reaction rate of hydrogen directly without a significant loss of generality, *i.e.*,

$$S_{\mathrm{H_2}} = -\frac{a^{\mathrm{eff,Pt}} i_{\mathrm{ref,H_2}}}{2F}\left(\frac{c_{\mathrm{H_2}}}{c_{\mathrm{H_2,ref}}}\right)^{1/2}\left(\frac{2F}{RT}\phi_{\mathrm{p}}\right), \tag{3.18}$$

where $a^{\mathrm{eff,Pt}}$ and $i_{\mathrm{ref,H_2}}$ are the effective specific area of the platinum catalyst and exchange current density of hydrogen oxidization, respectively, and $c_{\mathrm{H_2,ref}}$ is the reference hydrogen concentration.

The electrochemical reactions take place at anode and cathode CL are hydrogen oxidation and oxygen reduction, respectively, and they are written as follows:

$$\mathrm{Anode\ CL} : 2\mathrm{H_2} \rightarrow 4\mathrm{H^+} + 4\mathrm{e^-} \tag{3.19}$$

$$\mathrm{Cathode\ CL} : \mathrm{O_2} + 4\mathrm{e^-} + 4\mathrm{H^+} \rightarrow 2\mathrm{H_2O}. \tag{3.20}$$

Hence, the overall source term for the proton transport is:

$$S_{\mathrm{p}} = \begin{cases} -2S_{\mathrm{H_2}}, \text{ in anode CL} \\ 4S_{\mathrm{O_2}}, \text{ in cathode CL} \end{cases} \tag{3.21}$$

In this thesis, it is assumed the the water produced from the electrochemical reaction is a source of liquid water. Hence, $-2S_{\mathrm{O_2}}$ is one of the source for liquid water transport in cathode CL.

3.4 Transport of Liquid Water

For porous media, such as GDL and CL, Darcy's law is employed to describe the flow of liquid water, where the liquid water flux is proportional to the gradient of liquid water

pressure p_{l} [34, 43]. The expression of liquid water flux is :

$$\mathbf{J}_{\mathrm{l}} = -\frac{c_{\mathrm{l}} k k_{\mathrm{rl}}}{\mu_{\mathrm{l}}} \nabla p_{\mathrm{l}}. \tag{3.22}$$

Liquid water pressure, p_{l}, equals the difference between gas pressure, p_{g}, and capillary pressure, p_{c}, and the gas pressure is assumed uniform in the through-plane direction [103], *i.e.*, $\nabla p_{\mathrm{g}} = 0$, the liquid water flux is reduced by:

$$\mathbf{J}_{\mathrm{l}} = \frac{c_{\mathrm{l}} k k_{\mathrm{rl}}}{\mu_{\mathrm{l}}} \nabla p_{\mathrm{c}}, \tag{3.23}$$

where c_{l} and μ_{l} are, respectively, the concentration and viscosity of liquid water. k is the absolute permeability of liquid water at GDL or CL, which measures the ability of the media to pass liquid water when they are completely flooded. In the case of partial flooding, a correction term known as the relative permeability k_{rl} is introduced for obtaining the effective permeability. The relative permeability depends on liquid water saturation, and the suggested expression [34] is written as $k_{\mathrm{rl}} = s^3$.

The capillary pressure is described as a function of the surface tension τ, contact angle θ, porosity ε, permeability k, and liquid saturation s:

$$p_{\mathrm{c}} = \tau \cos\theta \left(\frac{\varepsilon}{k}\right)^{0.5} L\left(s\right), \tag{3.24}$$

where $L(s)$ is Leverett function , which is a polynomial of liquid water saturation that depends on the wettability of the porous media as given below [36]:

$$L(s) = \begin{cases} 1.417s - 2.12s^2 + 1.263s^3 & ,\theta > \frac{\pi}{2} \\ 1.417(1-s) - 2.12(1-s)^2 + 1.263(1-s)^3 & ,\theta < \frac{\pi}{2} \end{cases}. \tag{3.25}$$

The interfacial mass exchange rate between water vapor and liquid water due to condensation or evaporation is declared as S_{vl}. The rate is assumed to be proportional to the difference between the water vapor pressure and the saturation water vapor pressure, and is expressed as follows [103]:

$$S_{\mathrm{vl}} = \left(\chi_{\mathrm{v}} p_{\mathrm{g}} - p^{\mathrm{sat}}\right) \begin{cases} \frac{k_{\mathrm{cond}} \varepsilon (1-s) \chi_{\mathrm{v}}}{RT} & ,\chi_{\mathrm{v}} p_{\mathrm{g}} > p^{\mathrm{sat}} \\ k_{\mathrm{evap}} \varepsilon s c_{\mathrm{l}} & ,\mathrm{otherwise} \end{cases}. \tag{3.26}$$

Here, p^{sat} is the saturation water vapor pressure that is temperature dependent and is calculated from the following expression:

$$\begin{aligned} p^{\mathrm{sat}} &= -2846.4 + 411.24(T - 273.15) \\ &\quad - 10.554(T - 273.15)^2 + 0.16636(T - 273.15)^3. \end{aligned} \tag{3.27}$$

3.5 Transport of Charge Species

Although electron conduction happens in PEM fuel cell, its effects on the ohmic overpotential is much smaller than that of proton transport. Therefore, the electron transport is not considered in this thesis.

Proton transports from anode to cathode via membrane results in a major ohmic overpotential in PEM fuel cell, and proton transport phenomenon is therefore considered in this thesis. The proton flux across the membrane is described by the Ohm's law as follows:

$$\mathbf{J}_{\mathrm{p}} = -\frac{\sigma_{\mathrm{p}}^{\mathrm{eff}}}{F}\nabla\phi_{\mathrm{p}}, \tag{3.28}$$

where F is Faraday's constant and $\sigma_{\mathrm{p}}^{\mathrm{eff}}$ is the effective conductivity of membrane. Bruggeman's correction [126] is adopted to calculate the effective conductivity in this thesis and is written as follows:

$$\sigma_{\mathrm{p}}^{\mathrm{eff}} = \varepsilon_{\mathrm{m}}^{1.5}\sigma_{\mathrm{p}}. \tag{3.29}$$

Here, ε_{m} represents the fraction of the media occupied by membrane phase, and σ_{p} is the intrinsic protonic conductivity of membrane. The empirical value of membrane conductivity is adopted [129]:

$$\sigma_{\mathrm{p}} = (0.514\lambda - 0.326)\exp\left[1268\left(\frac{1}{303} - \frac{1}{T}\right)\right]. \tag{3.30}$$

Here, λ is water content of membrane, which represents the water concentration in membrane.

3.6 Transport of Dissolved Water

In membrane, dissolved water is transported by three mechanisms, *i.e.*, diffusion, electro-osmotic drag and pressure-driven permeation. They are represented by the first, second and third term on the right hand side of the following equation, respectively.

$$\mathbf{J}_{\mathrm{d}} = -D_{\mathrm{d}}\nabla c_{\mathrm{d}} + n_{\mathrm{d}}\mathbf{J}_{\mathrm{p}} - c_{\mathrm{l}}\frac{K_{\mathrm{l}}}{\mu_{\mathrm{l}}}\nabla p_{\mathrm{l}}, \tag{3.31}$$

where, in the first term, D_{d} is the diffusion coefficient of dissolved water, and its expression was suggested by by Motupally *et al.* [130]:

$$D_{\mathrm{d}} = \exp\left(-\frac{2436}{T}\right)\begin{cases} 3.1\times10^{-7}\lambda\left(e^{0.28\lambda}-1\right) & ,\lambda\in(0,3) \\ 4.17\times10^{-8}\lambda\left(161e^{-\lambda}+1\right) & ,\lambda\geq 3 \end{cases}. \tag{3.32}$$

Moreover, the dissolved water concentration, c_{d}, is given as the product of dry membrane concentration, c_{m}, and water content, λ. For the second term, n_{d} represents the electro-osmotic drag coefficient that is linearly dependent on the water content as suggested by Springer *et al.* [129], *i.e.*, $n_{\mathrm{d}} = 2.5\lambda/22$. The last term represents the pressure-driven permeation [131], and in this term, K_{l} is the relative permeability of dissolved water within the membrane.

The dissolved water mass exchange is formulated by the rate-limited model assuming that sorption/disorption happens when the membrane's hydration is not in equilibrium with the water activity at the cathode CL. Hence,

$$S_{\mathrm{d}} = k_{\mathrm{d}} c_{\mathrm{m}} \left(\lambda_{\mathrm{eq}} - \lambda\right). \tag{3.33}$$

The k_{d} denotes the water transfer rate coefficient of the membrane. Although the exact function of the equilibrium-state λ_{eq} is not known, it can be approximated as follow [132]:

$$\begin{aligned} \lambda_{\mathrm{eq}} &= \lambda_l s + \lambda_v \left(1 - s\right) \\ &= 22s + \left(0.3 + 10.8a_v - 16a_v^2 + 14.1a_v^3\right)\left(1 - s\right). \end{aligned} \tag{3.34}$$

The symbol a_v is the local water vapor activity given by the ratio of water vapor pressure to the saturation water vapor pressure.

The water release from desorption of membrane can be either in liquid water or water vapor but the exact mechanism is under investigation. Therefore, in this thesis, two approaches are used. One is assumed that desorption is a source of water vapor in CL; and the another is assumed that the ratio between the water release in the form of vapor and liquid depends on the liquid water saturation at the CL.

3.7 Conclusion

In this chapter, the mathematical models that describe the transports of gaseous reactant, liquid water, dissolved water and protons are discussed. Gaseous reactant transport is governed by diffusion. Liquid water transport is governed by capillary action that originates from the pressure difference between the liquid and gas phases of water. Dissolved water transport is governed by electro-osmotic drag, back-diffusion and pressure-driven permeation. Finally, proton transport is governed by the Ohm's law.

Chapter 4

Derivation of a Two-Phase GC Model

4.1 Introduction

Many one-dimensional PEM fuel cell models have been developed to address the water flooding issue, which contributed significantly to the understanding of two-phase water transport in cathode [34–40, 79, 92, 103, 105–109]. However, these models only focused on GDL and CL flooding but neglected GC flooding, in which case a zero saturation was typically taken as the boundary condition at GDL-GC interface [34, 35, 38–40, 92, 103, 106]. This formulation is based on the assumption that the vapor removal rate in GC is infinite hence water flooding in GC becomes negligible. Ziegler *et al.* [79] proposed to use the average liquid water saturation across GDL as the boundary value at GDL-GC interface but neglected the influences of two-phase flow in GC. Other authors, Pasaogullari *et al.* [36], Weber *et al.* [37, 107] and Wang *et al.* [105], introduced a

zero capillary pressure as the boundary condition which represents a more physical assumption. However, such an approach gives rise to a boundary condition that does not vary directly with the inlet conditions, but is only related to the properties of GDL.

GC water flooding and its influences on the fuel cell's performance have been recently reported by several authors through experimental studies [133–137]. Tüber *et al.* [133] constructed a PEM fuel cell with transparent cathode to obtain clear images of water formed inside the cathode GC, and the authors ascribed the performance drop of PEM fuel cell during operation to GC flooding. Yang *et al.* [134] conducted an experiment to observe the evolution of water in GC through a transparent PEM fuel cell. It was found that water first emerges from some preferential locations on GDL surface and grows until it touches GC wall where a water film is formed. This water flow is forced to exit GC by the shear stress of the inlet air flow. From the experimental data of Masuda *et al.* [136], an inverse relationship between the amount of liquid water inside GC and the output voltage of the fuel cell was observed. This indicates that the liquid water saturation at GDL-GC interface due to GC flooding will impede the water removal from MEA, thus causing water flooding and poor oxygen transport. This mass-transport loss is one of the major considerations due to two-phase flow in GC as discussed by Wang *et al.* [110]. Therefore, a more comprehensive fuel cell model that includes GC flooding is crucial to achieving a deeper understanding of the impact of the presence of liquid water on the fuel cell's performance.

In addition to experimental investigations, numerical investigations have been performed to study the effects of GC flooding [82, 89, 108, 109, 138, 139]. Meng *et al.* [89, 138], Ju [109], and Liu *et al.* [139] examined the influences of GDL-GC interface to the water distribution on the porous electrode. It was reported that the liquid water distribution in MEA is significantly affected by the chosen liquid water saturation value at GDL-GC interface. For instance, in [89], it was simulated that there is a 16% drop in PEM fuel cell's performance when the liquid water saturation at GDL-GC is increased from zero to 0.15. In addition to the steady-state performance, the liquid water accumulated at GDL-GC interface due to GC flooding also affects the transient response of PEM fuel cell. Meng [82] investigated the transient response of the fuel cell under a step change of voltage. It was shown that the magnitude of the corresponding over- and under-shoots of current density are increased by the liquid water accumulated at the GDL-GC interface. Song *et al.* [108] reported that the time constant of the dynamic liquid water transport in GDL depends on the liquid water saturation at the GDL-GC interface. However, the level of liquid water saturation at the GDL-GC interface imposed in these simulations was not related to the inlet operating conditions of fuel cell.

One-dimensional fuel cell models with more detailed treatments of GC flooding have been recently developed by Shah *et al.* [72, 80] and Gerteisen *et al.* [81]. Shah *et al.* suggested that the rate of change of liquid water saturation is directly proportional to the liquid water saturation at the GDL-GC interface based on the assumption that the

presence of more liquid water at the interface leads to a larger water removal rate. On the other hand, Gerteisen *et al.* [81] assumed that the flow rate of inlet air is linearly related to the water removal rate since the shear stress on liquid water increases as the velocity of inlet air flow increases. Moreover, the water removal rate was assumed to be a quadratic function of the effective liquid water saturation. Although Gerteisen's model is able to capture the influences of inlet air flow rate on the water distribution in MEA, the treatment is mainly qualitative due to the use of an artificial coefficient in describing the quadratic function. In addition, the effects of the relative humidity of inlet air, which has strong influences on the water distribution in MEA, was also neglected in these models.

In the present chapter, it is our aim to develop a more realistic PEM fuel cell model that includes the effects of two-phase flow in cathode GC to achieve a better understanding of the correlations between inlet conditions and fuel cell's performance. The model descriptions are given, and the formulation of the governing equations and the boundary conditions for GC are discussed. The proposed two-phase model is verified against some published experimental data and the simulation results from a computational fluid dynamics (CFD) model. In particular, the influences of inlet conditions on the fuel cell's performance and the liquid water distribution inside the fuel cell are discussed.

4.2 Two Phase Water Transport in Gas Channel

4.2.1 Background

Most of the reported models that consider two-phase flow in GC are based on the CFD approach for handling the non-linear terms in the momentum balance equation based on the volume-of-fluid method [95–97, 100, 101]. However, this approach is not suitable for developing models for use in control-oriented simulation of fuel cell system due to the high computational cost involved. Therefore, a simplified treatment of the momentum balance equation is necessary to provide a computationally efficient solution to the liquid water saturation.

Although numerous types of PEM fuel cell flow-field designs have been proposed and developed, the resulting GCs, in general, are straight channels with a width and depth ranging from 10^{-4} to 10^{-3} m as shown in Fig. 4.2.1 [110]. A structure of this dimension can be categorized as mini- or micro-channels with small hydraulic diameters, which is also a common design for micro-heat pipes for applications in thermal management of micro-components. The working fluid contained in the pipes is used for heating or cooling, evaporation or condensation takes place during the fluid transport and thus two-phase flow is commonly found in micro-heat pipes applications. Among the two-phase models developed in the literature for micro-heat pipes [140–148], one of the computationally efficient methods to approximate two-phase flow in micro- or

mini-channels is by the adoption of the Darcy's law, as is done in [141, 144–147], to analyze the heat transfer.

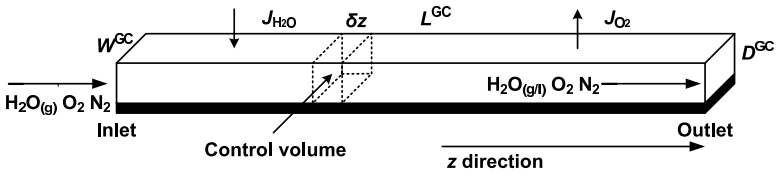

Figure 4.1: The schematic of structure of straight GC considered in two-phase GC model.

In this section, we approximate the momentum balance equation of the two-phase flow in GC by Darcy's law; the same approximation was also adopted by Wang *et al.* [110] and Basu *et al.* [28, 29] to correlate the pressure drop along GC to the liquid water saturation and to investigative the reactant's maldistribution in PEM fuel cell, respectively. The derivation of the model and the assumptions made are given in the following sections.

4.2.2 Darcy's Law Formulation

We begin by considering a single-phase gas flow along GC. This flow is well described by the Poiseuille flow since the Reynolds number is small as estimated by Eq. (4.1) under the typical conditions as shown in Table 4.1 and its entry length as estimated from Eq. (4.2) [149] is typically short compared to the length of GC.

$$Re \approx \frac{\rho_{\mathrm{g}} D_{\mathrm{h}} v_{\mathrm{g},0}}{\mu_{\mathrm{g}}} \sim 300 < 2000, \tag{4.1}$$

$$\text{Entry Distance} \approx \frac{ReD_{\mathrm{h}}}{30} \sim 1/100, \tag{4.2}$$

where D_{h} is the hydraulic diameter defined as four times the ratio between GC cross-section and perimeter. Moreover, supposing that the output current density of PEM fuel cell is $2\ \mathrm{A\ cm^{-2}}$ under the typical conditions, the average normal gas velocity at the GDL surface can be approximated as follows:

$$v_{\mathrm{normal}} = \frac{I}{4Fc_{\mathrm{g},0}\chi_{\mathrm{O_2},0}} = 5 \times 10^{-3}\ \mathrm{m\ s^{-1}}. \tag{4.3}$$

This velocity is much smaller compared to the inlet air velocity, that is $\sim 10\ \mathrm{m\ s^{-1}}$, under the same conditions, and hence it is reasonable to assume that the gas flow has a non-zero component along the channel only.

Table 4.1: Base-Case Operating Conditions.

Parameter	Symbol	Value(Unit)
Inlet operating temperature	T	80 °C (353 K)
Inlet air pressure	p_{air}	1.5 atm
Inlet hydrogen pressure	$p_{\mathrm{H_2}}$	1 atm
Cathode inlet relative humidity	Θ_{c}	100%
Anode inlet relative humidity	Θ_{a}	100%
Inlet air stoichiometry	ζ_{air}	2
Inlet hydrogen stoichiometry	$\zeta_{\mathrm{H_2}}$	1.2

Since it is assumed that there is only one non-zero velocity component in the Poiseuille flow along the channel, hence the momentum equation or the Navier-Stokes equation, reduces to an equation of creeping motion [150], which gives a good correlation be-

tween the average velocity and the pressure drop of the flow:

$$v = -\frac{2D_{\mathrm{h}}^2}{a\mu}\frac{dp}{dz}. \tag{4.4}$$

Here, z denotes the direction along GC, and the constant a depends on the shape of GC (≈ 56 for square GC [151]).

We further define the permeability k as $2D_{\mathrm{h}}^2/a$, and rewrite the average velocity in the form of Darcy's law. This is analogous to the derivation of Carman equation for permeability of porous medium [125].

Finally, Darcy's law is extended to two-phase flow in GC in resemblance to the extension of Darcy's law from a single-phase to two-phase consideration when modeling fluid transport in porous media. Thus, the momentum equations for two-phase flow in GC along GC direction are obtained as follows:

$$\begin{aligned} v_{\mathrm{g}} &= -\frac{k_{\mathrm{g}}}{\mu_{\mathrm{g}}}\frac{dp_{\mathrm{g}}}{dz}, \\ v_{\mathrm{l}} &= -\frac{k_{\mathrm{l}}}{\mu_{\mathrm{l}}}\frac{dp_{\mathrm{l}}}{dz}. \end{aligned} \tag{4.5}$$

In Eq. (4.5), the effective permeability of a given phase k_α increases with the saturation of its own phase, and equals the absolute permeability k when the saturation is

unity. Specifically, k_g and k_l are expressed as:

$$k_{\mathrm{g}} = kk_{\mathrm{rg}} = k\left(1-s\right)^{n},$$
$$k_{\mathrm{l}} = kk_{\mathrm{rl}} = ks^{n}. \tag{4.6}$$

The function $k_{\mathrm{r}\alpha}$ is known as the relative permeability and is typically a power function of the saturation. In this chapter, the exponent n is taken as five after the experimental validation by Wang *et al.* [110].

The two phases interact with each other and give rise to a pressure difference known as capillary pressure, which is expressed by the Young-Laplace equation [125] as a function of the surface tension τ and radius of curvature r:

$$p_{\mathrm{c}} = p_{\mathrm{g}} - p_{\mathrm{l}} = -\frac{\tau}{r}. \tag{4.7}$$

The liquid phase within GC forms a film or a droplet on GDL-GC interface and hence the radius of curvature can be determined as a function of the liquid water saturation by a simple geometry that is also adopted from the modeling works on the micro-heat pipes [140, 142–145, 147, 148]. The geometry of the liquid phase is assumed to be a circular segment as shown in Fig 4.2.

As the liquid water saturation increases in GC, the radius of curvature of the liquid water decreases gradually until it reaches its minimum that is the half of the width

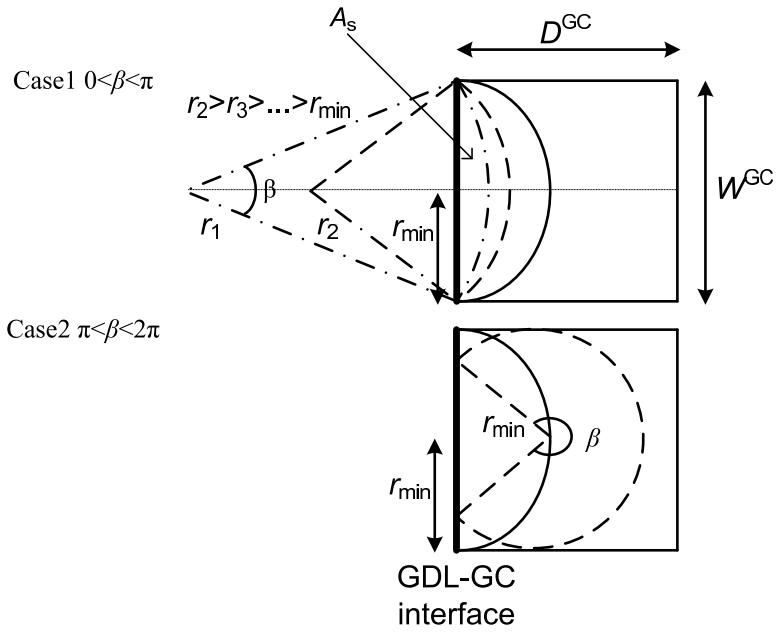

Figure 4.2: The schematic of the geometry of liquid water on the GDL-GC interface.

of GC as illustrating in Fig. 4.2. Due to the simplicity of the proposed geometry of segment, the relation between the radius of curvature and the liquid water saturation can be determined by introducing an angel β which is shown in Fig. 4.2. In Case 1, *i.e.*, β is larger than zero but smaller than π, the radius of curvature is a function of β and is expressed as follows:

$$r = \frac{W^{\mathrm{GC}}}{2\sin(\beta/2)}. \tag{4.8}$$

By considering the area of the cross-section of the liquid phase, another relation is

obtained:

$$A_{\mathrm{s}} = sW^{\mathrm{GC}}D^{\mathrm{GC}} = \frac{r^2\left(\beta - \sin\beta\right)}{2}, \tag{4.9}$$

hence the radius of curvature can be calculated by Eqs. (4.8) and (4.9). If the liquid water saturation keeps increasing such that the angel β is larger than π, the given relation reduces to the following equation:

$$r = r_{\min} = \frac{W^{\mathrm{GC}}}{2}. \tag{4.10}$$

The radius of curvature attains its minimum, while the corresponding capillary pressure attains its maximum at this case.

4.2.3 Governing Equations

The integral formulation of the conservation of species for considering a control volume along GC states that:

$$\begin{aligned}
\frac{\partial}{\partial t}\left(\varepsilon_\alpha c_\alpha \chi_{\alpha,i}\right) &= \left[\left(c_\alpha \chi_{\alpha,i} v_\alpha\right)_z - \left(c_\alpha \chi_{\alpha,i} v_\alpha\right)_{z+\delta z}\right] \frac{W^{\mathrm{GC}} D^{\mathrm{GC}}}{W^{\mathrm{GC}} D^{\mathrm{GC}} \delta z} + \frac{J_{\alpha,i}|_{\mathrm{GDL-GC}} W^{\mathrm{GC}} \delta z}{W^{\mathrm{GC}} D^{\mathrm{GC}} \delta z} \\
&= -\frac{d}{dz}\left(c_\alpha \chi_{\alpha,i} v_\alpha\right) + \frac{1}{D^{\mathrm{GC}}} J_{\alpha,i}|_{\mathrm{GDL-GC}} \\
&\equiv -\frac{d}{dz}\left(c_\alpha \chi_{\alpha,i} v_\alpha\right) + S_{\alpha,i},
\end{aligned} \tag{4.11}$$

where $c_\alpha \chi_{\alpha,i}$ is the concentration of species i in phase α. The void fraction ε_α is the saturation of α-phase in GC. The molar flux $J_{\alpha,i}|_{\mathrm{GDL-GC}}$ represents the species exchange at GDL-GC interface, and $S_{\alpha,i}$ is the source term.

Although anode GC flooding has been reported for some fuel cell designs that include MPLs in GDL [152], a single-phase formulation is assumed valid in the this thesis since MPL is absent from the fuel cell structure considered. The influences of the more important cathode GC flooding are the emphasis of the present model.

As water emerges into cathode GC, it can exist in the form of liquid water or vapor, depending on the local water vapor pressure in GC. Here, local thermodynamics equilibrium between vapor and liquid water is assumed. When the local water vapor pressure exceeds the saturation vapor pressure, the water emerged in GC is in the form of liquid. Otherwise, the water emerged in GC is assumed to be in form of vapor. The source terms are written as follows by introducing the Heaviside step function Γ for switching between liquid water and vapor formation:

$$\begin{aligned} S_{\mathrm{l,l}}(\text{simply denote as } S_{\mathrm{l}}) &= \frac{J_{\mathrm{H_2O}}|_{\mathrm{GDL-GC}}}{D^{\mathrm{GC}}} \Gamma \left(c_{\mathrm{v}} - c_{\mathrm{v}}^{\mathrm{sat}} \right), \\ S_{\mathrm{g,v}}(\text{simply denote as } S_{\mathrm{v}}) &= \frac{J_{\mathrm{H_2O}}|_{\mathrm{GDL-GC}}}{D^{\mathrm{GC}}} \Gamma \left(c_{\mathrm{v}}^{\mathrm{sat}} - c_{\mathrm{v}} \right), \end{aligned} \tag{4.12}$$

where $c_{\mathrm{v}}^{\mathrm{sat}}$ is calculated from the ideal gas law as p^{sat}/RT.

For a partially humidified inlet operating condition, two-phase condition does not

exist over the entire cathode GC, especially near the inlet. By assuming a net water source in GC, there is a position known as the phase transition position z^{sat} [110], where the saturation water vapor pressure is attained and liquid water begins to form. Therefore, the Heaviside step function in Eq. (4.12) can be rewritten as:

$$\Gamma\left(c_{\mathrm{v}}^{\mathrm{sat}} - c_{\mathrm{v}}\right) = \Gamma\left(z - z^{\mathrm{sat}}\right). \tag{4.13}$$

Other species such as oxygen and nitrogen in cathode, and hydrogen in anode exist only in gas phase and do not affect the water formation in GC, hence the source terms of these species are written as follows:

$$S_{\mathrm{g},i}(\text{simply denote as } S_i) = \frac{J_{\mathrm{g},i}\big|_{\mathrm{GDL-GC}}}{D^{\mathrm{GC}}}. \tag{4.14}$$

At steady state, the set of governing equations describing cathode GC is given by (summarizing the Eqs. (4.11)–(4.14)):

$$\frac{dJ_{\mathrm{g}}}{dz} = S_{\mathrm{O_2}} + S_{\mathrm{v}}, \tag{4.15}$$

$$\frac{dJ_{\mathrm{l}}}{dz} = S_{\mathrm{l}}, \tag{4.16}$$

$$\frac{d}{dz}\left(J_{\mathrm{g}}\chi_{\mathrm{v}}\right) = S_{\mathrm{v}}, \tag{4.17}$$

$$\frac{d}{dz}\left(J_{\mathrm{g}}\chi_{\mathrm{O_2}}\right) = S_{\mathrm{O_2}}, \tag{4.18}$$

where J_α equals $c_\alpha v_\alpha$. The same governing equations are used for anode except that only water vapor is considered in the formulation.

4.3 Analytical Solution for Steady State

4.3.1 Single-Phase Region

For the single-phase region, the solution of the conservation equation of water vapor, *i.e.*, Eq. (4.17), can be obtained via integration, hence we have:

$$c_{\mathrm{g}}\chi_{\mathrm{v}} = \frac{1}{v_{\mathrm{g}}}\left[\int_0^{\mathrm{z}} d\left(c_{\mathrm{g}}\chi_{\mathrm{v}}v_{\mathrm{g}}\right) + c_{\mathrm{g},0}\chi_{\mathrm{v},0}v_{\mathrm{g},0}\right] = \frac{S_{\mathrm{v}}z}{v_{\mathrm{g}}} + \frac{c_{\mathrm{g},0}\chi_{\mathrm{v},0}v_{\mathrm{g},0}}{v_{\mathrm{g}}}. \tag{4.19}$$

Here $c_{\mathrm{g},0}$, $\chi_{\mathrm{v},0}$ and $v_{\mathrm{g},0}$, respectively, represents the total gas concentration, mole fraction of water vapor, and air velocity at the inlet of GC (*i.e.*, at $z = 0$).

The inlet air velocity is calculated in terms of the air stoichiometry, ζ_{air}, the inlet oxygen concentration, $c_{\mathrm{g},0}\chi_{\mathrm{O_2},0}$, the oxygen source in GC, $S_{\mathrm{O_2}}$, and the length of GC, L^{GC}:

$$v_{\mathrm{g},0} \;=\; \frac{\zeta_{\mathrm{air}}S_{\mathrm{O_2}}L^{\mathrm{GC}}}{c_{\mathrm{g},0}\chi_{\mathrm{O_2},0}}. \tag{4.20}$$

Additionally, the air velocity gradient in single-phase flow is small along GC due to the high content of nitrogen in air. Thus, the air velocity in the single-phase region

$[0, z^{\mathrm{sat}}]$ closely approximates to the inlet air velocity $v_{\mathrm{g},0}$. The conservation equation of water vapor can be rewritten as follow:

$$c_{\mathrm{g}}\chi_{\mathrm{v}} = c_{\mathrm{g},0}\chi_{\mathrm{v},0} + \frac{S_{\mathrm{v}}z}{v_{\mathrm{g},0}} \text{ when } z \leq z^{\mathrm{sat}}. \tag{4.21}$$

The phase transition position is calculated by substituting the saturated water vapor concentration in the left hand side of Eq. (4.21):

$$z^{\mathrm{sat}} = \frac{\left(c_{\mathrm{v}}^{\mathrm{sat}} - c_{\mathrm{g},0}\chi_{\mathrm{v},0}\right) v_{\mathrm{g},0}}{S_{\mathrm{v}}}. \tag{4.22}$$

The oxygen concentration along GC is calculated via a similar treatment to the water vapor concentration, *i.e.*,

$$c_{\mathrm{O}_2} = c_{\mathrm{g},0}\chi_{\mathrm{O}_2,0} + \frac{S_{\mathrm{O}_2}z}{v_{\mathrm{g},0}}. \tag{4.23}$$

4.3.2 Two-Phase Region

In the two-phase region, the vapor flux $J_{\mathrm{g}}\chi_v$ and liquid water flux J_{l} are described by the following equations derived from Eqs. (4.16) and (4.17):

$$J_{\mathrm{g}}\chi_v = c_{\mathrm{v}}^{\mathrm{sat}} v_{\mathrm{g},z^{\mathrm{sat}}} \approx c_{\mathrm{v}}^{\mathrm{sat}} v_{\mathrm{g},0}, \tag{4.24}$$

$$J_{\mathrm{l}} = S_{\mathrm{l}} \left(z - z^{\mathrm{sat}} \right). \tag{4.25}$$

Applying the definition of capillary pressure, $p_{\mathrm{c}} = p_{\mathrm{g}} - p_{\mathrm{l}}$, $J_{\mathrm{g}}\chi_v$ can be rewritten in terms of J_{l} and dp_{c}/dz:

$$J_{\mathrm{g}}\chi_v = \frac{c_{\mathrm{v}}^{\mathrm{sat}} k_{\mathrm{g}} \mu_{\mathrm{l}}}{c_{\mathrm{l}} k_{\mathrm{l}} \mu_{\mathrm{g}}} J_{\mathrm{l}} - \frac{c_{\mathrm{v}}^{\mathrm{sat}} k_{\mathrm{g}}}{\mu_{\mathrm{g}}} \frac{dp_{\mathrm{c}}}{dz}. \tag{4.26}$$

By substituting Eqs. (4.24) and (4.25) into Eq. (4.26), an ordinary differential equation of the liquid water saturation is obtained. Although a numerical solution can be obtained given a known capillary function, an approximate analytical formula is desired. Since the viscous force is dominant over the capillary force, which is valid as indicated by the large capillary number, $Ca = v_\alpha \mu_\alpha / \tau$ (compared to the critical value 10^{-4} from [153]), it is possible to find an analytical solution to Eq. (4.26) by neglecting

the capillary pressure gradient along GC. Hence, Eq. (4.26) is reduced to Eq. (4.27):

$$c_{\mathrm{v}}^{\mathrm{sat}} v_{\mathrm{g},0} = \frac{c_{\mathrm{v}}^{\mathrm{sat}} k_{\mathrm{g}} \mu_{\mathrm{l}}}{c_{\mathrm{l}} k_{\mathrm{l}} \mu_{\mathrm{g}}} S_{\mathrm{l}} \left(z - z^{\mathrm{sat}} \right). \tag{4.27}$$

Recalling that $k_{\mathrm{rl}} = s^n$ and $k_{\mathrm{rg}} = (1-s)^n$, then an expression for the liquid water saturation is obtained by rearranging Eq. (4.27):

$$s = \left\{ 1 + \left[\frac{\mu_{\mathrm{g}} c_{\mathrm{l}} v_{\mathrm{g},0}}{\mu_{\mathrm{l}} S_{\mathrm{l}} \left(z - z^{\mathrm{sat}} \right)} \right]^{1/n} \right\}^{-1}. \tag{4.28}$$

The oxygen and water vapor concentration along GC are the objects of the interest. In the two-phase region, the water vapor is saturated, hence $c_{\mathrm{v}} = c_{\mathrm{v}}^{\mathrm{sat}}$. The oxygen concentration is determined from the conservation equations:

$$c_{\mathrm{O_2}} = c_{\mathrm{g},0} \chi_{\mathrm{O_2},0} + \frac{S_{\mathrm{O_2}} z}{v_{\mathrm{g},0}}. \tag{4.29}$$

4.4 Numerical Treatment of GDL-GC Interface

Many two-phase PEM fuel cell models imposed a continuous liquid water saturation across different domains, for instance at GDL-CL [71, 72, 80, 103], GDL-MPL [80] and GDL-GC [71] interfaces; however, imposing a continuous liquid water saturation at the interfaces as a boundary condition is still questionable.

Liquid water transport in porous medium is mainly governing by the capillary action for convenient PEM fuel cell [35]. As a result, the capillary pressure across the interface of different layers should be continuous, and a continuous capillary pressure have been imposed at GDL-MPL and GDL-CL interfaces as a boundary condition [35–40, 81, 104, 105, 139, 154]. This assumption always lead a discontinuous liquid water saturation at the interfaces because the capillary properties of different porous medium are not the same, and the liquid water saturation jump have been showed in the literature.

Liquid water saturation accumulated in GC builds up a capillary pressure at GDL-GC interface, which depends on the capillary property of GC and resists the liquid water removal from GDL to GC. When the capillary pressure in GC is larger than that in GDL, the liquid water in GC is absorbed in the void pores in GDL, which is known as imbibition, and increases the liquid water saturation in GDL and also the entire MEA. This is another important mechanism that contributes to the liquid water accumulation in GDL and CL besides the influence of capillary transport due to capillary pressure gradient [138]. This leads to a high diffusion resistance to oxygen since its diffusive path is blocked and becomes more tortuous, and results in a large concentration gradient of oxygen across GDL and CL in order to provide a sufficient oxygen flux for electrochemical reactions.

In order to capture the above phenomena, it is important to determine the capillary pressure of GC. As a result, a submodel that is adopted to determine the capillary

pressure in GC from the simulated liquid water saturation is presented in the previous section. In this section, it is assumed to use the z-averaged value of capillary pressure of GC as a boundary condition for determining the liquid water saturation jump across GDL-GC interface. *i.e.*,

$$p_{\mathrm{c}}|_{\mathrm{GDL-GC}} = \left\langle -\frac{\tau\Gamma\left(z - z^{\mathrm{sat}}\right)}{r} \right\rangle_z , \tag{4.30}$$

where the operator $\langle\rangle_z$ denotes as $\left(\int_0^{L^{\mathrm{GC}}} dz\right)/L^{\mathrm{GC}}$.

In addition to the boundary condition for liquid water transport, other proper boundary conditions at cathode GDL-GC interface, are also necessary to determine the vapor and oxygen concentration at the interface. In this work, the z-averaged value are calculated from the two-phase cathode GC model and are mathematically written as:

$$c_{\mathrm{v}}|_{\mathrm{GDL-GC}} = \left\langle \Gamma\left(z^{\mathrm{sat}} - z\right)\left(c_{\mathrm{v},0}\chi_{\mathrm{v},0} + \frac{S_{\mathrm{v}}z}{v_{\mathrm{g},0}}\right) + \Gamma\left(z - z^{\mathrm{sat}}\right)c_{\mathrm{v}}^{\mathrm{sat}} \right\rangle_z , \tag{4.31}$$

$$c_{\mathrm{O_2}}|_{\mathrm{GDL-GC}} = \left\langle c_{\mathrm{g},0}\chi_{\mathrm{O_2},0} + \frac{S_{\mathrm{O_2}}z}{v_{\mathrm{g},0}} \right\rangle_z . \tag{4.32}$$

On the other hand, a single-phase formulation is adopted for anode GC, hence the boundary condition for liquid water transport is absent in anode GC, and the necessary

boundary conditions are

$$c_i|_{\mathrm{GDL-GC}} = \left\langle c_{\mathrm{g},0}\chi_{i,0} + \frac{S_i z}{v_{\mathrm{g},0}} \right\rangle_z , \tag{4.33}$$

where i denotes hydrogen or water vapor in anode GC.

4.5 Results and Discussion

4.5.1 Model Descriptions

In this section, the proposed GC model is integrated to MEA model based on the presentation given in Chapter 3 to form an improved one-dimensional (*i.e.*, pseudo-two-dimensional), two-phase PEM fuel cell for studying the influences of inlet operating conditions on GC flooding and its effects on the fuel cell's performance.

We focus on a typical PEM fuel cell consisting of an anode, a cathode and a PEM, which is a multi-layer structure as shown in Fig. 4.3. Besides the CLs, all other layers such as GDLs and GCs are considered to be identical in materials, dimensions and structures for both cathode and anode sides. Moreover, the structural parameters of these layers are given in Table 4.2.

The emphasis of the numerical study in this chapter is cathode concentration overpotential due to the water flooding in cathode, especially in cathode GC. To capture the influences of cathode concentration overpotential due to water flooding, two-phase

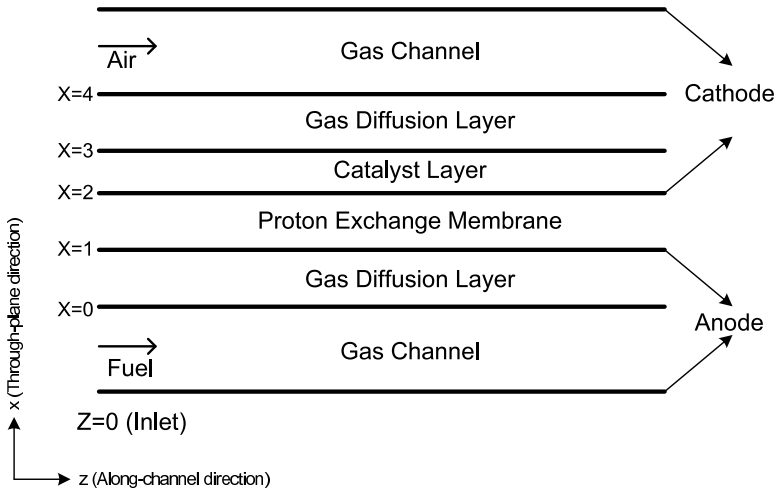

Figure 4.3: The schematic of the computation's domain of PEM fuel cell model. Through-plane and along-channel directions are denoted as x- and z-axes, respectively.

flow is considered in the entire cathode region including GC. In particular, a two-phase cathode GC submodel is adopted to determine the liquid water distribution and capillary pressure in GC that are significantly affected by the inlet operating conditions. The liquid water transport in cathode GDL is also considered such that the influences of the liquid water saturation at GDL-GC interface on the liquid water distribution in cathode GDL are captured. Finally, a detailed cathode CL model based on thin film-agglomerate approach is included due to the importance of cathode activation overpotential caused by the slow kinetics of the oxygen reduction reaction.

On the other hand, the influences of liquid water on anode side are neglected to simplify the analysis because the liquid water concentration and concentration overpotential at anode side are much lower compared to cathode side. Moreover, anode CL is modeled as an interface that the thin film-agglomerate approach is not adopted since the model

Table 4.2: Structural Parameters for MEA and GC in the Simulation.

Parameter	Value
Gas Channel	
Length, $L^{\mathrm{GC}}\,(\mathrm{m})$	0.5
Width, $W^{\mathrm{GC}}\,(\mathrm{mm})$	0.5
Depth, $D^{\mathrm{GC}}\,(\mathrm{mm})$	0.5
Gas Diffusion Layer	
Absolute permeability, $k^{\mathrm{GDL}}\,(\mathrm{m}^2)$ [72, 80]	8.7×10^{-12}
Porosity, $\varepsilon^{\mathrm{GDL}}$	0.55
Contact angle, $\theta^{\mathrm{GDL}}\,(^{\mathrm{o}})$	95
Thickness, $l^{\mathrm{GDL}}\,(\mu\mathrm{m})$	250
Catalyst Layer	
Absolute permeability, $k^{\mathrm{CL}}\,(\mathrm{m}^2)$ [72, 80]	10^{-13}
Porosity, $\varepsilon^{\mathrm{CL}}$	0.2
Contact angle, $\theta^{\mathrm{CL}}\,(^{\mathrm{o}})$	90.5
Thickness, $l^{\mathrm{CL}}\,(\mu\mathrm{m})$	15
Fraction of electrolyte, $\varepsilon_{\mathrm{m}}^{\mathrm{CL}}$	0.3
Critical pore radius, $r_{\mathrm{crit}}\,(\mathrm{nm})$	25
Specific surface area of catalyst Pt, $a^{\mathrm{pt}}\,(\mathrm{m}^2\,\mathrm{kg}^{-1})$ [121]	10^5
Catalyst Pt loading, $m^{\mathrm{pt}}\,(\mathrm{kg\,m}^{-2})$ [103]	0.004
Reference oxygen concentration, $c_{\mathrm{O_2,ref}}\,(\mathrm{mol\,m}^{-3})$	$101325 H_{\mathrm{m,O_2}}^{-1}$
Reference exchange current density of oxygen reduction, $i_{\mathrm{ref,O_2}}\,(\mathrm{A\,m}^{-2})$ [79]	10^{-3}
Proton Exchange Membrane	
Thickness, $l^{\mathrm{m}}\,(\mu\mathrm{m})$	50
Dry membrane concentration, $c_{\mathrm{m}}\,(\mathrm{mol\,m}^{-3})$ [138]	1800
Agglomerate	
Outer surface area of the agglomerates, $a^{\mathrm{agg}}\,(\mathrm{m}^{-1})$	9×10^5
Thickness of membrane covering, $d_{\mathrm{m}}\,(\mathrm{nm})$	20
Radius of the agglomerate, $r^{\mathrm{agg}}\,(\mathrm{nm})$ [155]	200
Fraction of PEM electrolyte in agglomerate, $\varepsilon_{\mathrm{m}}^{\mathrm{agg}}$	0.4

is mainly used to capture the flooding phenomena and its effects on the concentration overpotential.

A summary of the governing equations used in this simulation is listed in Table 4.3, and the boundary conditions that give the constrict the solution of the governing equations is listed in Table 4.4.

Table 4.3: Governing Equations of the Improved PEM Fuel Cell Model.

Variables	AGDL	Membrane	CCL	CGDL
$c_{\mathrm{O_2}}$	-	-	$\nabla \cdot \mathbf{J}_{\mathrm{O_2}} = -S_{\mathrm{O_2}}$	$\nabla \cdot \mathbf{J}_{\mathrm{O_2}} = 0$
$c_{\mathrm{H_2}}$	$\nabla \cdot \mathbf{J}_{\mathrm{H_2}} = 0$	-	-	-
c_{v}	$\nabla \cdot \mathbf{J}_{\mathrm{v}} = 0$	-	$\nabla \cdot \mathbf{J}_{\mathrm{v}} = -S_{\mathrm{vl}} - S_{\mathrm{d}}$	$\nabla \cdot \mathbf{J}_{\mathrm{v}} = -S_{\mathrm{vl}}$
ϕ_{p}	-	$\nabla \cdot \mathbf{J}_{\mathrm{p}} = 0$	$\nabla \cdot \mathbf{J}_{\mathrm{p}} = -4S_{\mathrm{O_2}}$	-
s	-	-	$\nabla \cdot \mathbf{J}_{\mathrm{l}} = 2S_{\mathrm{O_2}} + S_{\mathrm{vl}}$	$\nabla \cdot \mathbf{J}_{\mathrm{l}} = S_{\mathrm{vl}}$
c_{d}	-	$\nabla \cdot \mathbf{J}_{\mathrm{d}} = 0$	$\nabla \cdot \mathbf{J}_{\mathrm{d}} = S_{\mathrm{d}}$	-

4.5.2 Verification of Two-Phase Model

The two-phase GC model is developed to study the influences of water flooding in GC on the fuel cell's performance. For this purpose, a single-phase GC model is also developed for comparison. Both the single-phase and two-phase models share a similar set of governing equations and boundary conditions, but the single-phase model ignores the water flooding in GC by imposing a zero saturation condition at GDL-GC interface. The simulation results from the single-phase and two-phase GC models are compared with the numerical results obtained from a CFD model [138] and the experimental data from [156] to demonstrate the significance of water flooding in GC on the predicted fuel cell's performance.

Fig. 4.4 shows a comparison between the predicted polarization curves under single-phase and two-phase GC conditions by using the present model and the model devel-

Table 4.4: Boundary Conditions of the Improved PEM Fuel Cell Model.

Variables	AGC-AGDL	GDL-MEM	MEM-CCL	CCL-CGDL	CGDL-CGC
c_{O_2}	-	-	-	continuous	Eq. (4.32)
$\mathbf{J}_{\mathrm{O}_2}$	-	-	0	continuous	-
c_{H_2}	Eq. (4.33)	-	-	-	-
$\mathbf{J}_{\mathrm{H}_2}$	-	$\mathbf{J}_{\mathrm{H}_2} = 0$	-	-	-
c_{v}	Eq. (4.33)	-	-	continuous	Eq. (4.31)
$\mathbf{J}_v$	-	$\mathbf{J}_{\mathrm{O}_2} = 0$	$\mathbf{J}_{\mathrm{O}_2} = 0$	continuous	-
ϕ_{p}	-	$\phi_{\mathrm{p}} = 0$	continuous	continuous	-
$\mathbf{J}_{\mathrm{p}}$	-	-	continuous	$\mathbf{J}_{\mathrm{p}} = 0$	-
s	-	-	-	$p_c^- = p_c^+$	Eq. (4.30)
$\mathbf{J}_{\mathrm{l}}$	-	-	$\mathbf{J}_{\mathrm{l}} = 0$	continuous	-
c_{d}	-	continuous	continuous	continuous	-
$\mathbf{J}_{\mathrm{d}}$	-	$\lambda = \lambda_{\mathrm{eq}} - J_{\mathrm{d}} l^{\mathrm{CL}} / c_{\mathrm{m}} D_{\mathrm{d}} \varepsilon_{\mathrm{m}}^{1.5}$	continuous	continuous	$\mathbf{J}_{\mathrm{d}} = 0$

oped by Meng *et al.* [138] for the same set of operating conditions. For both GC conditions, the simulated results from the present model agree qualitatively and quantitatively with those from the three-dimensional model developed by Meng *et al.*. Both our model and the model of Meng *et al.*'s predicted that the limiting current density is significantly lower when water flooding exists in GC. A difference of 21% and 20% was predicted by our model and the model of Meng *et al.*'s, respectively, indicating the importance of a more accurate treatment of two-phase water transport in GC on the overall fuel cell's performance.

The predicted polarization curves under various inlet humidification levels were calculated by the present model using the single-phase and two-phase GC assumptions and compared to the experimental data from Yan *et al.* [156], and the results are shown in Fig. 4.5. The predicted trends match favorably with the experimental data that the cell performance at high current density is strongly related to the humidification level of the inlet air.

The locations of the crossovers between the polarization curves for the 100-70% and 70-50% pairs, and the differences in the polarization curves between the 100% and 70% case at high current density reflect more closely the experimentally observed trends when a two-phase GC model was used in the calculations. There is nearly no difference in the polarization curve between 100% and 70% case when a single-phase GC model was considered, indicating that the fuel cell's performance is less sensitive to

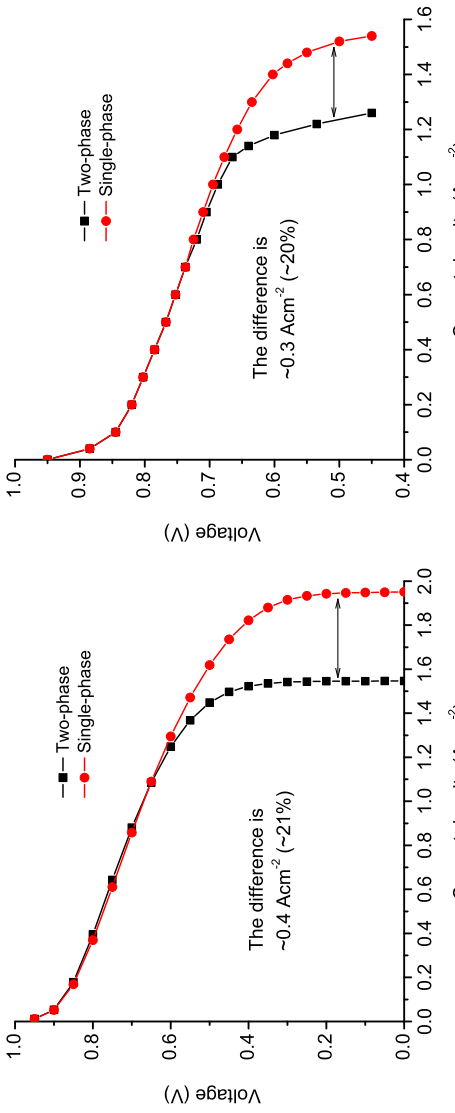

(b) Meng *et al.*'s model.

(a) The present model.

Figure 4.4: Comparisons of polarization curves under single-phase and two-phase GC conditions between the present model and Meng *et al.*'s model. The polarization curves in Fig. (a) are calculated under the same set of operating conditions used in Meng *et al.*'s model.

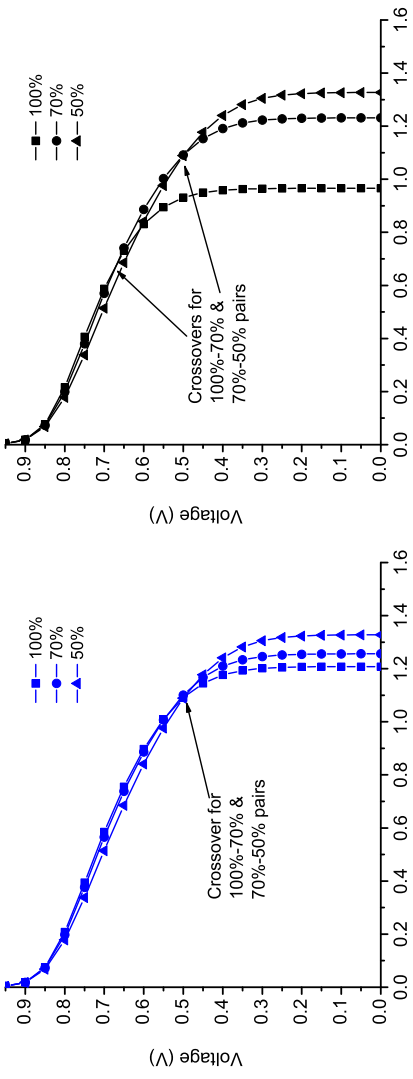

(a) Predicted trends with single-phase GC.

(b) Predicted trends with two-phase GC.

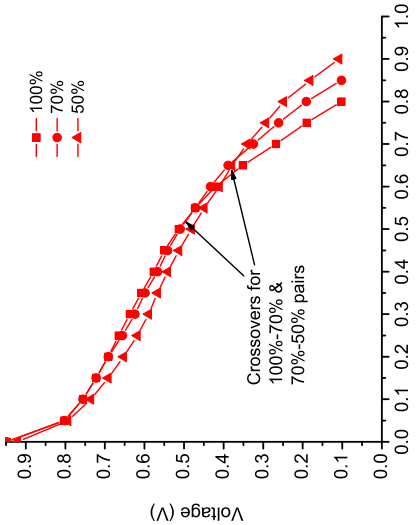

(c) Experimental data from Yan *et al.* [156].

Figure 4.5: Comparisons of polarization curves predicted under various inlet humidification levels of inlet air by the present model with single-phase/two-phase GC to the experimental data from Yan *et al.*. The polarization curves in Figs. (a) and (b) are calculated under the same set of operating conditions used in Yan *et al.*'s experiments.

the inlet humidification level, which contradicts the observations by experiments. The influences of the inlet humidification level as observed in the experiment and predicted by the two-phase GC model are close, however the abrupt fall in cell voltage due to excessive concentration loss at very high current density is less obvious in the experimental polarization curves possibly due to the higher ohmic voltage loss that could arise from the thicker membrane used in the experimental cell. The high ohmic voltage loss consequently screens the voltage drop contributed by the water flooding at the high current density.

4.5.3 Comparisons between Two-Phase and Single-Phase Gas Channel Model

In this section, we discuss the differences between the predicted polarization curves by using the two-phase and single-phase GC model under various inlet conditions. The base-case conditions used in these simulations are given in Table 4.1, which are the typical values used in the practical operations of PEM fuel cell. For each comparison, we focus on one type of inlet condition and analyze its influences while other conditions are kept unchanged.

Liquid Water Saturation

Here we introduce an average liquid water saturation, *i.e.*,

$$\langle s \rangle_x = \left(\int_0^l s dx \right) / l, \tag{4.34}$$

to represent the degree of water flooding in GDL and CL.

The influences of inlet air pressure and flow rate on the liquid water saturation in various regions are illustrated in Figs. 4.6 and 4.7. In these plots, the single-phase GC model predicted no difference in the liquid water saturation at GDL or CL under all inlet air pressures and flow rates. In contrary, inlet air pressure and flow rate have strong influences on the saturation level inside MEA when the two-phase GC model was considered. A higher inlet air pressure gives rise to a higher saturation level as shown in Fig. 4.6. Since a lower air velocity is required as the inlet air pressure increases under the same air stoichiometry, according to Eq. (4.20), this leads to a higher saturation level at GC as can be seen in Fig. 4.6(a). The inlet air flow rate, on the other hand, has an opposite effect. As the flow rate increases from 1 to 5 stoichiometry, the saturation level at GC decreases because the air velocity in GC increases, and is capable of removing water more effectively from the fuel cell.

According to Eqs. (4.20) and (4.30), a high air flow rate or low air pressure gives rise to a large air velocity, and leads to a low saturation level at GC. Thus, the single-phase GC model gives accurate predictions on the water distribution only when the inlet air flow is sufficiently large or the inlet air pressure is sufficiently small, thus acting as a good approximation to the more general two-phase GC model.

One feature of the two-phase GC model is to offer a close correlation between the fuel cell operation to the humidification level of the inlet air. A higher humidification

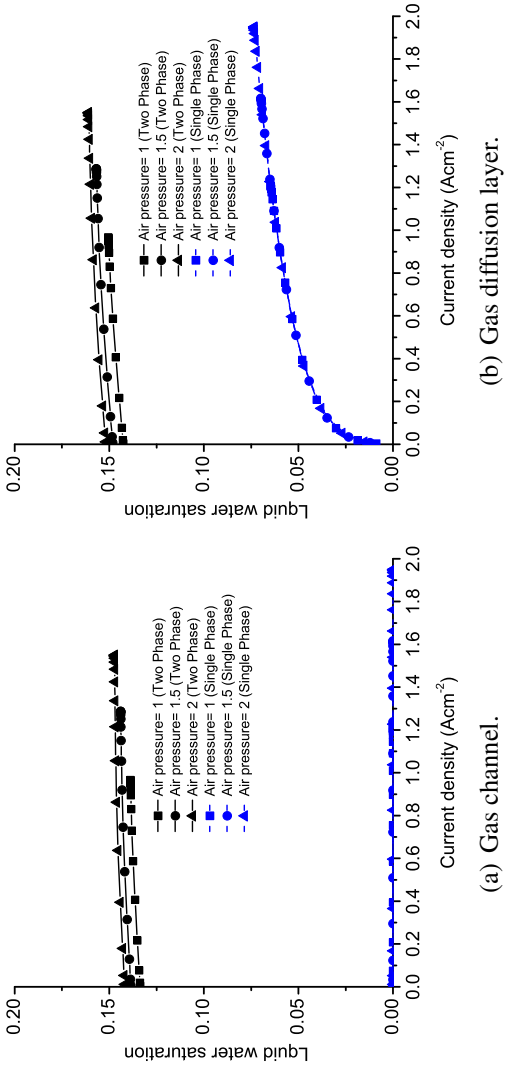

(a) Gas channel.

(b) Gas diffusion layer.

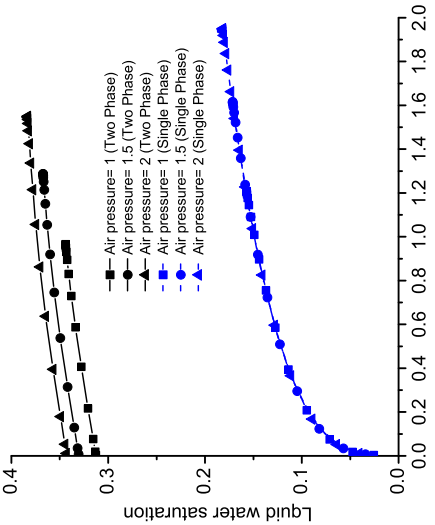

(c) Catalyst layer.

Figure 4.6: Predicted liquid water saturation under various inlet air pressures. The base-case conditions used in these simulations are given in Table 4.1.

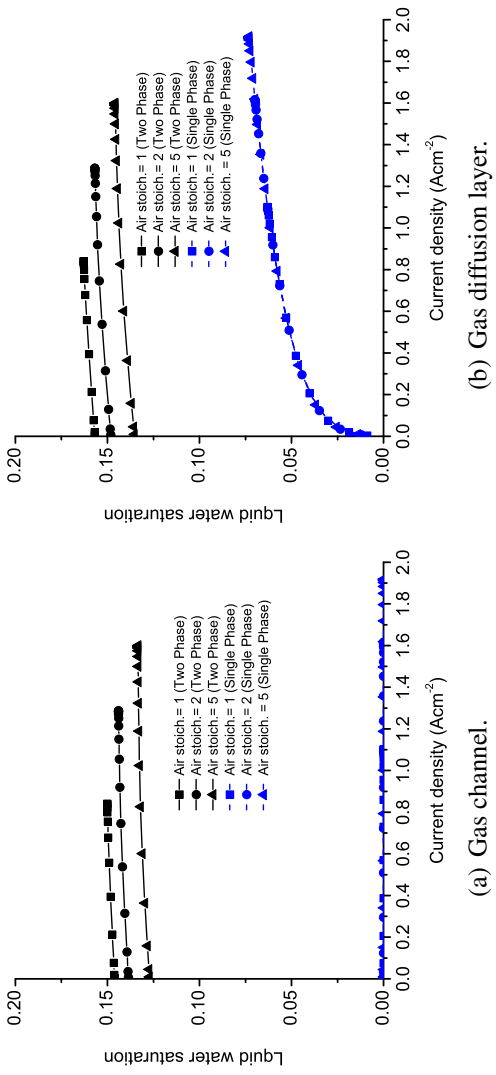

(a) Gas channel.

(b) Gas diffusion layer.

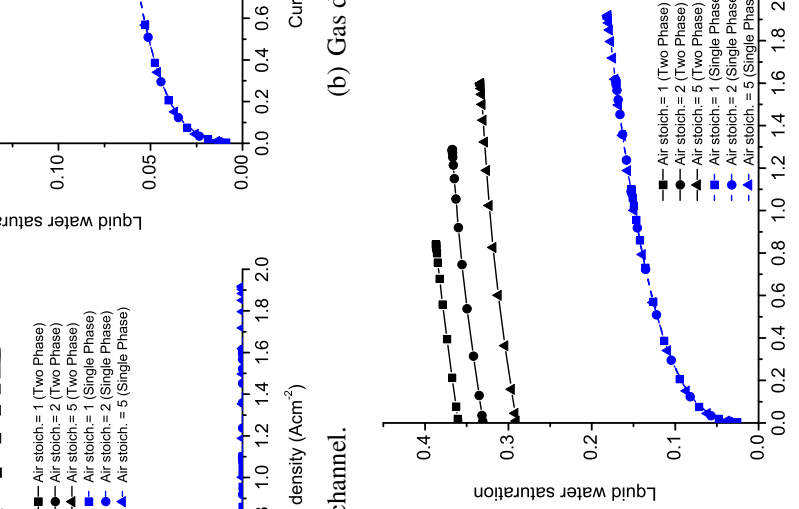

(c) Catalyst layer.

Figure 4.7: Predicted liquid water saturation under various inlet air flow rates. The base-case conditions used in these simulations are given in Table 4.1.

level, in accordance with Eq. (4.30), leads to a more severe water flooding in GC as illustrated in Fig. 4.8(a). Since a higher humidification level limits the vapor removal rate from GC due to an increase in the water vapor concentration in GC, more liquid water becomes accumulated in GC, hence leads to a higher saturation level in MEA as seen in Fig. 4.8.

On the other hand, a single-phase GC model assumes an infinitely large water evaporation rate in GC, therefore the water removal rate is solely determined by the conditions in MEA. As a result, the differences in the predicted saturation levels at GDL and CL under various humidification levels are relatively small.

Voltage-Current Characteristics

Figs. 4.9(a) and 4.9(b) illustrate the effects of inlet air pressure and flow rate on the fuel cell's performance, respectively. Generally, the single-phase GC model predicted significantly higher limiting current densities for the conditions being considered. It also predicted marginally larger ohmic voltage losses compared to those predicted by the two-phase GC model. At the ohmic region, more liquid water exists in MEA when the two-phase GC model is used, which implies a higher proton conductivity in the membrane but not a significantly higher concentration overpotential because the effect of the limitation on oxygen transport is not significant in this region. Therefore, a marginally improved fuel cell's performance is predicted by the two-phase GC model.

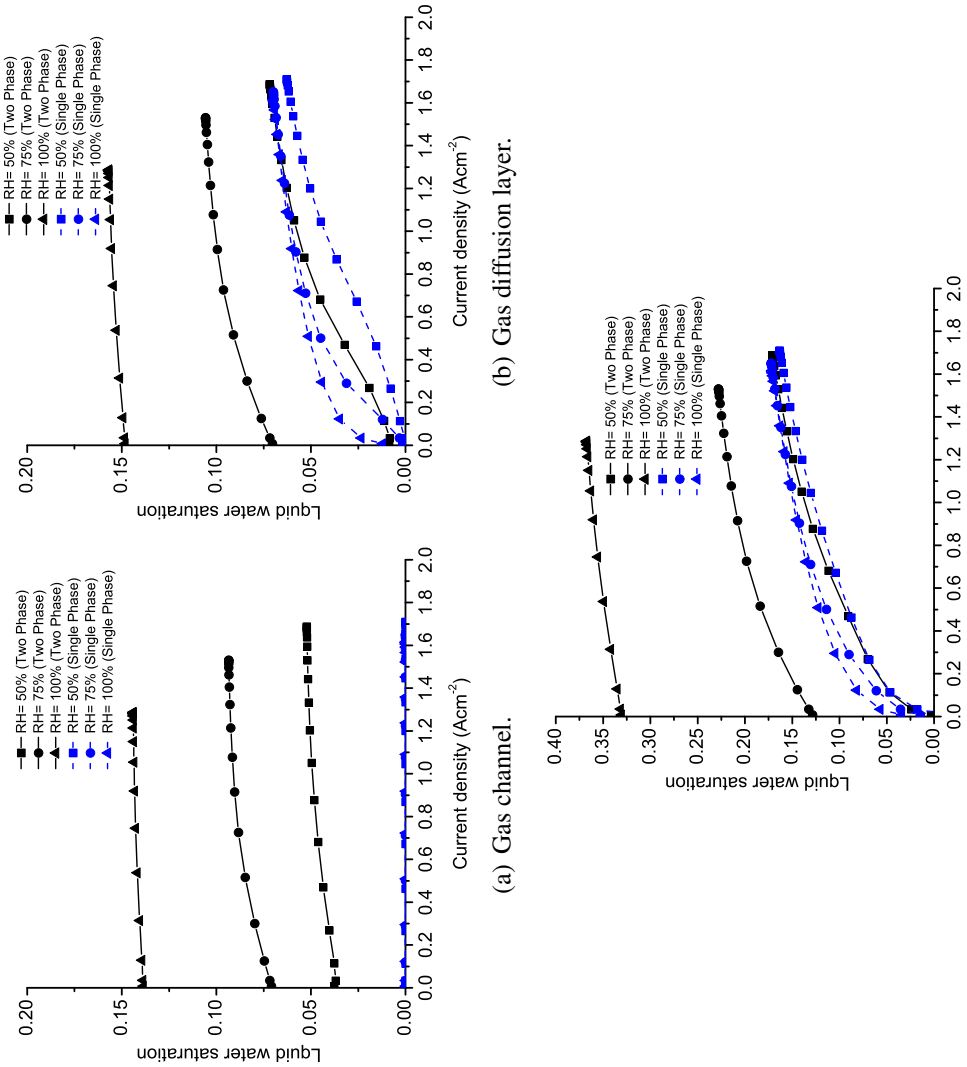

(a) Gas channel.

(b) Gas diffusion layer.

(c) Catalyst layer.

Figure 4.8: Predicted liquid water saturation under various inlet air humidification levels. The base-case conditions used in these simulations are given in Table 4.1.

In accordance with Fig. 4.9(c), the single-phase GC model predicted small differences in the cell performances at high current densities under various inlet air humidification levels, since similar levels of liquid water saturation are predicted in GDL and CL regions for all humidification levels, as shown in Fig. 4.8. On the other hand, the two-phase GC model predicted larger differences in the cell performances for different inlet air humidification levels. This is due to the differences in the predicted water distribution in MEA, which are strongly correlated to the water removal ability of GC under various inlet air humidification levels, a factor that is omitted in the single-phase GC model. This leads to significantly different oxygen concentrations at the CL and hence the corresponding limiting current densities.

4.6 Conclusion

In this chapter, a two-phase GC submodel is developed to correlate the liquid water saturation in GC to the inlet operating conditions. The formulation and assumption of this GC submodel is presented, and the numerical treatment to intergrade the submodel to the two-phase MEA submodel of PEM fuel cell is also discussed.

The intergraded PEM fuel cell model is a pseudo-two-dimensional, two-phase, steady-state PEM fuel cell model including the treatment of two-phase GC is adopted to address the influences of water flooding in GC on the fuel cell's performance. A one-dimensional modeling framework is adopted here for a good computational efficiency.

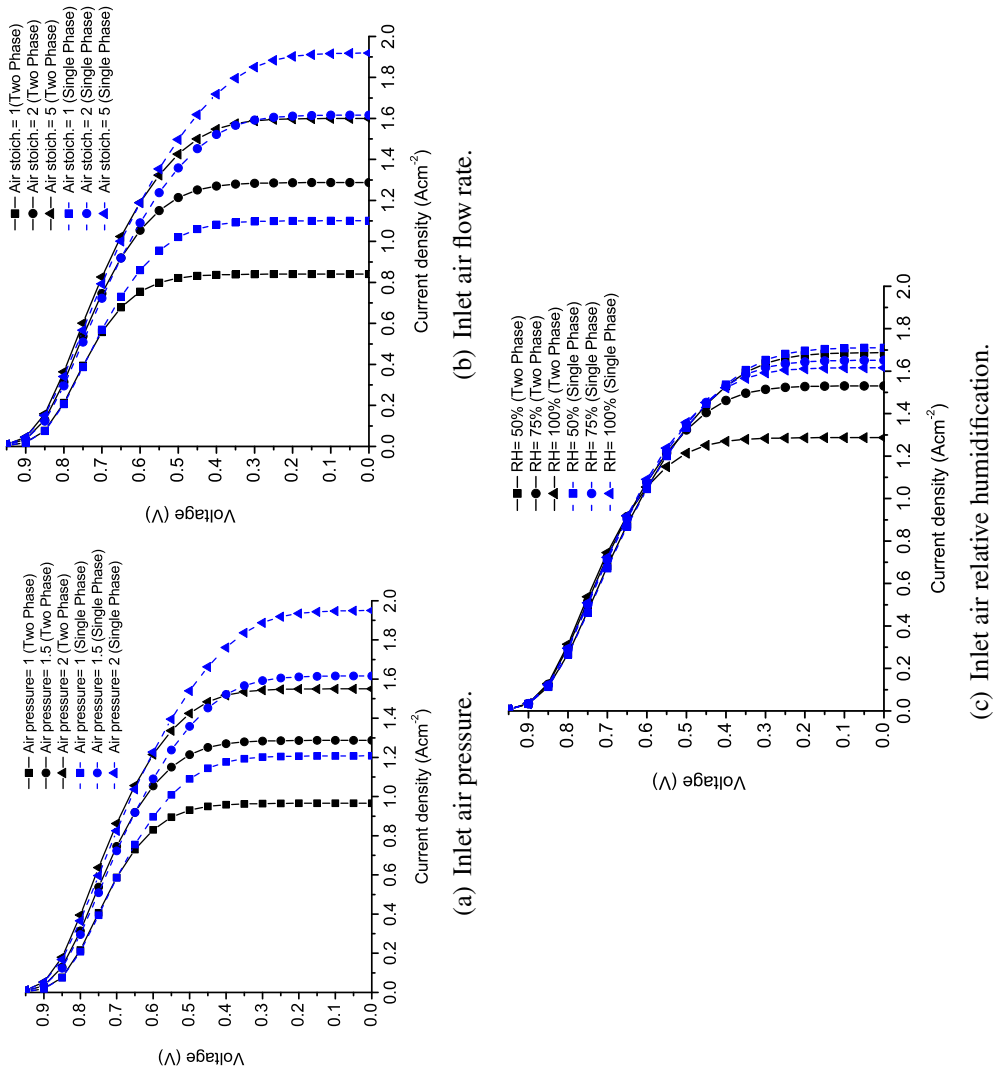

(a) Inlet air pressure.

(b) Inlet air flow rate.

(c) Inlet air relative humidification.

Figure 4.9: Predicted polarization curves under various inlet operating conditions. The base-case conditions used in these simulations are given in Table 4.1.

The two-phase GC model provides a more realistic boundary value of capillary pressure calculated from the liquid water saturation at cathode GDL-GC interface for coupling to MEA model with the objective to capture the influences of inlet conditions on the liquid water distribution inside MEA.

The model predicts that GC conditions, which are closely correlated to the inlet conditions, significantly affect the liquid water saturation level in MEA. An increase in the inlet air pressure or humidification level leads to a more severe water flooding, while an increase in the inlet air flow rate helps mitigating the severity of water flooding. The simulated voltage-current characteristics under various inlet conditions are verified against experimental data and simulation results of a published computational fluid dynamics (CFD) model. They indicate that the relative humidity and stoichiometry of inlet air are crucial to the fuel cell's performance, particularly at high current densities, due to their influences on the liquid water distribution in the fuel cell. The correlations between the inlet conditions and the fuel cell's performance are addressed in the proposed model through a more accurate treatment of the two-phase water transport in cathode MEA and GC. These are important for an appropriate water management in fuel cell.

Chapter 5

Inlet Relative Humidity Control

5.1 Introduction

Water management is a critical issue since the performance of PEM fuel cell is strongly influenced by its internal water distribution. A sufficient hydration of the membrane is essential to facilitate protonic transport for an efficient fuel cell's operation and to avoid irreversible physical degradation to the membrane due to dehydration [23–26]. In this respect, external humidification, where moisture is carried by inlet reactant gases to the internal of fuel cell, is often adopted to ensure that the membrane remains well hydrated, however, when excess water accumulates in the fuel cell, water flooding might be resulted at the cathode region and degrades the PEM fuel cell's performance. Both dehydration and water flooding should be avoided to maintain a satisfactory fuel cell's performance and to protect the fuel cell from physical damages. A balanced water

distribution, which is vital to optimizing PEM fuel cell's performance, should therefore be pursued.

A good understanding of the influences of inlet relative humidity on PEM fuel cell's operation is important as the first step to optimize its performance. In this chapter, a comprehensive study based on this objective is performed through the use of a two-phase PEM fuel cell model based on the improved GC submodel presented in Chapter 4. The different roles of the inlet relative humidity at anode and cathode on the overall water distribution in the PEM fuel cell, and their interactions with other fuel cell's operating conditions, such as air stoichiometries, are discussed in depth. It is the aim of this chapter to provide an unified view of the mechanism of the inlet relative humidity control and to theoretically quantify its effectiveness as a practical method for optimizing the performance of the PEM fuel cell.

5.2 Model Description

In this chapter, a steady-state, pseudo-two-dimensional, two-phase, isothermal unit PEM fuel cell model that bases on the two-phase MEA and GC submodels developed in previous chapters is used to study the influences of the relative humidity of inlet reactant gases on the performance of PEM fuel cell. The model describes a typical unit PEM fuel cell that consists of anode, cathode, and the membrane as shown in Fig. 5.1. Each layer is assumed to be homogenous and the fuel cell's physical processes are described

in the through-plane direction only, except GC, where the transport phenomena along GC direction are considered. Moreover, the structural parameters adopted in this model is shown in Tables 5.1 and 5.2

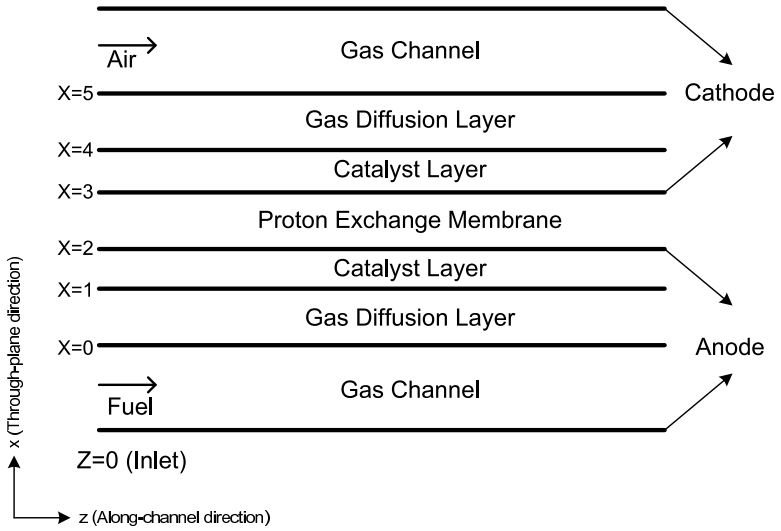

Figure 5.1: The schematic of the computation's domain of PEM fuel cell model. The domain includes two GCs, GDLs and CLs, and a PEM. Through-plane and along-channel directions are denoted as x- and z-axes, respectively.

The anode and cathode, each consists of a GC, a GDL and a CL, are assumed to be symmetrical about the PEM, and are constructed from materials having the same physical properties. The MEA is held between the anode and cathode GCs that deliver reactant gases to the assembly for electrochemical reactions.

The main difference between the present model and the model prevented in Chapter 4 is located in the MEA. In this mode, a more detailed anode CL submodel is developed, in which the anode CL is assumed to have dimension such that the hydrogen, proton, vapor transport and the electrochemical reaction of hydrogen oxidation can be

Table 5.1: Structural Parameters used in the Simulation: Part 1

Parameter	Value
Gas channel	
Length, $L^{\mathrm{GC}}\,(\mathrm{m})$	0.5
Width, $W^{\mathrm{GC}}\,(\mathrm{mm})$	0.5
Depth, $D^{\mathrm{GC}}\,(\mathrm{mm})$	0.5
Gas diffusion layer	
Absolute permeability, $k^{\mathrm{GDL}}\,(\mathrm{m}^2)$ [72, 80]	8.7×10^{-12}
Porosity, $\varepsilon^{\mathrm{GDL}}$	0.55
Contact angle, $\theta^{\mathrm{GDL}}\,(^{\mathrm{o}})$	93.5
Thickness, $l^{\mathrm{GDL}}\,(\mu\mathrm{m})$	250
Proton exchange membrane	
Thickness, $l^{\mathrm{m}}\,(\mu\mathrm{m})$	30
Dry membrane concentration, $c_{\mathrm{m}}\,(\mathrm{mol\ m}^{-3})$ [138]	1800

considered. The formulation of the GC submodel of this model is the same to that presented in Chapter 3 that the cathode GC is described by a two-phase, along-the-channel model so that the channel flooding phenomenon and the drying effect of inlet gas flow can be modeled to more realistically couple the inlet operating conditions to the assembly.

The governing equations of this model is shown in the Table 5.3. Most of the momentum and source terms are described in the Chapter 3 and are not repeated in this chapter. The boundary conditions imposed in this model is listed in the Table. 5.4.

Table 5.2: Structural Parameters used in the Simulation: Part 2

Parameter	Value
Catalyst layer	
Absolute permeability, $k^{\mathrm{CL}}\ (\mathrm{m}^2)$ [72, 80]	10^{-13}
Porosity, $\varepsilon^{\mathrm{CL}}$	0.2
Contact angle, $\theta^{\mathrm{CL}}\ (^{\mathrm{o}})$	90.5
Thickness, $l^{\mathrm{CL}}\ (\mu\mathrm{m})$	15
Fraction of electrolyte, $\varepsilon_{\mathrm{m}}^{\mathrm{CL}}$	0.3
Critical pore radius, $r_{\mathrm{crit}}\ (\mathrm{nm})$	50
Specific surface area of catalyst Pt, $a^{\mathrm{pt}}\ (\mathrm{m}^2\ \mathrm{kg}^{-1})$ [121]	10^5
Catalyst Pt loading, $m^{\mathrm{pt}}\ (\mathrm{kg\ m}^{-2})$ [103]	0.004
Reference oxygen concentration, $c_{\mathrm{O_2,ref}}\ (\mathrm{mol\ m}^{-3})$	$101325H_{\mathrm{m,O_2}}^{-1}$
Reference hydrogen concentration, $c_{\mathrm{H_2,ref}}\ (\mathrm{mol\ m}^{-3})$	34.52
Reference exchange current density of oxygen reduction, $i_{\mathrm{ref,O_2}}\ (\mathrm{A\ m}^{-2})$ [79]	10^{-3}
Reference exchange current density of hydrogen oxidization, $i_{\mathrm{ref,H_2}}\ (\mathrm{A\ m}^{-2})$	18.75
Agglomerate	
Outer surface area of the agglomerates, $a^{\mathrm{agg}}\ (\mathrm{m}^{-1})$	5×10^6
Thickness of membrane covering, $d_{\mathrm{m}}\ (\mathrm{nm})$	20
Radius of the agglomerate, $r^{\mathrm{agg}}\ (\mathrm{nm})$ [155]	200
Fraction of PEM electrolyte in agglomerate, $\varepsilon_{\mathrm{m}}^{\mathrm{agg}}$	0.4

5.3 Experimental Verification of Model

In this section, the developed PEM fuel cell model is verified by comparison with some published experimental data in the literature in order to examine its ability to predict the performance of PEM fuel cell under various inlet operating conditions. The data produced by the two experiments conducted by Williams *et al.* [47] and Saleh *et al.* [73] are used for verification. These reported experiments include detailed polarization curves that were measured under various inlet humidification conditions, hence are useful for

Table 5.3: Governing Equations.

Variables	AGDL	ACL	Membrane	CCL	CGDL
$c_{\mathrm{O_2}}$	-	-	-	$\nabla \cdot \mathbf{J}_{\mathrm{O_2}} = -S_{\mathrm{O_2}}$	$\nabla \cdot \mathbf{J}_{\mathrm{O_2}} = 0$
$c_{\mathrm{H_2}}$	$\nabla \cdot \mathbf{J}_{\mathrm{H_2}} = 0$	$\nabla \cdot \mathbf{J}_{\mathrm{H_2}} = -S_{\mathrm{H_2}}$	-	-	-
c_{v}	$\nabla \cdot \mathbf{J}_{\mathrm{v}} = 0$	$\nabla \cdot \mathbf{J}_{\mathrm{v}} = -S_{\mathrm{d}}$	-	$\nabla \cdot \mathbf{J}_{\mathrm{v}} = -S_{\mathrm{vl}} - (1-s)\, S_{\mathrm{d}}$	$\nabla \cdot \mathbf{J}_{\mathrm{v}} = -S_{\mathrm{vl}}$
ϕ_{p}	-	$\nabla \cdot \mathbf{J}_{\mathrm{p}} = 2S_{\mathrm{H_2}}$	$\nabla \cdot \mathbf{J}_{\mathrm{p}} = 0$	$\nabla \cdot \mathbf{J}_{\mathrm{p}} = -4S_{\mathrm{O_2}}$	-
s	-	-	-	$\nabla \cdot \mathbf{J}_{\mathrm{l}} = 2S_{\mathrm{O_2}} + S_{\mathrm{vl}} - sS_{\mathrm{d}}$	$\nabla \cdot \mathbf{J}_{\mathrm{l}} = S_{\mathrm{vl}}$
c_{d}	-	$\nabla \cdot \mathbf{J}_{\mathrm{d}} = S_{\mathrm{d}}$	$\nabla \cdot \mathbf{J}_{\mathrm{d}} = 0$	$\nabla \cdot \mathbf{J}_{\mathrm{d}} = S_{\mathrm{d}}$	-
p_{l}	$p_{\mathrm{l}} = p_{\mathrm{g}} - p_{\mathrm{c}}$	$p_{\mathrm{l}} = p_{\mathrm{g}} - p_{\mathrm{c}}$	$\frac{d^2 p_{\mathrm{l}}}{dx^2} = 0$	$p_{\mathrm{l}} = p_{\mathrm{g}} - p_{\mathrm{c}}$	$p_{\mathrm{l}} = p_{\mathrm{g}} - p_{\mathrm{c}}$

Table 5.4: Boundary Conditions in the Simulation.

Variables	AGC-AGDL	GDL-ACL	ACL-MEM	MEM-CCL	CCL-CGDL	CGDL-CGC
c_{O_2}	-	-	-	-	continuous	Eq. (4.32)
$\mathbf{J}_{O_2}$	-	-	-	0	continuous	-
c_{H_2}	Eq. (4.33)	continuous	-	-	-	-
$\mathbf{J}_{H_2}$	-	continuous	0	-	-	-
c_v	Eq. (4.33)	continuous	-	-	continuous	Eq. (4.31)
$\mathbf{J}_v$	-	continuous	0	0	continuous	-
ϕ_{p}	-	continuous	continuous	continuous	continuous	-
$\mathbf{J}_{\mathrm{p}}$	0	continuous	continuous	continuous	continuous	0
s	-	-	-	-	$p_c^- = p_c^+$	Eq. (4.30)
$\mathbf{J}_{\mathrm{l}}$	-	-	-	0	continuous	-
c_{d}	-	continuous	continuous	continuous	continuous	-
$\mathbf{J}_{\mathrm{d}}$	0	continuous	continuous	continuous	continuous	0
p_{l}	$p_{\mathrm{l}} = p_{\mathrm{g}}$	continuous	continuous	continuous	continuous	$p_{\mathrm{l}} = p_{\mathrm{g}}$

verifying the model's accuracy in respect of modeling the influences of inlet humidification on the performance of PEM fuel cell.

The polarization curves obtained under the conditions studied in the experiment of Williams *et al.* are simulated by the model. The predicted polarization curves are plotted in Fig. 5.2, and the results are compared with the experimental data of Williams *et al.* plotted in the same figure. The experimental result shows that, when the inlet cathode humidification is completely removed, the test cell can function properly and maintain an adequate output voltage when the anode's hydrogen gas remains fully humidified. The same is predicted by the model, which theoretically demonstrates the practical feasibility of dry-cathode operation. On the contrary, when the inlet anode humidification is removed, the performance of the test cell degrades significantly as can be justified from the large difference between the measured polarization curves under 100/0 and 0/0 conditions ($\Theta_{\mathrm{a}}/\Theta_{\mathrm{c}}$ denotes the inlet relative humidity at anode and cathode in %, respectively). The simulated polarization curves show that a similar case is predicted by the model. Although there are some mismatches between the measured and predicted polarization curves in numerical values, the model has generally demonstrated the ability to produce close qualitative predictions on the influences of inlet anode and cathode humidification on the performance of PEM fuel cell.

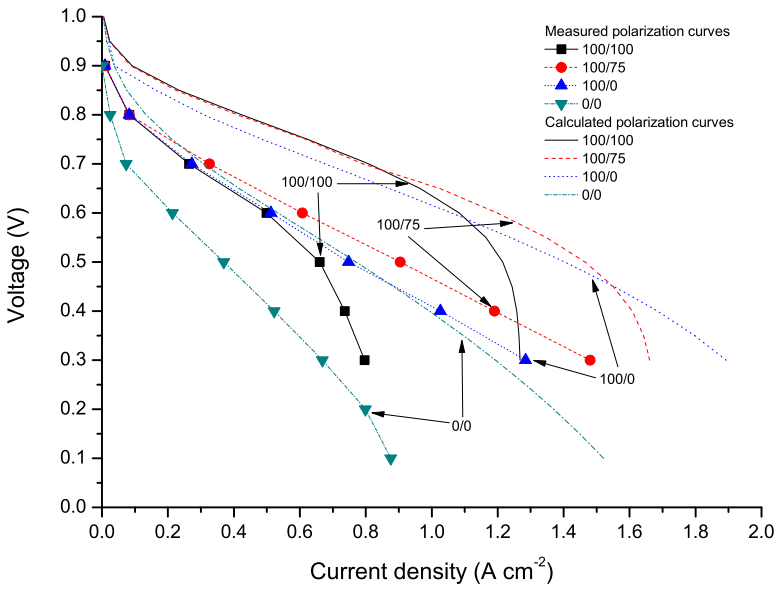

Figure 5.2: A comparison of polarization curves between the data from experimental studies in Williams *et al.* and the results based on the simulation in this paper. The inlet relative humidities shown includes 100/100, 100/75, 100/0 and 0/0 (Θ_a/Θ_c). The polarization curves simulated are under the same set of inlet operating conditions used in the experiments conducted by Williams *et al.*

By inspecting the measured polarization curves, when the inlet relative humidity at anode is fixed at 100%, different limiting current densities are produced under various inlet cathode humidification conditions. As the inlet relative humidity at cathode is reduced from 100%, to 75%, and to 0%, it is observed that the test cell's performance has improved by producing a higher limiting current density, hence a wider operating range is obtained. On the other hand, by examining the intermediate current density region, an increase in ohmic overpotential is observed as the inlet relative humidity at cathode is reduced, leading to a higher ohmic power loss when the test cell operates at this current density region. One exception to these trends is the case when both anode and cathode are fully humidified, *i.e.*, 100/100, where the measured curve shows an

early fall in output voltage, indicating that the gain in performance due to the reduced ohmic overpotential in a strongly hydrated membrane is largely offset by the increased concentration overpotential resulting from a more severe flooding. In general, these trends have been successfully captured by the model, where the simulation results are plotted in Fig. 5.2 for comparison.

In the experimental work conducted by Saleh *et al.* [73], the polarization curves of a PEM fuel cell operating under various symmetrical (with respect to anode and cathode) inlet humidification conditions were measured and the results are shown in Fig. 5.3. For comparison, these cases are simulated by the model and the predicted results are also plotted in Fig. 5.3. It can be seen from the experimental studies that a higher inlet relative humidity generally improves the performance of PEM fuel cell at the intermediate current density region, as expected, due to the reduced ohmic overpotential in the presence of a well-hydrated membrane. A similar trend is demonstrated by the predicted polarization curves shown in Fig. 5.3. In respect of limiting current density, an opposite trend is concluded from both the experimental and simulation results. In general, a higher inlet relative humidity does not favor the operation of PEM fuel cell at high current density since it could lead to a more severe flooding condition and degrade the fuel cell's performance by enhancing concentration overpotential.

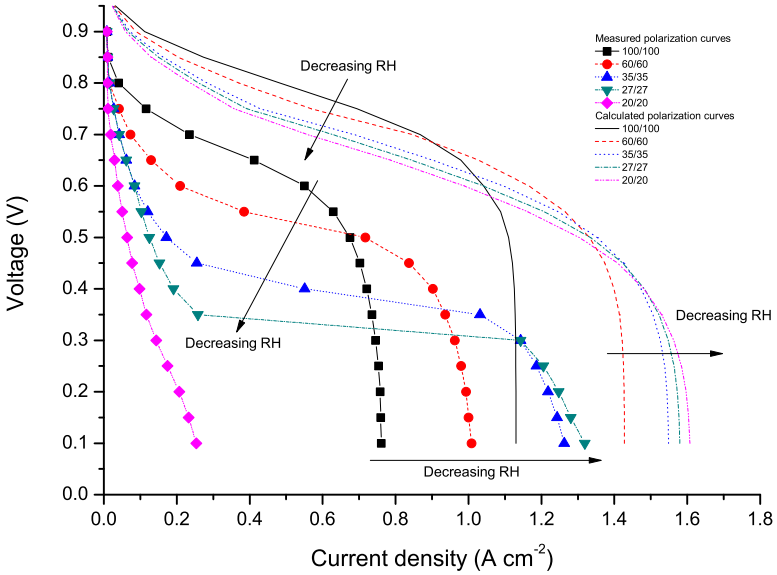

Figure 5.3: A comparison of polarization curves between the data from experimental studies in Saleh *et al.* and the results based on the simulation in this paper. The inlet relative humidities shown includes 100/100, 60/60, 35/35, 27/27 and 0/0 (Θ_a/Θ_c). The polarization curves simulated are under the same set of inlet operating conditions used in the experiments conducted by Saleh *et al.*

From these experimental and simulation studies, the dual-role of water in the operation and performance of PEM fuel cell is implied. On one hand, water is required for hydrating membrane; on the other hand, the presence of excessive water impedes the transportation of reactant gases, especially for oxygen at cathode. Therefore, a balanced water management is needed for optimizing the performance of PEM fuel cell. While external humidification provides a direct control over the rate of water supply to a fuel cell, the volume flow rates of reactant gases can also be utilized to control the rate of water removal from the fuel cell due to their drying effects. The interplay between these control parameters in a single PEM fuel cell system should be understood when designing an appropriate water management scheme. In the next section, the verified model

is used to perform a detailed simulation study on the influences of inlet humidification and volume flow rate conditions on the performance of PEM fuel cell. Compared to oxygen at cathode, the naturally fast hydrogen oxidation kinetics at anode tends to have a weak impact on the overall performance of PEM fuel cell and, in practice, its flow rate is typically kept close to one stoichiometry for minimization of wastage, therefore the volume flow rate of hydrogen is excluded from the study in order to keep a clear presentation of the essential ideas only.

5.4 Results and Discussion

In this section, the model is used to perform a detailed simulation study on the influences of various combinations of inlet anode and cathode humidification and air flow rate conditions (see Table 5.5) on the performance of PEM fuel cell.

Table 5.5: Range of Operating Conditions in the Simulation.

Inlet condition	Symbol	Value
Inlet operating temperature	T	80 °C (353 K)
Inlet hydrogen and air pressure	$p_{\mathrm{H_2/air}}$	1 atm
Inlet anode stoichiometry	ζ_{a}	1.2
Inlet cathode stoichiometry	ζ_{c}	1, 2 & 4
Anode inlet relative humidity	$\Theta_{\mathrm{H_2}}$	20, 60 & 100%
Cathode inlet relative humidity	Θ_{Air}	20, 60 & 100%

The predicted polarization curves are plotted in Figs. 5.4 and 5.5 and some general conclusions are drawn by a systematic analysis of these curves. The figure sets in Figs. 5.4 and 5.5 are conveniently arranged in a matrix form, where each matrix's element represents a case of variation of one parameter while the other two parameters are

kept constant. For instance, in Fig. 5.4, each matrix's element represents the case where the inlet relative humidity at cathode and air stoichiometry are kept constant while the inlet relative humidity at anode is varied from 20%, to 60%, and to 100%. Other elements in the same column are repeated similarly for other inlet cathode humidification conditions, whereas other elements in the same row are repeated similarly for other air stoichiometry values. Fig. 5.5 follows the same arrangement but with the inlet relative humidity at cathode varied from 20%, to 60%, and to 100% while the inlet relative humidity at anode and air stoichiometry are kept constant for each matrix's element. The reason for adopting such an arrangement for Figs. 5.4 and 5.5 is to enable a clearer visualization of the individual role or contribution of inlet anode and cathode humidification on the overall fuel cell's performance in the presence of various air flow rates.

From Fig. 5.4, it can be seen that inlet anode humidification mainly affects the polarization curves of the simulated PEM fuel cell at the intermediate current density region where ohmic overpotential dominates. As shown by each matrix's element in the figure set, the limiting current density remains virtually unchanged under various inlet anode humidification conditions when inlet cathode humidification is kept constant. On the contrary, Fig. 5.5 shows that the variation of inlet cathode humidification has an almost negligible effect on the polarization curves at the intermediate current density region, but produces a significant influence on the value of limiting current density and hence the operating range of the simulated fuel cell. From these simulated trends, it appears

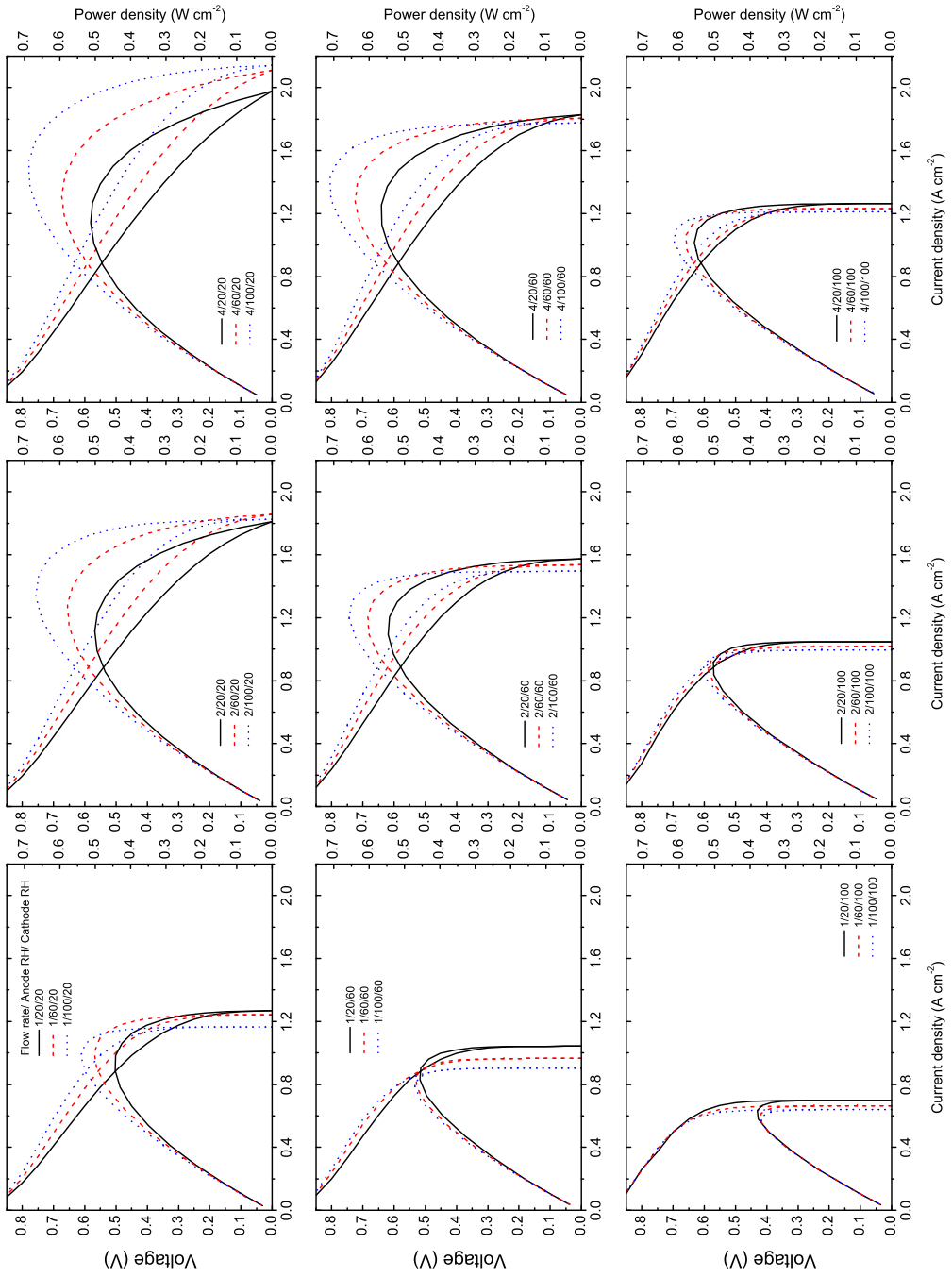

Figure 5.4: Performances of PEM fuel cell are calculated under various inlet operating conditions that are listed in Table. 5.5 shown in matrix form. In this figure, the emphasis is the influences of inlet anode humidification on the performances of PEM fuel cell. Each matrix's element represents the cases where only the inlet anode humidification is varied from 20%, to 60%, and to 100% while other inlet operating conditions are kept constant. ($\zeta_c/\Theta_a/\Theta_c$ stand for the cathode stoichiometry, inlet anode and cathode relative humidity, respectively).

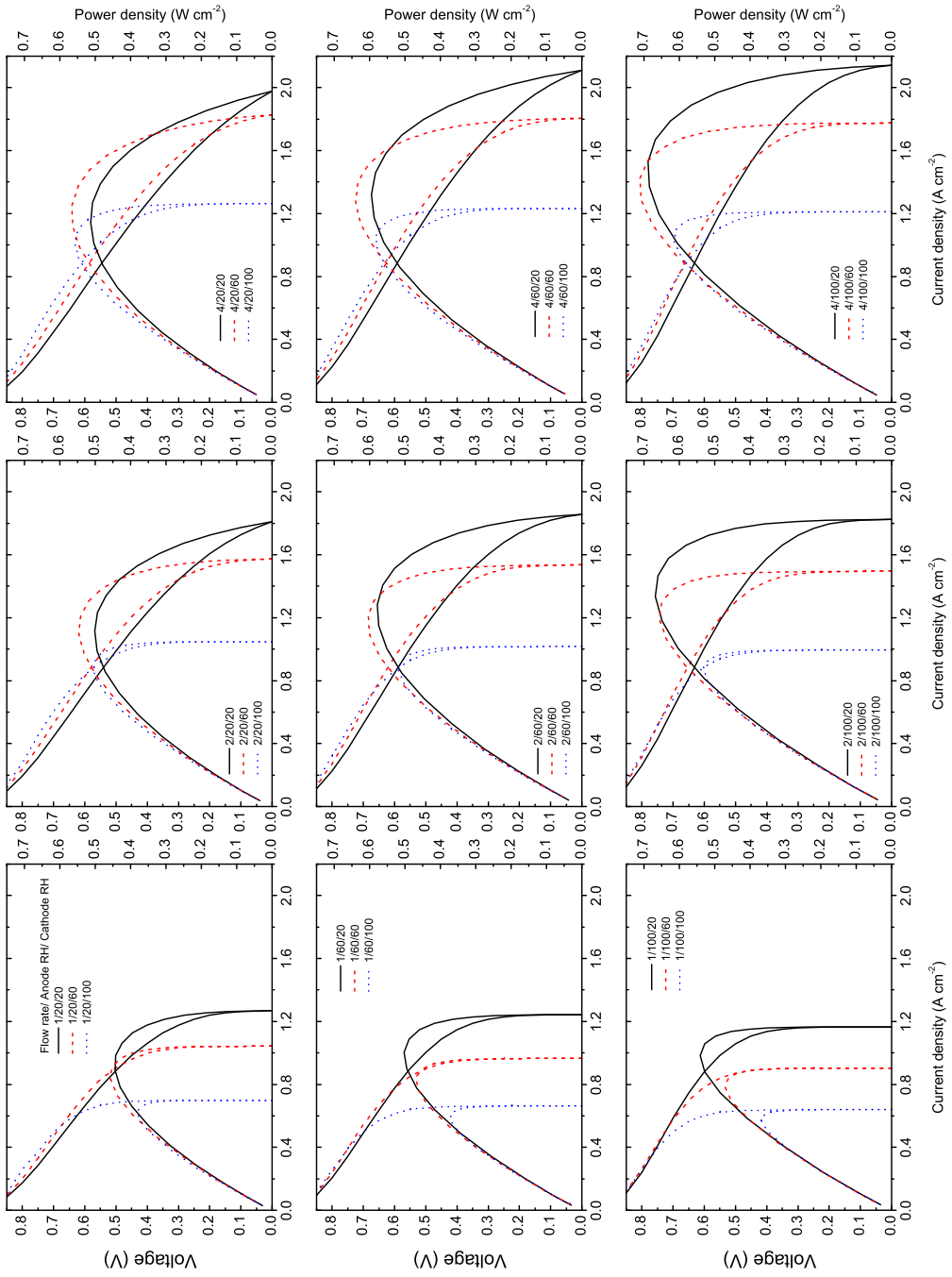

Figure 5.5: Performances of PEM fuel cell are calculated under various inlet operating conditions that are listed in Table. 5.5 shown in matrix form. In this figure, the emphasis is the influences of inlet cathode humidification on the performances of PEM fuel cell. Each matrix's element represents the cases where only the inlet cathode humidification is varied from 20%, to 60%, and to 100% while other inlet operating conditions are kept constant. ($\zeta_c/\Theta_a/\Theta_c$ stand for the cathode stoichiometry, inlet anode and cathode relative humidity, respectively).

that the role of inlet anode and cathode humidification are asymmetrical in nature under the operating conditions being studied. Thus, we propose to consider their roles individually in the following discussion and attempt to optimize the performance of fuel cell by controlling these parameters separately.

The origin of this asymmetry lies in the formation of water at the cathode of PEM fuel cell that constantly maintains the cathode at an adequately hydrated state. Since water also arrives from anode by electro-osmotic drag, and water desorption from membrane for removal through cathode GDL is an inherently slow process, water tends to accumulate at the cathode region near the interface between membrane and CL. By means of back-diffusion and even pressure-driven permeation, the high water content at the cathode region then acts as a concentration barrier to prevent further incoming water from anode by electro-osmotic drag. In this way, any incoming water due to inlet anode humidification will tend to be circulated and confined within the membrane by the counteracting actions of electro-osmotic drag and back-diffusion, aided by the blocking action of the high water concentration at cathode, and pressure-driven permeation. The back-diffusion process further helps to distribute water more evenly across the membrane, a mechanism that is well known from the literature, and lower the overall membrane's resistivity. Since the amount of water to be circulated within the membrane is mainly determined by the incoming water from inlet anode humidification, the membrane's resistivity, and hence ohmic overpotential, becomes highly susceptible to the

variation of inlet relative humidity at anode. Therefore, for each matrix's element in Fig. 5.4, fully humidified anode always gives rise to the smallest ohmic overpotential and hence the maximum deliverable power density. This is supported by the plots of water content and ohmic overpotential in Fig. 5.6.

Due to the same mechanism as described above, in the presence of electro-osmotic drag that transports water in the opposite direction, the water accumulated at the cathode region cannot be effectively transported through membrane by back-diffusion and pressure-driven permeation towards anode for subsequent removal. Therefore, this water should be mainly removed by transportation through cathode GDL in the form of water vapor or liquid water, and the effectiveness of this method relies critically on the humidification condition in cathode GDL and GC, hence the inlet cathode humidification condition. By means of this reasoning, it can be argued that the removal of the accumulated water will become more impeded as the inlet relative humidity at cathode is increased. The excessive accumulation of water then leads to the formation of liquid water that occupies the GDL pores and partially blocks the transportation of oxygen to CL; these effects of increased inlet cathode humidification are reflected by the plots of liquid water saturation and the corresponding concentration overpotential in Fig. 5.7. It can be seen from Figs. 5.5 and 5.6 that although inlet cathode humidification does affect water content, the effect is less significant compared to its effect on concentration overpotential and hence the limiting current density. In summary, the influence of in-

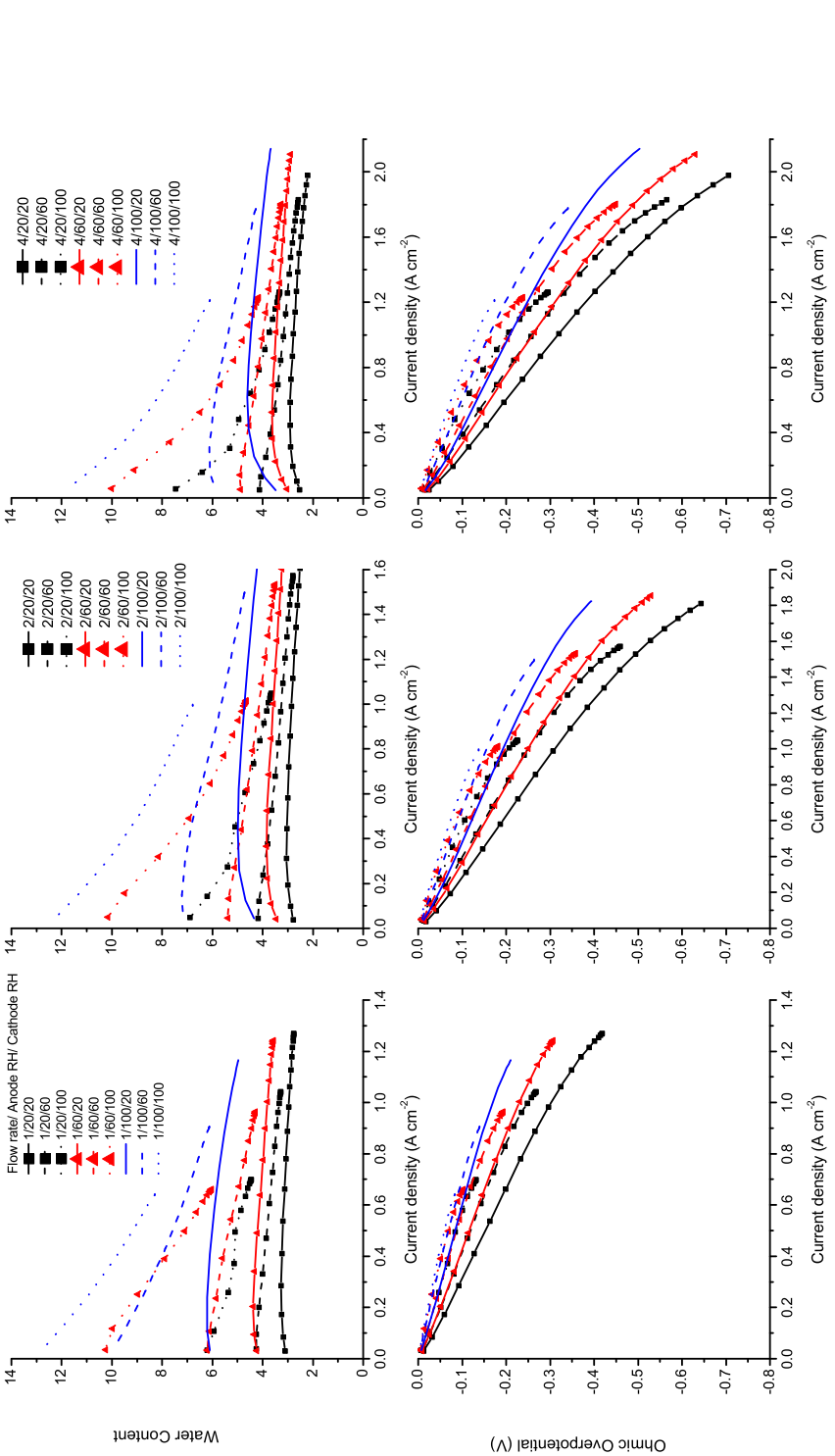

Figure 5.6: Averaged water content and ohmic overpotential are simulated under various inlet operating conditions that are listed in Table 5.5. Upper and lower rows represent, respectively, the averaged water content and ohmic overpotential. The air stoichiometry of each column are kept constant.

let cathode humidification on the performance of PEM fuel cell is more pronounced in respect of its contribution to the control of liquid water saturation at the cathode region.

Therefore, the simulation study shows that, in accordance to the asymmetrical roles of anode and cathode humidification, as discussed, the inlet relative humidity at anode should be ideally kept at 100% in order to maintain a well hydrated membrane for minimizing ohmic overpotential (at the intermediate current density region), while the inlet relative humidity at cathode should be kept very low to minimize concentration overpotential by preventing the formation of liquid water, *i.e.*, flooding, in cathode GDL and GC. These conditions typically give rise to an absolute maximum power density under a given air flow rate. However, a closer look at Fig. 5.5 reveals an exceptional case that deserves further explanation. It can be seen that, when the air stoichiometry is increased to 4, the maximum power density point is attained when the inlet relative humidity at cathode is 60% instead of 20%. The high air stoichiometry is responsible for an enhanced drying of cathode GDL and GC, as shown by the reduced liquid water saturation and concentration overpotential in Fig. 5.7, which also undesirably drains water from membrane and decreases its conductivity. The combined effect of increased oxygen supply and water removal under a high air stoichiometry diminishes the role of concentration overpotential, and the fuel cell's performance becomes dominated by ohmic overpotential. Hence, when such a high air flow rate is needed, the dehydration of membrane should be remedied (or the loss of water compensated) by increasing the

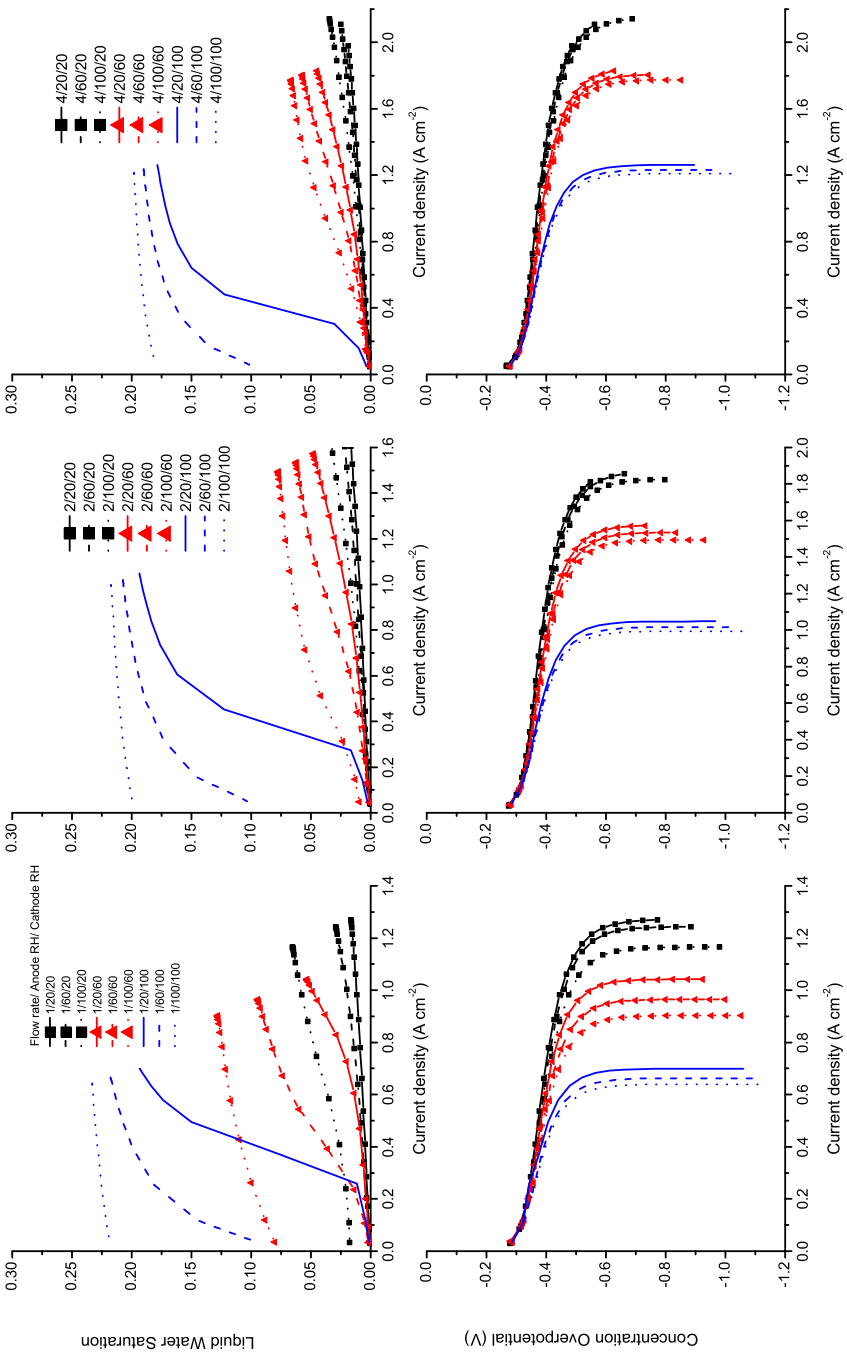

Figure 5.7: Averaged liquid water saturation (at cathode GDL) and concentration overpotential are simulated under various inlet operating conditions that are listed in Table 5.5. Upper and lower rows represent, respectively, the averaged liquid water saturation and concentration overpotential. The air stoichiometry of each column are kept constant.

inlet relative humidity at cathode. However, it can be seen that the performance gain by increasing the inlet cathode humidification from 20% to 60% is very limited considering the apparently weak influence of inlet cathode humidification on membrane's resistivity due to the water transportation mechanism discussed previously. From the simulated case, it is clear that the performance gain is offset by the much more significant reduction in the limiting current density.

The influences of inlet anode and cathode humidification can be utilized in two ways to control the performance of PEM fuel cell, and each is now illustrated by using a simulated example. The first example relates to the case when a PEM fuel cell is intended to operate at *static* condition and an absolute maximum power density is always desired, such as in grid-connected power generation. For analysis, a comparison between the highest and lowest maximum power density under each air stoichiometry value is made, as shown in Fig. 5.8. They correspond to the highest and lowest maximum power density extracted from the nine output power curves plotted in Fig. 5.4 or Fig. 5.5. It is interesting and important to note that the maximum power density attained under a given air stoichiometry can vary significantly depending on the inlet anode and cathode humidification conditions under which a PEM fuel cell operates. For example, under one air stoichiometry, 0.37 $\mathrm{W\ cm^{-2}}$ is obtained when both anode and cathode are fully humidified, but it can be improved significantly to 0.54 $\mathrm{W\ cm^{-2}}$ by simply reducing the inlet relative humidity at cathode from 100% to 20%. For other air stoichiometry

values, different absolute maximum power density values can be obtained similarly.

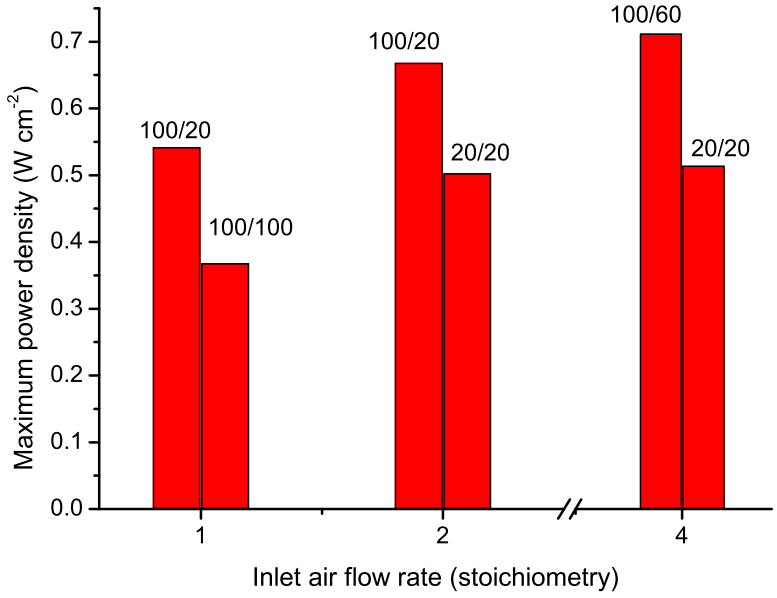

Figure 5.8: Predicted highest and lowest maximum power density of PEM fuel cell under various air flow rates.

The second example relates to the case when a PEM fuel cell is intended to operate at *moving-static* condition in response to a slowly changing load. In this case, the inlet humidification should be adjusted according to the operating point of the fuel cell. The polarization curves shown in Fig. 5.9 are used for the following discussion. It can be seen that at low current density, both anode and cathode should be fully humidified in order to minimize ohmic overpotential. However, these conditions cannot sustain the fuel cell's operation at intermediate current density due to the excessive concentration overpotential that occurs at about 1 $\mathrm{A\ cm^{-2}}$. To avoid the collapse of voltage and power, the inlet relative humidity at cathode should be reduced to 60%, with which the fuel cell will continue to operate until the current density reaches about 1.5 $\mathrm{A\ cm^{-2}}$. Similar as

before, when the fuel cell operates beyond 1.5 $\mathrm{A\,cm^{-2}}$, the inlet relative humidity at cathode should be further reduced to 20% for sustaining its operation at high current density. It is evident from the discussion that the primary objective of the dynamic humidity control is to maximize the fuel cell's power density at each current density by dynamically tracing the outer envelope of the polarization and power density curves. With the same control, the practical operating range of the fuel cell is maximized compared to the case where fixed humidification is employed.

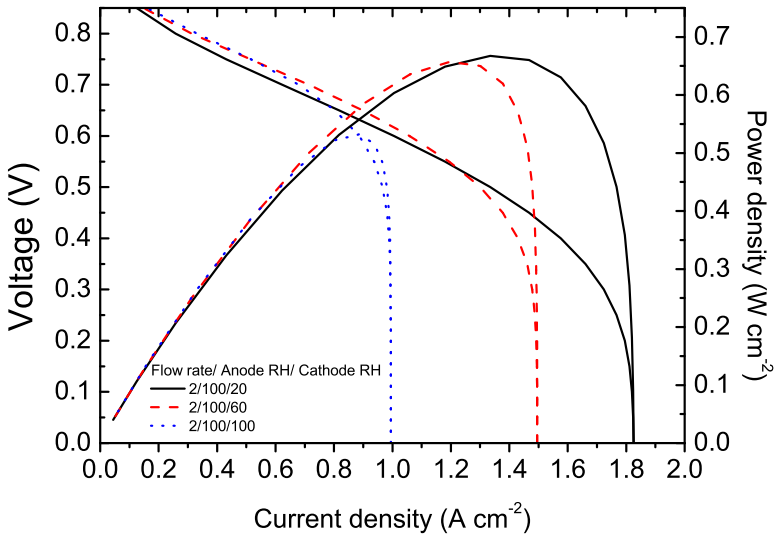

Figure 5.9: Calculated polarization curves under various inlet cathode relative humidity, 2 stoichiometries and 100% inlet anode relative humidity. Other inlet operating conditions are listed in Table 5.5.

5.5 Conclusion

In this work, the engineering feasibility of optimizing the performance of PEM fuel cell by means of inlet relative humidity control has been theoretically studied with the aid of a pseudo two-dimensional, two-phase, isothermal unit PEM fuel cell model. The indi-

vidual influences of the inlet relative humidity at anode and cathode have been systematically investigated by simulating the polarization curves under various combinations of inlet anode and cathode humidification and air stoichiometry conditions. It is found that, under the operating conditions being studied, the influences of the inlet relative humidity at anode and cathode are highly asymmetrical with the former mainly affecting membrane's conductivity while the latter mainly influences the level of liquid water saturation, hence the severity of flooding, at the cathode region. The origin of these asymmetrical influences is postulated as due to the pressure-driven permeation and the formation of water at cathode, which establishes a concentration barrier that, on one hand, helps circulate membrane's water and renders ohmic overpotential susceptible to inlet anode humidification, and, on the other hand, drives water to cathode GDL and GC with a removal rate that is governed by inlet cathode humidification. From the simulation study, it is concluded that a fully humidified anode and a dry cathode are typically required to maximize the power density delivered by a PEM fuel cell, unless a high air flow rate is employed, in which case the cathode should be operated with an intermediate relative humidity. Based on the developed understanding of the individual influences of inlet anode and cathode humidification, two examples on the use of inlet relative humidity control for maximizing the volumeric power density and operating range of PEM fuel cell have been discussed. Its usefulness as a simple and effective method for the performance optimization of PEM fuel cell has been theoretically demonstrated.

Chapter 6

Derivation of a Fast Two-Phase Dynamic PEM Fuel Cell Model

In Chapter 5, the influences of external humidification on the performance of PEM fuel cell have been studied systematically by using a steady-state pseudo two-dimensional two-phase PEM fuel cell model. The numerical results of the study show that the volumetric power density and operating range of PEM fuel cell can be adjusted by controlling the inlet relative humidity. In a practical PEM fuel cell system, however, a dynamic water management scheme is often employed due to the time-varying loading condition, thus requiring a two-phase dynamic PEM fuel cell model for aiding a simulation study. A PEM fuel cell system, in general, consists of a PEM fuel cell and various auxiliary subsystems, such as humidifiers, mass flow controllers and *etc*, that are used to support the operation of PEM fuel cell. A complete dynamic PEM fuel cell system

model including all these components is complicated and the simulation is time consuming. In view of this, although a PEM fuel cell model considering the sophisticated two-phase water transport can accurately capture the influences of liquid water transport in PEM fuel cell, it is challenging to integrate the model with other auxiliary subsystem models and yet form a computationally efficient system model. Therefore, a fast two-phase dynamic PEM fuel cell model is desired for this application. In view of this, in this chapter, a computationally efficient two-phase dynamic PEM fuel cell model is derived in order to provide a sufficiently accurate two-phase model while maintaining the simulation time of the complete PEM fuel cell system to within a reasonable time scale.

6.1 Modeling Description and Assumptions

The computation domains of the two-phase dynamic PEM fuel cell model presented in this chapter include an anode, a cathode and a PEM. Both electrodes include a GDL and a CL. The CLs are assumed to be infinitely thin and are modeled as interfacial layers lumped together to GDL, and the water produced by the electrochemical reaction is assumed to be taking place at the interfacial layer between the membrane and the cathode. The state of phase of the produced water depends on the water activity at the cathode GDL-membrane interface. Water activity in GDL is calculated by assuming a phase equilibrium between water vapor and liquid water. Liquid water is only assumed to exist in the cathode only, while no liquid water is assumed to exist in the anode.

The transient responses of the water content in membrane and the liquid water saturation in GDL are much slower compared to the concentrations of gaseous species, and the slow re-distribution of water within the membrane and GDL are main causes that lead a slow transient of PEM fuel cell [84, 85]. Therefore, the dynamic responses of the water content and liquid water saturation are considered, while the concentrations of gaseous species are assumed to exist in steady-state during the computation of the slowly changing parameters: water content in membrane and liquid water saturation.

6.2 Governing Equations

6.2.1 Reactant Gas Transport

The mass transport of reactant gases is derived from the conservation equation given by:

$$\frac{\partial}{\partial t}\left[(1-s)\,\varepsilon c_i\right] - \frac{\partial}{\partial x}\left(D_i^{\text{eff}}\frac{\partial c_i}{\partial x}\right) = 0, \tag{6.1}$$

where D_i^{eff} is the effective diffusion coefficient of gas species i that is described in Chapter 3. In the present chapter, the expression suggested by Nam *et al.* [34] is used to model D_i^{eff}, *i.e.*,

$$D_i^{\text{eff}} = \varepsilon\left(\frac{\varepsilon - 0.11}{1 - 0.11}\right)^{0.785}(1-s)^2\,. \tag{6.2}$$

The dynamic response of reactant gases is fast with a typical characteristic time in

the order of centiseconds [84,85]. On the other hand, the characteristic times associated with the water transport in membrane and the capillary flow of liquid water in GDL are in the order of seconds. It is expected that these water transport mechanisms are the main factors that limit the dynamic response of PEM fuel cell. The transient term of reactant gases is therefore neglected in this model. A static equation of reactant gases, as shown before, is thus used in this model to calculate the diffusive flow of reactant gases in order to enhance the computational efficiency of the model.

$$J_i = -\frac{\partial}{\partial x}\left(D_i^{\text{eff}}\frac{\partial c_i}{\partial x}\right). \tag{6.3}$$

6.2.2 Water Transport

Water concentration inside the membrane is described by the water content of membrane, λ, which is defined as the number of dissolved water molecules held per sulphonic acid group. The change of water content is governed by mass conservation considering the diffusion and the electro-osmotic drag and is expressed as the following equation:

$$\frac{\partial}{\partial t}\left(c_{\text{m}}\lambda\right) + \frac{\partial}{\partial x}\left(\frac{2.5\lambda I}{22F} - c_{\text{m}}D_{\text{d}}\frac{\partial \lambda}{\partial x}\right) = 0. \tag{6.4}$$

The first term in the equation represents the transient response of the water transport in membrane. The second term is the spatial derivative of the dissolved water flux in

membrane, and the dissolved water flux originates from both the back-diffusion and electro-osmotic drag. Their physical details are presented in Chapter 3.

Two-phase flow is commonly found in the cathode GDL, and it is considered in this model. The liquid water distribution in the cathode GDL is governed by the conservation equation shown as the following:

$$\frac{\partial\left(\varepsilon s c_{\mathrm{l}}\right)}{\partial t}-\frac{\partial}{\partial x}\left(c_{\mathrm{l}} D_{\mathrm{c}} \frac{\partial s}{\partial x}\right)=0. \tag{6.5}$$

The term $\partial\left(\varepsilon s c_{\mathrm{l}}\right)/\partial t$ is the transient term of liquid water transport. The second term, $-\frac{\partial}{\partial x}\left(c_{\mathrm{l}} D_{\mathrm{c}} \frac{\partial s}{\partial x}\right)$, represents the spatial derivative of the liquid water flux in GDL, *i.e.*,

$$J_{\mathrm{l}}=-c_{\mathrm{l}} D_{\mathrm{c}} \frac{\partial s}{\partial x}. \tag{6.6}$$

The water diffusion coefficient, D_{c}, is a parameter that depends on the properties of the porous media and the liquid water saturation. In order to obtain a computationally efficient model, a constant capillary pressure coefficient is used [43].

6.3 Numerical Procedure

The governing equations prescribed are solved using standard finite difference method. The approach is to transform a partial differential equation into recursive algebraic equation by two basic procedures, namely the discretization of computation domain and the

approximation of partial derivative operation.

The time domain is discretized and labeled by the index n, and its derivative is approximated by forward finite difference approximation as follows:

$$\left.\frac{\partial y}{\partial t}\right|_{t=n} = \frac{y^{n+1} - y^n}{\Delta t}. \tag{6.7}$$

The spatial domain is divided into $P-1$ regions with P grid points labeled from 1 to P. By using the normalized spatial variable, $\bar{x} = x/L$, the grid size is given by:

$$\Delta\bar{x} = \frac{1}{P-1}. \tag{6.8}$$

The first and second spatial derivatives are approximated by using the central difference approach.

$$\left.\frac{\partial y}{\partial \bar{x}}\right|_{\bar{x}=i} = \frac{y_{i+1} - y_{i-1}}{2L\Delta\bar{x}}, \tag{6.9}$$

$$\left.\frac{\partial^2 y}{\partial \bar{x}^2}\right|_{\bar{x}=i} = \frac{y_{i-1} - 2y_i + y_{i+1}}{L^2\Delta\bar{x}^2}. \tag{6.10}$$

Recursive algebraic equations are obtained by applying Eqs. (6.7) and (6.10) to the governing equations, *i.e.*, Eqs. (6.4) and (6.5).

6.4 Boundary Conditions

The concentration of reactant gases decreases linearly along GC due to a uniform consumption by MEA. This effect is considered in this model by computing the average concentration at GC-GDL interface as follows:

$$c_{\mathrm{H_2,GC|GDL}} = c_{\mathrm{H_2,inlet}} \left(1 - \frac{1}{\zeta_{\mathrm{H_2}}}\right),$$
$$c_{\mathrm{O_2,GC|GDL}} = c_{\mathrm{O_2,inlet}} \left(1 - \frac{1}{\zeta_{\mathrm{air}}}\right). \tag{6.11}$$

The equilibrium values of the water content at the left and right boundary of the membrane are taken as the boundary values for solving the transport equation of the dissolved water in the membrane. The equilibrium values are calculated from the water activity at the anode-membrane and cathode-membrane interfaces by the following empirical expression:

$$\lambda_{\mathrm{eq}} = 0.3 + 10.8a_v - 16a_v^2 + 14.1a_v^3. \tag{6.12}$$

where a_{v} is the water activity. In order to calculate the value of water activity, the vapor concentration at the GDL-membrane interface should be first computed by solving the static equation as shown in Eq. (6.3).

Assuming the water flux across the anode GDL-membrane interface is continuous,

the vapor flux at anode CL can be calculated from Eq. (6.13).

$$J_{v,AGDL|MEM} = J_{\mathrm{d,AGDL|MEM}} = \left(-D_{\mathrm{d}}\frac{\partial c_{\mathrm{d}}}{\partial x} + n_{\mathrm{d}}J_{\mathrm{p}}\right)_{\mathrm{AGDL|MEM}}. \tag{6.13}$$

There are two water sources at the cathode CL. Water is generated at the cathode CL due to electrochemical reactions at a rate which equal to $I/2F$, and water is transported from the anode CL to the cathode CL through the membrane. The total amount of water present in the cathode CL determines if liquid water will be formed. It is assumed that a phase equilibrium between water vapor and liquid water is established in the cathode CL. If the vapor concentration is lower than saturation water vapor concentration, water exists in vapor form only, and only diffusive flow of water vapor is considered in GDL. On the contrary, when the saturation water vapor concentration is exceeded, water exists in two phases including water vapor and liquid water, and liquid water starts to emerge and floods the GDL. In order to capture the formation of two-phase flow at the cathode CL, two alternative boundary conditions that depend on the vapor concentration at the cathode GDL-membrane interface.

If $c_{\mathrm{v,CGDL-MEM}}$ is smaller than $c_{\mathrm{v}}^{\mathrm{sat}}$, *i.e.*, p^{sat}/RT, single-phase flow is determined

and the corresponding vapor and liquid water fluxes are:

$$J_{v,CGDL|MEM} = J_{\mathrm{d,CGDL|MEM}} + \frac{I}{2F}, \tag{6.14}$$

$$J_{l,CGDL|MEM} = 0. \tag{6.15}$$

Otherwise, two-phase flow is established and the corresponding vapor and liquid water fluxes are:

$$J_{v,CGDL|MEM} = J_{\mathrm{v,max}}, \tag{6.16}$$

$$J_{l,CGDL|MEM} = J_{\mathrm{d,CGDL|MEM}} + \frac{I}{2F} - J_{\mathrm{v,max}}, \tag{6.17}$$

where $J_{\mathrm{v,max}}$ is the maximum diffusive flux of water vapor attained when the saturation water vapor concentration is reached at cathode CL. Moreover, the calculated liquid water flux is used as the boundary condition to calculate the liquid water saturation within the cathode GDL. Another boundary condition is required for solving the liquid water transport equation. In this model, liquid water saturation is assumed to be zero at the cathode GDL-GC interface.

6.5 Cell Voltage

The output voltage of the fuel cell, V_{cell}, can be calculated by subtracting the ohmic overpotential, η_{ohmic}, and activation overpotential, η_{act} from the open-circuit voltage of

fuel cell, $V_{\rm oc}$.

The membrane's conductivity, as expressed by Eq. (3.30), is first determined from the water content calculated from the dissolved water transport equation of the membrane, Eq. (6.4). The ohmic overpotential is then calculated as the following equation:

$$\eta_{\rm ohmic} = \int_0^{l^{\rm m}} \frac{dx}{\sigma_{\rm p}}. \tag{6.18}$$

The activation overpotential is calculated from a modified Butler-Volmer equation proposed by [43] as follows:

$$\eta_{\rm act} = \frac{RT}{0.5F} \ln\left(\frac{I}{i_{\rm ref}} \frac{p_{\rm O_2,ref}}{p_{\rm O_2,CCL}} \frac{1}{1-s}\right). \tag{6.19}$$

The effect of anode activation overpotential due to hydrogen oxidation is neglected in this model since its magnitude is considerably smaller compared to that due to the oxygen reduction at cathode. Finally, the output voltage of fuel cell is computed from:

$$V_{\rm cell} = V_{\rm oc} - \eta_{\rm act} - \eta_{\rm ohmic}. \tag{6.20}$$

6.6 Results and Discussion

In this thesis, we aim to propose an effective water management scheme using inlet relative humidity control. In order to achieve this objective, the proposed two-phase

dynamic PEM fuel cell model should be able to capture the influences of water transport in at least in two aspects. First, the model should be able to predict the influences of inlet relative humidity under static and dynamic conditions; and second, it should be able to model the dynamic response of PEM fuel cell due to the dynamic re-distribution of water within the cell.

In this section, the developed two-phase dynamic PEM fuel cell model is examined from the perspectives of these two aspects. First, the steady polarization curves under various inlet relative humidity are simulated to demonstrate the ability of the proposed model in describing the influences of inlet relative humidity. Secondly, the dynamic responses of PEM fuel cell due to various step changes of current density are simulated to measure the ability of the proposed model in describing the dynamic response of PEM fuel cell.

Table 6.1 shows the operating conditions used in the simulations. All simulations are performed under the conditions of $80\ ^{\circ}\mathrm{C}$, hydrogen stoichiometry of 1.2, air stoichiometry of 2, 1 atm pressure of reactant gases. For validating the steady-state behavior of the proposed model, polarization curves are simulated under various inlet anode and cathode relative humidity values, including 50%, 60%, 70% and 80%, respectively. The base-case conditions used to simulate the dynamic response of PEM fuel cell under step changes of current density are 80% for anode and 60% for cathode. Four step changes of current density with an initial current density of 0.25 A m^{-2} are considered, and the

final current density are 0.7, 0.9, 1.1 and 1.3 A m^{-2}. Under all cases, the parameters used in the simulations are listed in Table 6.2.

Table 6.1: Operating Conditions used in the Simulation.

Inlet condition	Symbol	Value
Inlet operating temperature	T	80 °C
Inlet anode and cathode pressure	$p_{\mathrm{a/c}}$	1 atm
Anode stoichiometry	ζ_{a}	1.2
Cathode stoichiometry	ζ_{c}	2
Anode inlet relative humidity	Θ_{a}	Various (base-case: 80%)
Cathode inlet relative humidity	Θ_{c}	Various (base-case: 60%)

Table 6.2: Structural Parameters used in the Simulation.

Parameter	Value
GDL's porosity, $\varepsilon^{\mathrm{GDL}}$	0.5
GDL's thickness, l^{GDL} $(\mu\mathrm{m})$	250
Membrane's thickness, l^{m} $(\mu\mathrm{m})$	100
Cathodic transfer coefficient for oxygen reduction, α_{c}	0.5
Reference exchange current density, i_{ref} $(\mathrm{A\ m}^{-2})$	20

6.6.1 Effects of RH on Steady-State Polarization Curves

The steady-state polarization curves under various inlet relative humidity are plotted in Figs. 6.1 and 6.2. In each figure, one of the inlet relative humidity is kept constant while the other inlet relative humidity is varied from 50% to 80%.

In Fig. 6.1, it is observed that inlet cathode relative humidity has a significant effect on the polarization curves of PEM fuel cell at high current density, but it has weak influences on the polarization curves at intermediate current density. On the other hand, inlet anode relative humidity has weak influences on the polarization curves at high

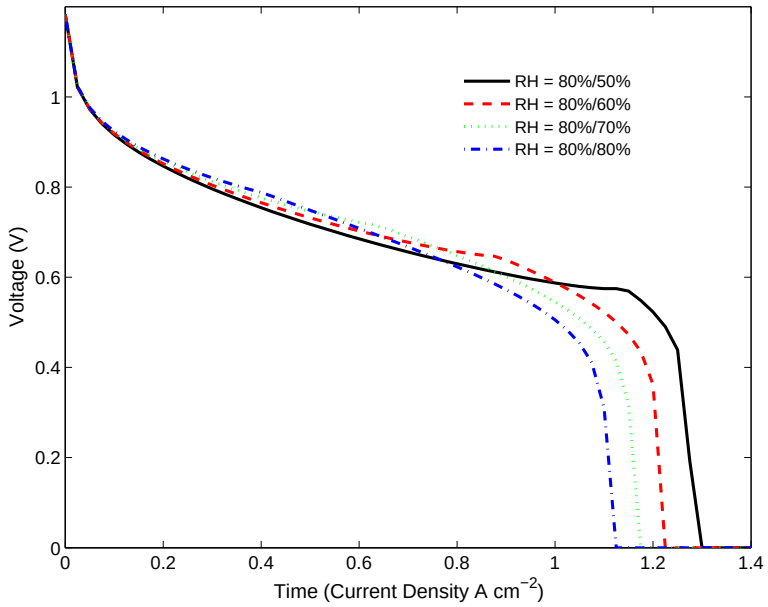

Figure 6.1: Calculated polarization curves under 80% inlet anode relative humidity and various inlet cathode relative humidity.

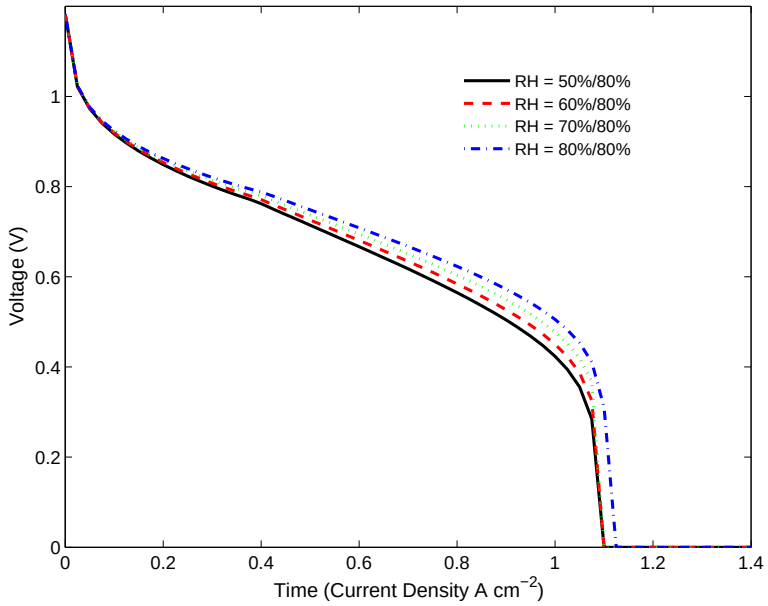

Figure 6.2: Calculated polarization curves under 80% inlet cathode relative humidity and various inlet anode relative humidity.

current density but has a more significant effect on the polarization curves at intermediate current density, as shown in Fig. 6.2. The asymmetrical role of inlet anode and cathode humidification, which is studied in detail in Chapter 5, is also captured in the simplified model with the main difference being the magnitude of their influences of the polarization curves compared to the more sophisticated model discussed in Chap 3 to 5.

6.6.2 Dynamic Responses to Step Changes of Current Density

The voltage undershoot observed during a step increase of load has been studied both experimentally [84] and numerically [85] in the literature, and the authors ascribed the initial undershoot to the time delay due to the water re-distribution in membrane. This general behavior can be considered as a performance indicator to measure the model's ability in describing the dynamic response of PEM fuel cell due to membrane's water transport. In Fig. 6.3, the calculated cell voltage responses of PEM fuel cell under various step changes of current density are plotted. Voltage undershoot is observed immediately after a step change of current density from low to high load, followed by a voltage recovery. As the current density suddenly changes from low to high, the water content of membrane remains virtually unchanged during the current step. The conductivity of membrane remains unchanged but the current density is increased. This causes a higher ohmic overpotential, an undershoot is formed.

The dynamic responses of ohmic overpotential under various step changes of current density are simulated and plotted in Fig. 6.4. It is found that the recovery process of

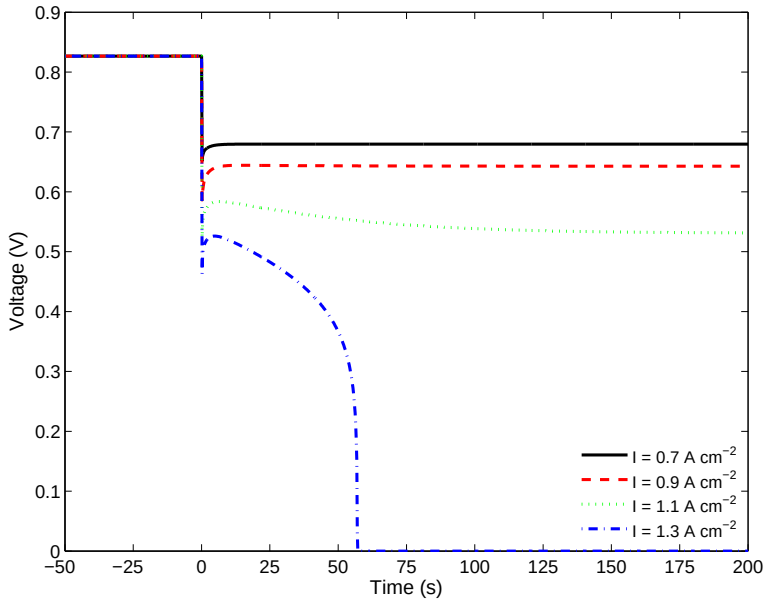

Figure 6.3: Calculated cell voltage response to various step changes of current density. The initial current density are all 0.25 A m^{-2}. The final current density vary from 0.7 to 1.3 A m^{-2}. Other operating conditions are listed in Table 6.1 with the base-case inlet relative humidity.

ohmic overpotential after a step change of current density lasts for several seconds, which is consistent with the time duration from undershoot to voltage recovery as shown in Fig. 6.3. This verifies the model's ability in describing the transient response of membrane's water transport under step changes of current density.

According to Loo *et al.* [85], voltage responses due to step changes can be categorized into four types depending on the liquid water saturation within GDL. Since the characteristic time of liquid water flux in GDL is longer compared to that of membrane's water flux, the liquid water distribution mainly affects the characteristics of voltage recovery after the initial undershoot due to time varying protonic resistivity. In our simulation, four different step changes of current density are considered, and each

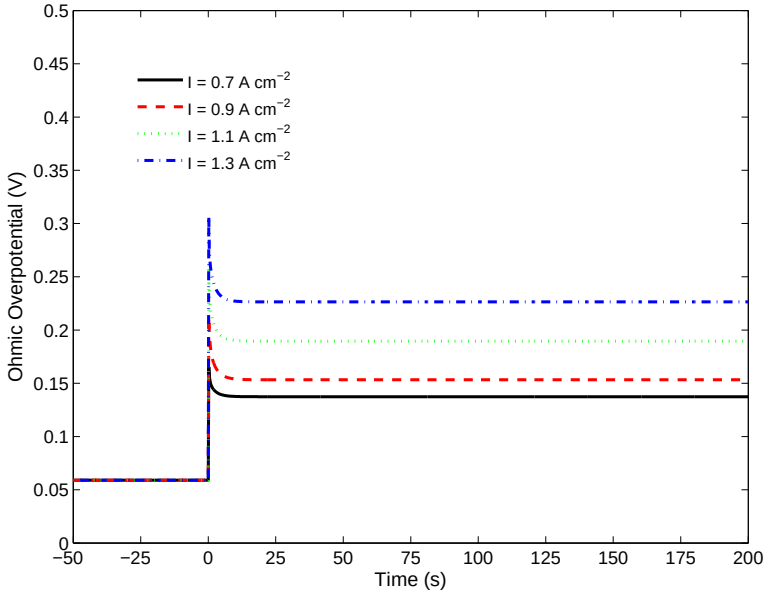

Figure 6.4: Calculated ohmic overpotential under various step changes of current density. The initial current density are all 0.25 A m^{-2}. The final current density vary from 0.7 to 1.3 A m^{-2}. Other operating conditions are listed in Table 6.1 with the base-case inlet relative humidity.

of them, respectively, represents one type of the voltage responses as mentioned.

When the step change of current density is relatively small, *i.e.*, the case of from 0.25 to 0.7 A m^{-2}, the cell voltage experiences an initial undershoot, and then it increases slowly to a maximum value during the voltage recovery process. After reaching the maximum value, voltage remains steady as shown in Fig. 6.3. Since the membrane's water transport solely affects the initial undershoot, it has a negligible effect on the voltage response after the initial undershoot. Moreover, no liquid water is accumulated in GDL due to low final current density, and thus the concentration overpotential remains unchanged (as shown in Fig: 6.5) after the step change of current density.

As the step change of current density is increased to the case of stepping from 0.25

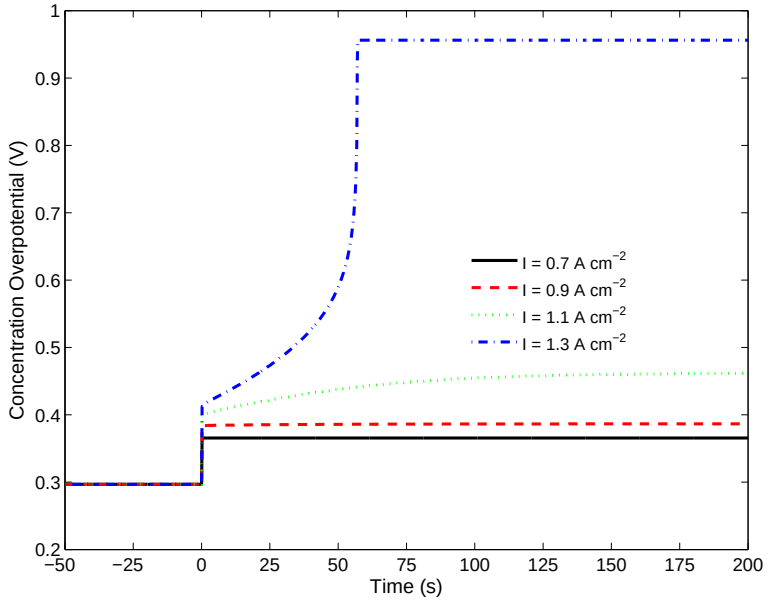

Figure 6.5: Calculated concentration overpotential under various step changes of current density. The initial current density are all 0.25 A m^{-2}. The final current density vary from 0.7 to 1.3 A m^{-2}. Other operating conditions are listed in Table 6.1 with the base-case inlet relative humidity.

to 0.9 A m^{-2}, liquid water starts to form in GDL as shown in Fig. 6.6. However, the level of liquid water is too low to have any dramatic effect on the oxygen transport within GDL, and a steady voltage is still observed after the initial undershoot.

As the step change of current density is further increased to the case of stepping from 0.25 to 1.1 A m^{-2}, an increased degree of water flooding occurs in GDL due to the high water generation rate at CL under high current density. The slow liquid water transport in the GDL gives rise to an overshoot (maximum voltage) followed by a long decay towards the steady-state. From Fig. 6.7, it is observed that the time required for liquid water re-distribution within the GDL is consistent with the slow decay time observed in the voltage response time after the initial undershoot.

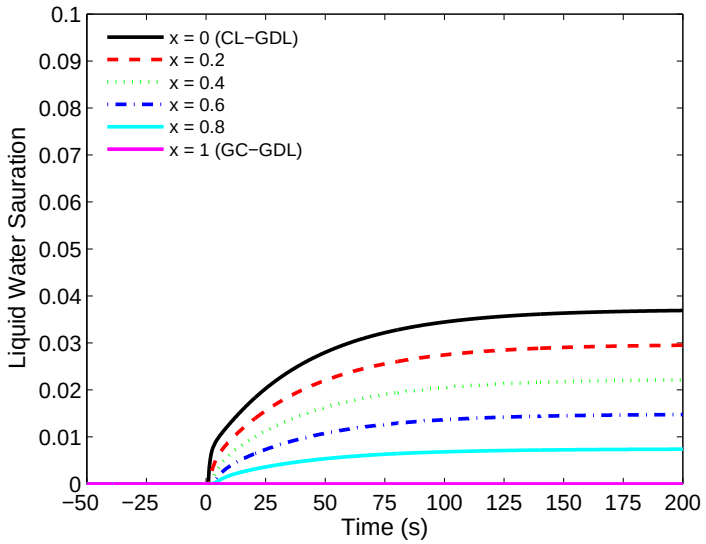

Figure 6.6: Calculated liquid water saturation under step change of current density from 0.25 to 0.9 A m^{-2}. Other operating conditions are listed in Table 6.1 with the base-case inlet relative humidity.

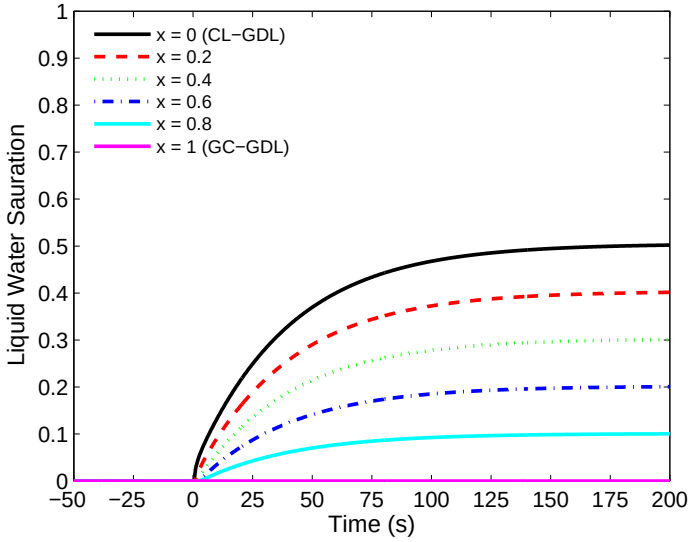

Figure 6.7: Calculated liquid water saturation under step change of current density from 0.25 to 1.1 A m^{-2}. Other operating conditions are listed in Table 6.1 with the base-case inlet relative humidity.

When the step change of current density is finally increased to the case of stepping from 0.25 to 1.3 $\mathrm{A\ m^{-2}}$, the water generation rate is further increased and the GDL is severely flooded. As shown in Fig. 6.8, the liquid water saturation keeps increasing after the step change of current density and reaches to a level where zero oxygen concentration is resulted at CL as shown in Fig. 6.9. First, the cell voltage increases to the maximum value due to the reduction of ohmic overpotnatial. Then, the cell voltage has a long decay and finally reaches zero because of the zero oxygen concentration at CL.

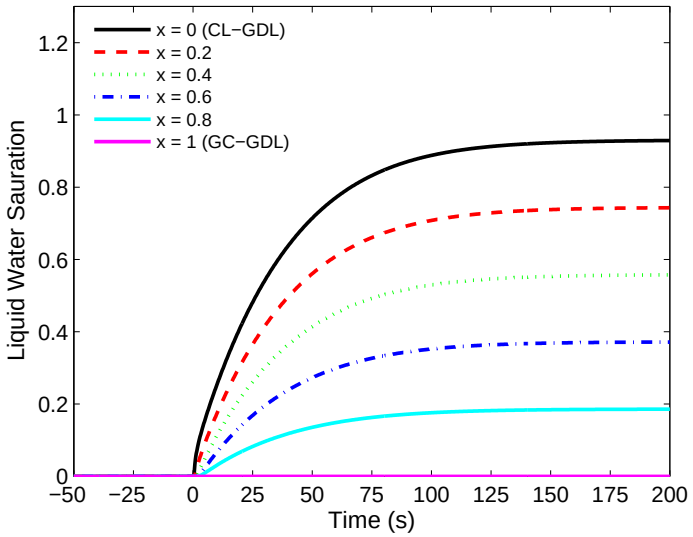

Figure 6.8: Calculated liquid water saturation under step change of current density from 0.25 to 1.3 $\mathrm{A\ m^{-2}}$. Other operating conditions are listed in Table 6.1 with the base-case inlet relative humidity.

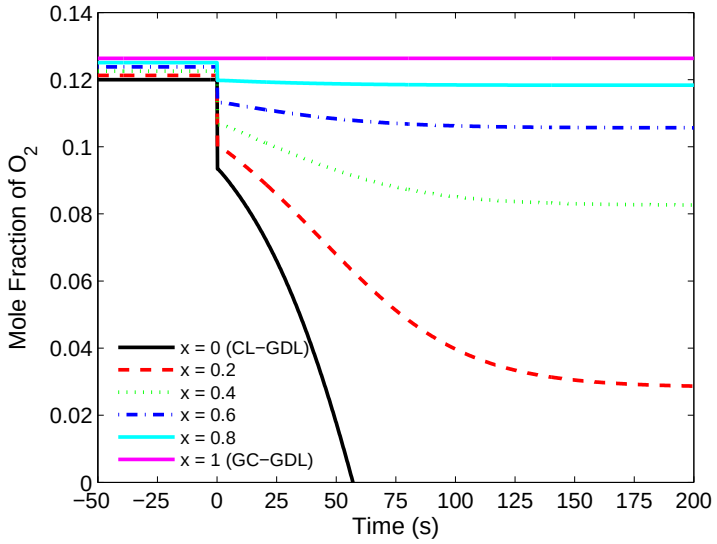

Figure 6.9: Calculated mole fraction of oxygen under step change of current density from 0.25 to 1.3 A m^{-2}. Other operating conditions are listed in Table 6.1 with the base-case inlet relative humidity.

Chapter 7

Conclusions

A balanced water distribution is typically required for a better utilization and performance of PEM fuel cell. It is also mandatory for enhancing the durability of PEM fuel cell by preventing the irreversible damages due to the improper water distribution. This is often achieved through water management design, which can be categorized into two types, namely active and passive water management schemes. The former aims to control the water distribution according to the operating conditions of PEM fuel cell, while the latter aims to utilize structural and material designs for achieving a balanced water distribution.

A real-time control of water distribution is not necessary when passive water management scheme is employed. However, a passive control of water distribution is not likely to guarantee a balanced water distribution under all operating conditions since the water distribution is inherently restricted by the operating conditions of PEM fuel

cell. On the contrary, an active water management provides a more flexible control over the water distribution by adjusting the inlet operating conditions of PEM fuel cell. This advantage of active water management scheme has initiated a numerical study of the influences of inlet operating conditions on the performance of PEM fuel cell as presented in this thesis.

A computational efficient two-phase GC model is derived in Chapter 4 in order to correlate the liquid water flooding in GC to the inlet operating conditions. This proposed model is then coupled to the MEA model presented in Chapter 3 to develop a steady-state pseudo two-dimensional two-phase PEM fuel cell model as a fundamental framework for analyzing the role of inlet operating conditions. The effects of inlet cathode operating pressure, inlet air flow rate and inlet cathode relative humidity are studied, and it is found that all inlet operating conditions affect the water distribution and the performance of PEM fuel cell. This simulated results show that the inlet operating conditions can act as effective control parameters for achieving a balanced water distribution in PEM fuel cell and optimizing its performance.

Although the inlet operating pressure and flow rate can have influences on the performance of PEM fuel cell, inlet relative humidity control is the most attractive control parameter because less power is consumed by this control approach. The influences of the inlet relative humidity at anode and cathode are thus systematically investigated by simulating the polarization curves under various combinations of inlet anode and

cathode humidification and air stoichiometry conditions. In this investigation, a general trend is observed, where it is found that the influences of the inlet relative humidity at anode and cathode are highly asymmetrical due to the properties of membrane and the water formation at cathode. Inlet anode humidification mainly affects the membrane's conductivity while inlet cathode humidification mainly influences the level of liquid water saturation at the cathode. Under the operating conditions being studied, it is concluded that a high inlet anode humidification tends to give rise to a smaller ohmic overpotential and a low cathode humidification tends to reduce the concentration overpotential. Therefore, a fully humidified anode and dry cathode are generally preferred for maximizing the output power density of PEM fuel cell by means of achieving a good protonic conduction and an unimpeded diffusion of reactant gases, in particular the diffusion of oxygen, simultaneously. However, if a high air flow rate is employed, the inlet cathode humidification should be adjusted to an intermediate value to prevent the dehydration of membrane so that a high output power density can be maintained. Finally, the usefulness of inlet relative humidity control as a simple and effective method for optimizing PEM fuel cell's performance has been demonstrated theoretically by using two examples, in which the use of inlet relative humidity control for maximizing the power density (in static condition) and extending the operating range (in moving-static condition) of PEM fuel cell have been presented.

In a PEM fuel cell system, inlet relative control of the fuel cell must be realized dy-

namically due to the time-varying loading condition, hence a two-phase dynamic PEM fuel cell model is required. Specifically, a fast model is desired due to the fact that various auxiliary components are included in the PEM fuel cell system. The derivation of a fast two-phase dynamic PEM fuel cell model is presented in this thesis. In the proposed model, the dynamic responses of the water content in membrane and the liquid water saturation in GDL are considered, while the concentration of reactant gases are assumed to be in steady state. This assumption is based on the fact that the transient responses of the water content and the liquid water saturation have significantly larger characteristic time constants compared to the concentration of reactant gases. This treatment decouples the governing equations that describe the liquid water saturation and the concentration of reactant gases, so a shorter computational time can be achieved. Steady-state polarization curves under various combinations of inlet relative humidity at anode and cathode are simulated using the fast model, it is shown that the asymmetrical influences of the inlet relative humidity at anode and cathode can be captured in the fast model. Moreover, the dynamic responses of PEM fuel cell due to step changes of current density are simulated. It is observed that the general trends of the influences on the PEM fuel cell's performance due to the re-distribution of water in membrane and liquid water saturation in GDL can be realistically captured.

7.1 Future Work

In this thesis, the feasibility of optimizing PEM fuel cell's performance by means of inlet relative humidity control has been examined. However, its practical implementation in a PEM fuel cell system has not yet been discussed. For this purpose, an effective control of the inlet relative humidity of reactant gases should be proposed. The first step to achieve the effective control should be the development of the model of humidifiers, and it should be suitable for integration with the two-phase dynamic PEM fuel cell model presented in Chapter 6.

The primary interest of the present work is to optimize the performance of PEM fuel cell by means of inlet relative humidity control. Furthermore, an actively controlled external humidification has the potential to extend the lifetime of PEM fuel cell since a balanced water distribution can prevent irreversible damages to the mechanical parts as a result of dehydration and flooding. A recommended approach to begin these studies is to develop a PEM fuel cell's degradation model to capture these effects, and to understand the role of inlet relative humidity on the physics of PEM fuel cell's degradation.

References

[1] J. Larminie and A. Dicks. *Fuel Cell Systems Explained*. Wiley, 2003.

[2] X. Li. *Principles of Fuel Cells*. Taylor & Francis, 2006.

[3] M.M. Mench. *Fuel Cell Engines*. Wiley, 2008.

[4] J. Marcinkoski, J.P. Kopasz, and T.G. Benjamin. Progress in the US DOE fuel cell subprogram efforts in polymer electrolyte fuel cells. *International Journal of Hydrogen Energy*, 33(14):3894 – 3902, 2008.

[5] A. Heinzel, C. Hebling, M. Müller, M. Zedda, and C. Müller. Fuel cells for low power applications. *Journal of Power Sources*, 105(2):250–255, 2002.

[6] K. Tüber, M. Zobel, H. Schmidt, and C. Hebling. A polymer electrolyte membrane fuel cell system for powering portable computers. *Journal of Power Sources*, 122(1):1–8, 2003.

[7] T. Ito, S. Kaneko, and M. Kunimatsu. Fabrication and characterization of a thin μ PEMFC with microfabricated grooves on electroformed current collector plate. *Electrochemical and Solid-State Letters*, 12(11):B154–B157, 2009.

[8] Y. Wang, L. Pham, G.P.S. de Vasconcellos, and M. Madou. Fabrication and characterization of micro PEM fuel cells using pyrolyzed carbon current collector plates. *Journal of Power Sources*, 195(15):4796 – 4803, 2010.

[9] P. Beckhaus, M. Dokupil, A. Heinzel, S. Souzani, and C. Spitta. On-board fuel cell power supply for sailing yachts. *Journal of Power Sources*, 145(2):639–643, 2005.

[10] K. Haraldsson, A. Folkesson, and P. Alvfors. Fuel cell buses in the Stockholm CUTE project–First experiences from a climate perspective. *Journal of Power Sources*, 145(2):620–631, 2005.

[11] M. Saxe, A. Folkesson, and P. Alvfors. A follow-up and conclusive report on the attitude towards hydrogen fuel cell buses in the CUTE project–from passengers in Stockholm to bus operators in Europe. *International Journal of Hydrogen Energy*, 32(17):4295–4305, 2007.

[12] M. Saxe, A. Folkesson, and P. Alvfors. Energy system analysis of the fuel cell buses operated in the project: Clean Urban Transport for Europe. *Energy*, 33(5):689–711, 2008.

[13] X. Li, J. Li, L. Xu, F. Yang, J. Hua, and M. Ouyang. Performance analysis of proton-exchange membrane fuel cell stacks used in Beijing urban-route buses trial project. *International Journal of Hydrogen Energy*, 35(8):3841–3847, 2010.

[14] K. Kendall, B.G. Pollet, A. Dhir, I. Staffell, B. Millington, and J. Jostins. Hydrogen fuel cell hybrid vehicles (HFCHV) for Birmingham campus. *Journal of Power Sources*, 196(1):325–330, 2011.

[15] G. Gigliucci, L. Petruzzi, E. Cerelli, A. Garzisi, and A. La Mendola. Demonstration of a residential CHP system based on PEM fuel cells. *Journal of Power Sources*, 131(1-2):62–68, 2004.

[16] M.T. Gencoglu and Z. Ural. Design of a PEM fuel cell system for residential application. *International Journal of Hydrogen Energy*, 34(12):5242–5248, 2009.

[17] E.M. Stewart, A.E. Lutz, S. Schoenung, M. Chiesa, J.O. Keller, J. Fletcher, G. Ault, J. McDonald, and A. Cruden. Modeling, analysis and control system development for the Italian hydrogen house. *International Journal of Hydrogen Energy*, 34(4):1638 – 1646, 2009.

[18] J.J. Hwang and M.L. Zou. Development of a proton exchange membrane fuel cell cogeneration system. *Journal of Power Sources*, 195(9):2579–2585, 2010.

[19] Ø. Ulleberg, T. Nakken, and A. Eté. The wind/hydrogen demonstration system at Utsira in Norway: Evaluation of system performance using operational data

and updated hydrogen energy system modeling tools. *International Journal of Hydrogen Energy*, 35(5):1841 – 1852, 2010.

[20] M.S. Yazici. UNIDO-ICHET support to hydrogen and fuel cell technologies in Turkey. *International Journal of Hydrogen Energy*, In Press, Corrected Proof, 2011.

[21] P. Costamagna and S. Srinivasan. Quantum jumps in the PEMFC science and technology from the 1960s to the year 2000: Part I. Fundamental scientific aspects. *Journal of Power Sources*, 102(1-2):242–252, 2001.

[22] D.E. Curtin, R.D. Lousenberg, T.J. Henry, P.C. Tangeman, and M.E. Tisack. Advanced materials for improved PEMFC performance and life. *Journal of Power Sources*, 131(1-2):41–48, 2004.

[23] S.D. Knights, K.M. Colbow, J. St-Pierre, and D.P. Wilkinson. Aging mechanisms and lifetime of PEFC and DMFC. *Journal of Power Sources*, 127(1-2):127–134, 2004.

[24] E. Endoh, S. Terazono, H. Widjaja, and Y. Takimoto. Degradation study of MEA for PEMFCs under low humidity conditions. *Electrochemical and Solid-State Letters*, 7(7):A209–A211, 2004.

[25] J. Yu, T. Matsuura, Y. Yoshikawa, M. N. Islam, and M. Hori. In situ analysis of performance degradation of a PEMFC under nonsaturated humidification. *Electrochemical and Solid-State Letters*, 8(3):A156–A158, 2005.

[26] X. Huang, R. Solasi, Y. Zou, M. Feshler, K. Reifsnider, D. Condit, S. Burlatsky, and T. Madden. Mechanical endurance of polymer electrolyte membrane and PEM fuel cell durability. *Journal of Polymer Science Part B: Polymer Physics*, 44(16):2346–2357, 2006.

[27] M. Gummalla, V.V. Atrazhev, D. Condit, N. Cipollini, T. Madden, N.Y. Kuzminyh, D. Weiss, and S.F. Burlatsky. Degradation of polymer-electrolyte membranes in fuel cells. *Journal of The Electrochemical Society*, 157(11):B1542–B1548, 2010.

[28] S. Basu, J. Li, and C.Y. Wang. Two-phase flow and maldistribution in gas channels of a polymer electrolyte fuel cell. *Journal of Power Sources*, 187(2):431 – 443, 2009.

[29] S. Basu, C.Y. Wang, and K.S. Chen. Two-phase flow maldistribution and mitigation in polymer electrolyte fuel cells. *Journal of Fuel Cell Science and Technology*, 6(3):031007, 2009.

[30] A. Taniguchi, T. Akita, K. Yasuda, and Y. Miyazaki. Analysis of degradation in PEMFC caused by cell reversal during air starvation. *International Journal of*

Hydrogen Energy, 33(9):2323–2329, 2008.

[31] A. Taniguchi, T. Akita, K. Yasuda, and Y. Miyazaki. Analysis of electrocatalyst degradation in PEMFC caused by cell reversal during fuel starvation. *Journal of Power Sources*, 130(1-2):42–49, 2004.

[32] Q. Yan, H. Toghiani, Y.W. Lee, K. Liang, and H. Causey. Effect of sub-freezing temperatures on a PEM fuel cell performance, startup and fuel cell components. *Journal of Power Sources*, 160(2):1242–1250, 2006.

[33] T.V. Nguyen and R.E. White. A water and heat management model for proton-exchange-membrane fuel cells. *Journal of The Electrochemical Society*, 140(8):2178–2186, 1993.

[34] J.H. Nam and M. Kaviany. Effective diffusivity and water-saturation distribution in single- and two-layer PEMFC diffusion medium. *International Journal of Heat and Mass Transfer*, 46(24):4595–4611, 2003.

[35] U. Pasaogullari and C.Y. Wang. Two-phase transport and the role of micro-porous layer in polymer electrolyte fuel cells. *Electrochimica Acta*, 49(25):4359 – 4369, 2004.

[36] U. Pasaogullari, C.Y. Wang, and K.S. Chen. Two-phase transport in polymer electrolyte fuel cells with bilayer cathode gas diffusion media. *Journal of The Electrochemical Society*, 152(8):A1574–A1582, 2005.

[37] A.Z. Weber and J. Newman. Effects of microporous layers in polymer electrolyte fuel cells. *Journal of The Electrochemical Society*, 152(4):A677–A688, 2005.

[38] Z. Zhan, J. Xiao, D. Li, M. Pan, and R. Yuan. Effects of porosity distribution variation on the liquid water flux through gas diffusion layers of PEM fuel cells. *Journal of Power Sources*, 160(2):1041–1048, 2006.

[39] Z. Zhan, J. Xiao, Y. Zhang, M. Pan, and R. Yuan. Gas diffusion through differently structured gas diffusion layers of PEM fuel cells. *International Journal of Hydrogen Energy*, 32(17):4443–4451, 2007.

[40] W. Shi, E. Kurihara, and N. Oshima. Effect of capillary pressure on liquid water removal in the cathode gas diffusion layer of a polymer electrolyte fuel cell. *Journal of Power Sources*, 182(1):112 – 118, 2008.

[41] T.V. Nguyen. A gas distributor design for proton-exchange-membrane fuel cells. *Journal of The Electrochemical Society*, 143(5):L103–L105, 1996.

[42] J.S. Yi and T.V. Nguyen. Multicomponent transport in porous electrodes of proton exchange membrane fuel cells using the interdigitated gas distributors. *Journal of The Electrochemical Society*, 146(1):38–45, 1999.

[43] W. He, J.S. Yi, and T.V. Nguyen. Two-phase flow model of the cathode of PEM fuel cells using interdigitated flow fields. *AIChE Journal*, 46(10):2053–2064, 2000.

[44] X.D. Wang, Y.Y. Duan, and W.M. Yan. Numerical study of cell performance and local transport phenomena in PEM fuel cells with various flow channel area ratios. *Journal of Power Sources*, 172(1):265 – 277, 2007.

[45] A.D. Le and B. Zhou. A generalized numerical model for liquid water in a proton exchange membrane fuel cell with interdigitated design. *Journal of Power Sources*, 193(2):665 – 683, 2009.

[46] F.N. Buchi and S. Srinivasan. Operating proton exchange membrane fuel cells without external humidification of the reactant gases. *Journal of The Electrochemical Society*, 144(8):2767–2772, 1997.

[47] M.V. Williams, H.R. Kunz, and J.M. Fenton. Operation of Nafion based PEM fuel cells with no external humidification: Influence of operating conditions and gas diffusion layers. *Journal of Power Sources*, 135(1-2):122–134, 2004.

[48] J. Zhang, Y. Tang, C. Song, X. Cheng, J. Zhang, and H. Wang. PEM fuel cells operated at 0% relative humidity in the temperature range of 23-120 ^{0}C. *Electrochimica Acta*, 52(15):5095–5101, 2007.

[49] X.G. Yang, N. Burke, C.Y. Wang, K. Tajiri, and K. Shinohara. Simultaneous measurements of species and current distributions in a PEFC under low-humidity operation. *Journal of The Electrochemical Society*, 152(4):A759–A766, 2005.

[50] H. Yu and C. Ziegler. Transient behavior of a proton exchange membrane fuel cell under dry operation. *Journal of The Electrochemical Society*, 153(3):A570–A575, 2006.

[51] M. Watanabe, H. Uchida, Y. Seki, M. Emori, and P. Stonehart. Self-humidifying polymer electrolyte membranes for fuel cells. *Journal of The Electrochemical Society*, 143(12):3847–3852, 1996.

[52] M. Watanabe, H. Uchida, and M. Emori. Analyses of self-humidification and suppression of gas crossover in Pt-dispersed polymer electrolyte membranes for fuel cells. *Journal of The Electrochemical Society*, 145(4):1137–1141, 1998.

[53] T.H. Yang, Y.G. Yoon, C.S. Kim, S.H. Kwak, and K.H. Yoon. A novel preparation method for a self-humidifying polymer electrolyte membrane. *Journal of Power Sources*, 106(1-2):328–332, 2002.

[54] H. Hagihara, H. Uchida, and M. Watanabe. Preparation of highly dispersed SiO2 and Pt particles in Nafion® 112 for self-humidifying electrolyte membranes in fuel cells. *Electrochimica Acta*, 51(19):3979–3985, 2006.

[55] S.H. Kwak, T.H. Yang, C.S. Kim, and K.H. Yoon. The effect of platinum loading in the self-humidifying polymer electrolyte membrane on water uptake. *Journal of Power Sources*, 118(1-2):200 – 204, 2003.

[56] M. Han, S.H. Chan, and S.P. Jiang. Investigation of self-humidifying anode in polymer electrolyte fuel cells. *International Journal of Hydrogen Energy*, 32(3):385–391, 2007.

[57] H. Su, L. Xu, H. Zhu, Y. Wu, L. Yang, S. Liao, H. Song, Z. Liang, and V. Birss. Self-humidification of a PEM fuel cell using a novel Pt/SiO2/C anode catalyst. *International Journal of Hydrogen Energy*, 35(15):7874 – 7880, 2010.

[58] Z. Qi and A. Kaufman. PEM fuel cell stacks operated under dry-reactant conditions. *Journal of Power Sources*, 109(2):469–476, 2002.

[59] W.H.J. Hogarth and J.B. Benziger. Operation of polymer electrolyte membrane fuel cells with dry feeds: Design and operating strategies. *Journal of Power Sources*, 159(2):968–978, 2006.

[60] S.H. Ge, X.G. Li, and I.M. Hsing. Water management in PEMFCs using absorbent wicks. *Journal of The Electrochemical Society*, 151(9):B523–B528, 2004.

[61] S. Ge, X. Li, and I.M. Hsing. Internally humidified polymer electrolyte fuel cells using water absorbing sponge. *Electrochimica Acta*, 50(9):1909–1916, 2005.

[62] S. Litster and J.G. Santiago. Dry gas operation of proton exchange membrane fuel cells with parallel channels: Non-porous versus porous plates. *Journal of Power Sources*, 188(1):82–88, 2009.

[63] R. Huizing, M. Fowler, W. Merida, and J. Dean. Design methodology for membrane-based plate-and-frame fuel cell humidifiers. *Journal of Power Sources*, 180(1):265–275, 2008.

[64] D. Kadylak and W. Merida. Experimental verification of a membrane humidifier model based on the effectiveness method. *Journal of Power Sources*, 195(10):3166–3175, 2010.

[65] S.K. Park, S.Y. Choe, and S.H. Choi. Dynamic modeling and analysis of a shell-and-tube type gas-to-gas membrane humidifier for pem fuel cell applications. *International Journal of Hydrogen Energy*, 33(9):2273 – 2282, 2008.

[66] S. Kang, K. Min, and S. Yu. Two dimensional dynamic modeling of a shell-and-tube water-to-gas membrane humidifier for proton exchange membrane fuel cell. *International Journal of Hydrogen Energy*, 35(4):1727–1741, 2010.

[67] S. Park and I.H. Oh. An analytical model of Nafion^{TM} membrane humidifier for proton exchange membrane fuel cells. *Journal of Power Sources*, 188(2):498–501, 2009.

[68] D. Chen and H. Peng. A thermodynamic model of membrane humidifiers for PEM fuel cell humidification control. *Journal of Dynamic Systems, Measurement, and Control*, 127(3):424–432, 2005.

[69] D. Natarajan and T.V. Nguyen. A two-dimensional, two-phase, multicomponent, transient model for the cathode of a proton exchange membrane fuel cell using conventional gas distributors. *Journal of The Electrochemical Society*, 148(12):A1324–A1335, 2001.

[70] D. Natarajan and T.V. Nguyen. Three-dimensional effects of liquid water flooding in the cathode of a PEM fuel cell. *Journal of Power Sources*, 115(1):66 – 80, 2003.

[71] C.I. Lee and H.S. Chu. Effects of cathode humidification on the gas-liquid interface location in a PEM fuel cell. *Journal of Power Sources*, 161(2):949 – 956, 2006.

[72] A.A. Shah, G.S. Kim, W. Gervais, A. Young, K. Promislow, J. Li, and S. Ye. The effects of water and microstructure on the performance of polymer electrolyte fuel cells. *Journal of Power Sources*, 160(2):1251 – 1268, 2006.

[73] M.M. Saleh, T. Okajima, M. Hayase, F. Kitamura, and T. Ohsaka. Exploring the effects of symmetrical and asymmetrical relative humidity on the performance of H_2/air PEM fuel cell at different temperatures. *Journal of Power Sources*, 164(2):503–509, 2007.

[74] F. Urbani, O. Barbera, G. Giacoppo, G. Squadrito, and E. Passalacqua. Effect of operative conditions on a pefc stack performance. *International Journal of*

Hydrogen Energy, 33(12):3137 – 3141, 2008.

[75] I.S. Hussaini and C.Y. Wang. Dynamic water management of polymer electrolyte membrane fuel cells using intermittent RH control. *Journal of Power Sources*, 195(12):3822–3829, 2010.

[76] C.H. Min. A novel three-dimensional, two-phase and non-isothermal numerical model for proton exchange membrane fuel cell. *Journal of Power Sources*, 195(7):1880 – 1887, 2010.

[77] J. Golbert and D.R. Lewin. Model-based control of fuel cells: (1) Regulatory control. *Journal of Power Sources*, 135(1-2):135 – 151, 2004.

[78] K.C. Lauzze and D.J. Chmielewski. Power control of a polymer electrolyte membrane fuel cell. *Industrial & Engineering Chemistry Research*, 45(13):4661–4670, 2006.

[79] C. Ziegler, H.M. Yu, and J.O. Schumacher. Two-phase dynamic modeling of PEMFCs and simulation of cyclo-voltammograms. *Journal of The Electrochemical Society*, 152(8):A1555–A1567, 2005.

[80] A.A. Shah, G.S. Kim, P.C. Sui, and D. Harvey. Transient non-isothermal model of a polymer electrolyte fuel cell. *Journal of Power Sources*, 163(2):793–806, 2007.

[81] D. Gerteisen, T. Heilmann, and C. Ziegler. Modeling the phenomena of dehydration and flooding of a polymer electrolyte membrane fuel cell. *Journal of Power Sources*, 187(1):165–181, 2009.

[82] H. Meng. Numerical investigation of transient responses of a PEM fuel cell using a two-phase non-isothermal mixed-domain model. *Journal of Power Sources*, 171(2):738 – 746, 2007.

[83] Y. Wang and C.Y. Wang. Two-phase transients of polymer electrolyte fuel cells. *Journal of The Electrochemical Society*, 154(7):B636–B643, 2007.

[84] J. Cho, H.S. Kim, and K. Min. Transient response of a unit proton-exchange membrane fuel cell under various operating conditions. *Journal of Power Sources*, 185(1):118–128, 2008.

[85] K.H. Loo, K.H. Wong, S.C. Tan, Y.M. Lai, and C.K. Tse. Characterization of the dynamic response of proton exchange membrane fuel cells - A numerical study. *International Journal of Hydrogen Energy*, 35(21):11861 – 11877, 2010.

[86] M. Grötsch and M. Mangold. A two-phase PEMFC model for process control purposes. *Chemical Engineering Science*, 63(2):434 – 447, 2008.

[87] B.A. McCain, A.G. Stefanopoulou, and I.V. Kolmanovsky. On the dynamics and control of through-plane water distributions in PEM fuel cells. *Chemical Engineering Science*, 63(17):4418 – 4432, 2008.

[88] B.A. McCain, A.G. Stefanopoulou, and I.V. Kolmanovsky. A dynamic semi-analytic channel-to-channel model of two-phase water distribution for a unit fuel cell. *Control Systems Technology, IEEE Transactions on*, 17(5):1055 –1068, 2009.

[89] H. Meng. Multi-dimensional liquid water transport in the cathode of a PEM fuel cell with consideration of the micro-porous layer (MPL). *International Journal of Hydrogen Energy*, 34(13):5488 – 5497, 2009.

[90] S.S. Hsieh, B.S. Her, and Y.J. Huang. Effect of pressure drop in different flow fields on water accumulation and current distribution for a micro pem fuel cell. *Energy Conversion and Management*, 52(2):975 – 982, 2011.

[91] Z.H. Wang, C.Y. Wang, and K.S. Chen. Two-phase flow and transport in the air cathode of proton exchange membrane fuel cells. *Journal of Power Sources*, 94(1):40–50, 2001.

[92] U. Pasaogullari and C.Y. Wang. Liquid water transport in gas diffusion layer of polymer electrolyte fuel cells. *Journal of The Electrochemical Society*, 151(3):A399–A406, 2004.

[93] T. Berning and N. Djilali. A 3D, multiphase, multicomponent model of the cathode and anode of a PEM fuel cell. *Journal of The Electrochemical Society*, 150(12):A1589–A1598, 2003.

[94] U. Pasaogullari and C.Y. Wang. Two-phase modeling and flooding prediction of polymer electrolyte fuel cells. *Journal of The Electrochemical Society*, 152(2):A380–A390, 2005.

[95] P. Quan, B. Zhou, A. Sobiesiak, and Z. Liu. Water behavior in serpentine microchannel for proton exchange membrane fuel cell cathode. *Journal of Power Sources*, 152:131 – 145, 2005.

[96] K. Jiao, B. Zhou, and P. Quan. Liquid water transport in parallel serpentine channels with manifolds on cathode side of a PEM fuel cell stack. *Journal of Power Sources*, 154(1):124 – 137, 2006.

[97] K. Jiao, B. Zhou, and P. Quan. Liquid water transport in straight micro-parallel-channels with manifolds for PEM fuel cell cathode. *Journal of Power Sources*, 157(1):226 – 243, 2006.

[98] X. Zhu, P.C. Sui, and N. Djilali. Dynamic behaviour of liquid water emerging from a gdl pore into a pemfc gas flow channel. *Journal of Power Sources*, 172(1):287 – 295, 2007.

[99] X. Zhu, P.C. Sui, and N. Djilali. Three-dimensional numerical simulations of water droplet dynamics in a pemfc gas channel. *Journal of Power Sources*, 181(1):101 – 115, 2008.

[100] A.D. Le and B. Zhou. A general model of proton exchange membrane fuel cell. *Journal of Power Sources*, 182(1):197 – 222, 2008.

[101] A.D. Le and B. Zhou. Fundamental understanding of liquid water effects on the performance of a PEMFC with serpentine-parallel channels. *Electrochimica Acta*, 54(8):2137 – 2154, 2009.

[102] N.P. Siegel, M.W. Ellis, D.J. Nelson, and M.R. von Spakovsky. A two-dimensional computational model of a pemfc with liquid water transport. *Journal of Power Sources*, 128(2):173 – 184, 2004.

[103] G. Lin, W. He, and T.V. Nguyen. Modeling liquid water effects in the gas diffusion and catalyst layers of the cathode of a PEM fuel cell. *Journal of The Electrochemical Society*, 151(12):A1999–A2006, 2004.

[104] Q. Ye and T.V. Nguyen. Three-dimensional simulation of liquid water distribution in a PEMFC with experimentally measured capillary functions. *Journal of The Electrochemical Society*, 154(12):B1242–B1251, 2007.

[105] X. Wang and T.V. Nguyen. Modeling the effects of capillary property of porous media on the performance of the cathode of a PEMFC. *Journal of The Electrochemical Society*, 155(11):B1085–B1092, 2008.

[106] S.M. Chang and H.S. Chu. A transient model of PEM fuel cells based on a spherical thin film-agglomerate approach. *Journal of Power Sources*, 172(2):790–798, 2007.

[107] A.Z. Weber, R.M. Darling, and J. Newman. Modeling two-phase behavior in PEFCs. *Journal of The Electrochemical Society*, 151(10):A1715–A1727, 2004.

[108] D. Song, Q. Wang, Z.S. Liu, and C. Huang. Transient analysis for the cathode gas diffusion layer of PEM fuel cells. *Journal of Power Sources*, 159(2):928–942, 2006.

[109] H. Ju. Analyzing the effects of immobile liquid saturation and spatial wettability variation on liquid water transport in diffusion media of polymer electrolyte fuel cells (pefcs). *Journal of Power Sources*, 185(1):55 – 62, 2008.

[110] Y. Wang, S. Basu, and C.Y. Wang. Modeling two-phase flow in PEM fuel cell channels. *Journal of Power Sources*, 179(2):603 – 617, 2008.

[111] V.P. Schulz, J. Becker, A. Wiegmann, P.P. Mukherjee, and C.Y. Wang. Modeling of two-phase behavior in the gas diffusion medium of pefcs via full morphology approach. *Journal of The Electrochemical Society*, 154(4):B419–B426, 2007.

[112] P.K. Sinha and C.Y. Wang. Pore-network modeling of liquid water transport in gas diffusion layer of a polymer electrolyte fuel cell. *Electrochimica Acta*, 52(28):7936 – 7945, 2007.

[113] B. Markicevic, A. Bazylak, and N. Djilali. Determination of transport parameters for multiphase flow in porous gas diffusion electrodes using a capillary network model. *Journal of Power Sources*, 171(2):706 – 717, 2007.

[114] J.T. Gostick, M.A. Ioannidis, M.W. Fowler, and M.D. Pritzker. Pore network modeling of fibrous gas diffusion layers for polymer electrolyte membrane fuel cells. *Journal of Power Sources*, 173(1):277 – 290, 2007.

[115] P.K. Sinha and C.Y. Wang. Liquid water transport in a mixed-wet gas diffusion layer of a polymer electrolyte fuel cell. *Chemical Engineering Science*, 63(4):1081 – 1091, 2008.

[116] O. Chapuis, M. Prat, M. Quintard, E. Chane-Kane, O. Guillot, and N. Mayer. Two-phase flow and evaporation in model fibrous media: Application to the gas diffusion layer of PEM fuel cells. *Journal of Power Sources*, 178(1):258 – 268, 2008.

[117] K.J. Lee, J.H. Nam, and C.J. Kim. Pore-network analysis of two-phase water transport in gas diffusion layers of polymer electrolyte membrane fuel cells. *Electrochimica Acta*, 54(4):1166 – 1176, 2009.

[118] K.J. Lee, J.H. Nam, and C.J. Kim. Steady saturation distribution in hydrophobic gas-diffusion layers of polymer electrolyte membrane fuel cells: A pore-network study. *Journal of Power Sources*, 195(1):130 – 141, 2010.

[119] F.P. Incropera and D.P. Dewitt. *Fundamentals of Heat and Mass Transfer*. John Wiley & Sons, 1990.

[120] D.R. Lide and W.M. Haynes. *CRC Handbook of Chemistry and Physics*. The CRC Press, 2010.

[121] T.V. Nguyen and W. He. *Ch.8 of Vol. 3 of Handbook of Fuel Cell-Fundamentals, Technology and Applications*. John Wiley & Sons, 2003.

[122] R.B. Bird, W.E. Stewart, and E.N. Lightfoot. *Transport Phenomena*. John Wiley & Sons, 1960.

[123] D.M. Bernardi and M.W. Verbrugge. Mathematical model of a gas diffusion electrode bonded to a polymer electrolyte. *AIChE Journal*, 37(8):1151–1163, 1991.

[124] J.C. Amphlett, R.M. Baumert, R.F. Mann, B.A. Peppley, P.R. Roberge, and T.J. Harris. Performance modeling of the Ballard mark IV solid polymer electrolyte fuel cell. *Journal of The Electrochemical Society*, 142(1):1–8, 1995.

[125] J. Bear. *Dynamics of fluids in porous media*. American Elsevier Pub. Co., New York, 1972.

[126] D.A.G. Bruggeman. Berechnung verschiedener physikalischer konstanten von heterogenen substanzen. *Ann. Phys.*, 416(24):636–664, 1935.

[127] N. Zamel, X. Li, and J. Shen. Correlation for the effective gas diffusion coefficient in carbon paper diffusion media. *Energy and Fuels*, 23(12):6070–6078, 2009.

[128] M. Eikerling. Water management in cathode catalyst layers of PEM fuel cells. *Journal of The Electrochemical Society*, 153(3):E58–E70, 2006.

[129] T.E. Springer, T.A. Zawodzinski, and S. Gottesfeld. Polymer electrolyte fuel cell model. *Journal of The Electrochemical Society*, 138(8):2334–2342, 1991.

[130] S. Motupally, A.J. Becker, and J.W. Weidner. Diffusion of water in Nafion 115 membranes. *Journal of The Electrochemical Society*, 147(9):3171–3177, 2000.

[131] X. Wang and T.V. Nguyen. Modeling the effects of the microporous layer on the net water transport rate across the membrane in a PEM fuel cell. *Journal of The Electrochemical Society*, 157(4):B496–B505, 2010.

[132] J.T. Hinatsu, M. Mizuhata, and H. Takenaka. Water uptake of perfluorosulfonic acid membranes from liquid water and water vapor. *Journal of The Electrochemical Society*, 141(6):1493–1498, 1994.

[133] K. Tüber, D. Púcza, and C. Hebling. Visualization of water buildup in the cathode of a transparent pem fuel cell. *Journal of Power Sources*, 124(2):403–414, 2003.

[134] X.G. Yang, F.Y. Zhang, A.L. Lubawy, and C.Y. Wang. Visualization of liquid water transport in a pefc. *Electrochemical and Solid-State Letters*, 7(11):A408–A411, 2004.

[135] X. Liu, H. Guo, F. Ye, and C.F. Ma. Water flooding and pressure drop characteristics in flow channels of proton exchange membrane fuel cells. *Electrochimica Acta*, 52(11):3607–3614, 2007.

[136] H. Masuda, K. Ito, T. Oshima, and K. Sasaki. Comparison between numerical simulation and visualization experiment on water behavior in single straight flow channel polymer electrolyte fuel cells. *Journal of Power Sources*, 177(2):303–313, 2008.

[137] I.S. Hussaini and C.Y. Wang. Visualization and quantification of cathode channel flooding in PEM fuel cells. *Journal of Power Sources*, 187(2):444–451, 2009.

[138] H. Meng and C.Y. Wang. Model of two-phase flow and flooding dynamics in polymer electrolyte fuel cells. *Journal of The Electrochemical Society*, 152(9):A1733–A1741, 2005.

[139] J. Liu, N. Oshima, E.K., and L.K. Saha. Transport phenomena within the porous cathode for a proton exchange membrane fuel cell. *Journal of Power Sources*, 195(19):6342–6348, 2010.

[140] B.R. Babin, G.P. Peterson, and D. Wu. Steady-state modeling and testing of a micro heat pipe. *Journal of Heat Transfer*, 112(3):595–601, 1990.

[141] C.Y. Wang, M. Groll, S. Roler, and C.J. Tu. Porous medium model for two-phase flow in mini channels with applications to micro heat pipes. *Heat Recovery Systems and CHP*, 14(4):377 – 389, 1994.

[142] J.M. Ha and G.P. Peterson. Analytical prediction of the axial dryout point for evaporating liquids in triangular microgrooves. *Journal of Heat Transfer*, 116(2):498–503, 1994.

[143] J.P. Longtin, B. Badran, and F.M. Gerner. A one-dimensional model of a micro heat pipe during steady-state operation. *Journal of Heat Transfer*, 116(3):709–715, 1994.

[144] K.K. Tio, C.Y. Liu, and K.C. Toh. Thermal analysis of micro heat pipes using a porous-medium model. *Heat and Mass Transfer*, 36:21–28, 2000.

[145] D. Sugumar and K.K. Tio. Thermal analysis of inclined micro heat pipes. *Journal of Heat Transfer*, 128(2):198–202, 2006.

[146] L.L. Vasiliev. Micro and miniature heat pipes – Electronic component coolers. *Applied Thermal Engineering*, 28(4):266 – 273, 2008.

[147] D. Sugumar and K.K. Tio. The effects of working fluid on the heat transport capacity of a microheat pipe. *Journal of Heat Transfer*, 131(1):012401, 2009.

[148] Y.M. Hung and K.K. Tio. Analysis of microheat pipes with axial conduction in the solid wall. *Journal of Heat Transfer*, 132(7):071301, 2010.

[149] A.M.O. Smith. Remarks on transition in a round tube. *Journal of Fluid Mechanics*, 7(04):565–576, 1960.

[150] D.J. Tritton. *Physical fluid dynamics*. Oxford University Press, New York, 1988.

[151] R.K. Shah and A.L. London. *Laminar flow forced convection in ducts*. Academic Press, New York, 1978.

[152] D. Spernjak, A.K. Prasad, and S.G. Advani. Experimental investigation of liquid water formation and transport in a transparent single-serpentine PEM fuel cell. *Journal of Power Sources*, 170(2):334 – 344, 2007.

[153] G.F. Pinder and G.G. William. *Essentials of multiphase flow and transport in porous media*. John Wiley & Sons, 2008.

[154] V. Gurau, Jr. T.A. Zawodzinski, and Jr. J.A. Mann. Two-phase transport in PEM fuel cell cathodes. *Journal of Fuel Cell Science and Technology*, 5(2):021009, 2008.

[155] S. Litster and G. McLean. PEM fuel cell electrodes. *Journal of Power Sources*, 130(1-2):61–76, 2004.

[156] Q. Yan, H. Toghiani, and H. Causey. Steady state and dynamic performance of proton exchange membrane fuel cells (PEMFCs) under various operating conditions and load changes. *Journal of Power Sources*, 161(1):492–502, 2006.